Valentin Steinwender, BSc

Improvement and Application of a Terpenoid Screening Assay

Master's Thesis

to achieve the university degree of

Diplom-Ingenieur

Master's degree programme: Biotechnology

submitted to

Graz University of Technology

Supervisor

Assoc.Prof. Dipl.-Ing. Dr.techn. Harald Pichler

Institute of Molecular Biotechnology

Sandra Moser, M.Sc.

Graz, March 2017

Affidavit

I declare that I have authored this thesis independently, that I have not used other than the declared sources/resources, and that I have explicitly indicated all material which has been quoted either literally or by content from the sources used. The text document uploaded to TUGRAZonline is identical to the present master's thesis.

Date

Signature

Danksagung

Mein Umfeld hat natürlich intensiv an der Entstehung dieser Arbeit mitgewirkt. An dieser Stelle möchte ich die Chance nutzen all denjenigen zu danken, die mich während der Entstehung dieser Arbeit und während des gesamten Studiums motiviert und unterstützt haben.

Zum einen gilt mein Dank der Technischen Universität Graz, dem Institut für Molekulare Biotechnologie und unserem Firmenpartner Isobionics für Möglichkeit in diesem Projekt mitarbeiten zu dürfen.

Weiters möchte ich mich bei Sandra Moser für die großartige Betreuung und Zusammenarbeit bedanken. Sie ist mir immer mit Rat und Tat zur Seite gestanden und hat mich im Labor unterstützt.

Meinem Arbeitsgruppenleiter Harald Pichler, der mir die Zusammenarbeit in einem spannenden internationalen Projekt ermöglicht hat, gilt ebenfalls größter Dank. Er stand immer mit Rat zur Seite und durch sein Wissen konnten unzählige Probleme gelöst werden.

Weiters gilt mein Dank auch Gerhard Thallinger, der sich regelmäßig Zeit genommen hat, um mit Rat für die Verbesserung unserer Auswertungsmethode beseitezustehen.

Natürlich möchte ich mich auch bei meiner Arbeitsgruppe bedanken, die mich mit ihrer großen Hilfsbereitschaft unterstützt hat. Danke liebe(r) Sandra, Anita, Tamara, Melissa, Matthias, Simon, Eva, Steffi, Meli and Corinna.

Ebenfalls müssen meine Freunde hier Erwähnung finden, die mir über die gesamte Dauer meines Studiums zur Seite gestanden sind. Meine Freundin Ceren hat mir vor allem während des Verfassens dieser Arbeit immer Mut zugesprochen.

Abschließend bedingt natürlich meiner Familie größter Dank. Ohne ihre Hilfe wäre mein Studium nicht möglich gewesen. Meine Eltern haben mich konstant in meinem Weg bestärkt und mir alle Möglichkeiten freigestellt. Besonders danken möchte ich auch meinem Onkel Edmund und Marianne, sowie meinen Großeltern Helene und Kurt für die stetige Unterstützung.

Contents

1 List of abbreviations

Abbreviation	Description
DWP	Deep well plate
hDWP	Half-high deep well plate
ddH2O	Water, double distilled
GC-FID	Gas chromatography - flame ionization detector
EtBr	Ethidium bromide
PCR	Polymerase chain reaction
kb	Kilo base pairs
Kan	Kanamycin (40 mg/L)
Neo	Neomycin (100 mg/L)
HTS	High-throughput screening
MTS	Medium-throughput screening
NR	Nile red
R	media control (originates from RS102)
WT	Wild type strain
TMSC	Trimethylsilyl cellulose
EtOH	Ethanol
MeOH	Methanol
n	Number of experiments
System Duetz	special fixing clamps for shakers
Pppa	constitutive promoter in *R. sphaeroides*
pmeV	p-m-Pppa-trx-ValCO Q492K L566S-mpmii alt wild type plasmid, present in *R. sphaeroides* #88

2 Abstract

Terpenoid biosynthesis has been strongly investigated during the last few decades. This is fostered by terpenoid applications in pharmaceutical, agricultural, flavor & fragrance and fuel industries. Biotechnology offers sustainable options for production of these compounds in microbes. Along these lines, terpenoid production can be improved by strain engineering so that seasonal changes in natural (re)sources do not influence overall terpenoid yields. Strain improvement frequently relies on screening procedures with sufficient throughput. Versatile terpenoid screening assays are largely missing in the field. This work describes the development and optimization of a screening method to directly detect and quantify microbially produced terpenes and terpenoids.

3 Zusammenfassung

Dem Feld der Terpenoidforschung wurde für lange Zeit zu wenig Beachtung geschenkt, obwohl die Pflanzenheilkunde ein integraler Bestandteil menschlicher Kulturgeschichte ist. Dies hat sich zuletzt geändert. Nicht nur die Pharmaindustrie hat ihr Interesse an der Wirkstoffforschung verstärkt, sondern auch die Agrarindustrie, die Aroma- und Duftstoff-Industrie sowie die Treibstoffindustrie sehen in der Terpenoidforschung Optionen für die Zukunft. Die Biotechnologie bietet interessante Möglichkeiten, Terpenoide nachhaltig und in hoher Reinheit mikrobiell zu produzieren. Allerdings fehlt es an Hochdurchsatz-fähigen Assays, um schnell und gezielt Stammverbesserungen feststellen zu können. Hier wird die Entwicklung und Verbesserung eines Screening Assays beschrieben, der es ermöglicht mikrobiell hergestellte Terpene und Terpenoide direkt zu detektieren und zu quantifizieren.

4 Introduction

The chemical class of terpenoids has been a booming field of research in the last decades. The reason for this trend is that terpenoids are used vastly in flavor&fragrance, pharmaceutical, agricultural and fuel industries. Until now about 55,000 natural terpenoids have been identified.

Originally, the name terpene comes from the turpentine tree (in German Terpentin), which was used for isolating the first compounds of this class. The chemical class of terpenoids is large and diverse. They are subdivided into the classes of terpenes, which are pure hydrocarbons, and terpenoids that comprise terpenes, but may additionally have functional groups added to the hydrocarbon skeleton. In nature, terpenoids are found in various areas. Almost all plants and some insects produce them. In many cases they protect plants by attracting predators which have herbivores as bait. Another protection mechanism is detering herbivores through their smell or intolerance. Terpenes and terpenoids often have a strong odor and are responsible for the distinct taste in our food.

In addition to their role in defence or attraction, they are also major biosynthetic building blocks in nearly every living organism. Compounds like steroids are synthesized from the precursor molecule squalene, a triterpene. Vitamin A also is a terpene. Every terpenoid is derived from the basic structure of isoprene C_5H_8, and follows the so-called isoprene rule. This basic, branched 5C-structure (refered to as isoprene units) are repetitively fused to form terpenes. The monomeric C5 structures can be fused in a head-to-tail, head-to-head or head-to-middle fashion. Due to this fusion mechanism, terpenoids can als be subdivided according to their size. Terpenoids containing only one isoprene unit are called hemiterpenes. Two fused isoprene units yield monoterpenes. With three isoprene units they are called sesquiterpenes. Structures with 20 carbon atoms are diterpenes, 30 carbon atoms make up triterpenes and with 40 carbon atoms they are called tetraterpenes. Terpene structures containing more than 40 carbon atoms are referred to by the term polyterpenes. Volatile terpenoids usually belong to classes with 5-15 carbon atoms like hemiterpenes, monoterpenes and sesquiterpenes. [1] For the biosynthesis of terpenoids, the two C5 precursor molecules dimethyl allyl diphosphate (DMAPP) and its isomer isopentenyl diphosphate (IPP) are needed. A condensation reaction catalyzed by a prenyl diphosphate synthase takes place to create a polyprenyl diphosphates. These polyprenyl diphosphates are further used by terpene synthases to create terpenes. Distinct pathways have been found in eukaryotes and prokaryotes for the generation of the precursors DMAPP and IPP. The mevalonate dependent (MEV) pathway is generally used by eukaryotes and archaea, while the deoxyxylulose-5-phosphate (DXP) pathway is more commonly used by bacteria. While the mevalonate pathway uses two molecules of acetyl-CoA in the beginning of the pathway, the DXP pathway connects pyruvate and D-glyceraldehyde-3-phosphate.[2]

The flavor&fragrance industry shows huge interest in terpenoids, because of their smell and taste. In nature, terpenoids are also used for communication purposes which makes them attractive for agriculture for example as an insect repellent. From the chemical perspective terpenoids have a high energy content due to their hydrocarbon structure. Therefore, there have been successful attempts to use terpenoids as an alternative fuel source. It has been shown that some essential oils harbour strong antimicrobial activity against for example methicilin-resistant *Staphylococcus aureus* (MRSA).[3] The pharmaceutical industry is trying to employ these properties or to use the relatively complex

structure as a precursor compound in their production pipelines. To generate terpenoids for the global market three different processes can be used: extraction from natural resources, chemical synthesis and cultivation of recombinant microbes. While extraction from natural resources and chemical synthesis are frequently neither commercially profitable nor ecologically sustainable, cultivation of recombinant microbes can use cheap feedstocks and turn them into high value products. Additionally natural sources may have the disadvantage of contamination with unwanted terpenoid impurities, of low terpenoid abundances in plants leading to high waste amounts and of variable quality due to seasonal variations. However, there may also be severe limitations in microbial terpenoid production, that should be overcome. To improve and circumvent these limitations, several approaches of directed evolution have been undertaken. Mostly, they focused on either engineering terpenoid synthesis or on the whole recombinant host. Microbial terpenoid production improvement can be classified in two main areas. One approach is to engineer microbial hosts in a way that they have a higher isoprene level for terpene synthesis. The second approach is improvement of terpene synthases. Since terpene synthases constitute the bottleneck in terpenoid synthesis with a turnover number of less than 0.5 per second on average, engineering these enzymes will massively boost productivity. Prenyl diphosphates are essential for cells. Not only secondary metabolite terpenoids are formed from them, but they are also precursors to squalene (and sterols), heme factors and ubiquinones. Therefore, there is strong competition taking place for the prenyl diphosphate pool. If terpene synthases are the bottleneck in microbial hosts an increase in enzyme amount by using a stronger promoter or promoter engineering can be another approach. Still microbial production hosts have not yet reached their limits, because easy-to-use, efficient, stable and reproducible high-throughput assays are largely missing in this field.[4][1]

The term "high-throughput" generally refers to 10.000 up to 100.000 screened clones per day. It can be achieved by manual work as well as fully automated robotic labor.[5] To date some groups found really creative approaches to achieve the throughput. They developed assays either for one special reaction or for general purposes. Most approaches are limited to low-throughput chromatography-based methods. Colorimetric assays would be easier and faster to evaluate, but terpenoids are mostly colorless and have to be coupled to a dye to be measured indirectly. [6] Nevertheless, a few color-based assays exist. For example, indirect screening approaches can be based on different carotenoid colony pigmentation. This can be coupled with fluorescence assisted cell sorting by flow cytometry and magnetic cell sorting.[7] Another approach that uses carotenoids for screening is based on competition during synthesis. This kind of selection systems focuses on the fact that precursors (isoprene units) of carotenoids are also used for terpenoid synthesis. The higher the output of for example sesquiterpenoid, the less isoprene units remain for the synthesis of carotenoids. And less carotenoids lead to less pigmentation. Furubayashi et al. (2014) used this strategy to screen mutant libraries of tobacco 5-epi-aristolochene synthase (TEAS), taxadiene synthase (TXS) and geraniol synthase (GES) in *E. coli* for higher activities.[8] A special use of the dye nile red and BODIPY was patented by Amyris, Inc. in 2012.[9] An assay was established that used these dyes to screen for improved activities of terpene synthases. Since the photophysical properties of nile red are highly dependent on the anisotropic environment, it seems also possible that other compounds can be screened for in this system.[10]

Plain selection can sometimes be done by the use of a certain concentration of selective compounds. Kirby et al. (2014) proposed the use of nonionic surfactants like Tween 20 to select for increased bisabolene titers in *Saccharomyces cerevisiae*. The group proved that Tween 20 created sufficient selective pressure to select between two bisabolene producing strains differing in titers by a factor of 2. Additionally, Tween 20 seemed also to sustain high production levels during fermentation. When cultivating bisabolene producing *S. cerevisiae* strains, the production titer inceased by a factor of four compared to using a dodecane overlay and by a factor of 20 without dodecane.[11]

Another approach to screen for improved terpenoid production is the use of colored by-products. One example is the malachite green assay that is based on the by-product pyrophosphate. During the cyclization reaction of farnesyl pyrophosphate (FPP) to sesquiterpenes the pyrophosphate is cleaved off. An inorganic pyrophosphatase from *S. cerevisiae* uses it for producing inorganic phosphate. Malachite, molybdate and the monophosphates create a turquoise complex that can be quantified by a standard UV spectrometer. The terpene synthases β-farnesene synthase from *Artemisia annua* (AaFS), amorpha-4,11-diene synthase from *A. annua* (AaADS) and 5-epi-aristolochene synthase from *Nicotiana tabacum* (TEAS) were successfully analyzed by this method.[12] A second example is the use of a vinyl methyl ether isoprenoid derivative ("Substrate 3") in combination with a coupled enzyme assay. During the cyclization reaction of Substrate 3, methanol is released as a by-product. This methanol molecule is further converted to formaldehyde by an alcohol oxidase. Subsequently, Purpald® and formaldehyde form a purple complex. This method was established by rapid optimization of conditions for stability and expression of the terpene synthase SSCG_02150, that produces (-)-δ-candinene. Moreover, the thermostability of the sesquiterpene synthase BcBOT2 from *Botrytis cinerea* was increased by 12°C with this assay.[13] Both methods based on assessing by-products have the downside of prior protein extraction though.

In the field of microbial terpenoid production a wide range of microorganism can be employed as hosts. Two frequently used microorganisms are the methylotrophic yeast *Pichia pastoris* and the purple bacterium *Rhodobacter sphaeroides*. The yeast is frequently used for the production of industrial enzymes and biopharmaceuticals. Advantages that make it so suitable for these tasks are availability of strong and tightly regulated promoters, growth to very high cell densities and the recominant protein production levels in an order of grams of recombinant protein per litre culture both intracellularly and extracellularly. In *P. pastoris* the *AOX1* promoter is commonly used as a very strong inducible promoter to uncouple the production state from the growth state. The *AOX1* promoter naturally drives alcohol oxidase 1 expression, in the presence of methanol. Therefore, production of a protein of interest regulated by the *AOX1* promoter is induced by addition of methanol. For constitutive expression, the *GAP* promoter is frequently used to start production from the beginning of inoculation. The *GAP* promoter is able to reach almost the same expression level on glucose as the *AOX1* promoter.[14][15]

The purple non-sulfur photosynthetic Eubacterium *R. sphaeroides* has been extensivley studied in photosynthesis research and for possible hydrogen production. It has a very diverse metabolism that can generate growth either by anaerobic or aerobic respiration, fermentation or photosynthesis. Organic compounds that enter the cytoplasm can be used as a carbon source or reductants for chemoheterotrophic and photoheterotrophic growth. In the autotrophic case, carbon dioxide is used

as a sole carbon source.[16] Additionally, *R. sphaeroides* has a large membrane system and an intrinsic DXP pathway which makes the organisms suitable for terpenoid production.

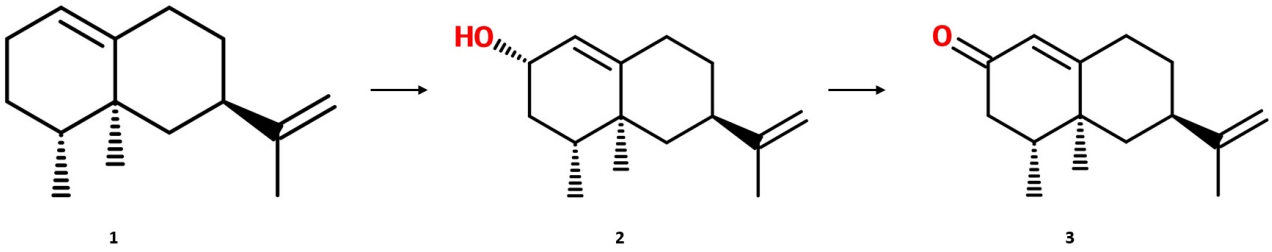

Figure 1: **Conversion of (+)-valencene (1) to trans-nootkatol (2) and (+)-nootkatone (3).**

The present work addresses the lack of high-throughput assays in the field of microbial terpenoid production. We developed and optimized a new technology to detect terpenoids and some other compounds. By using the volatility of compounds/terpenoids it is possible to detect and quantify them. As production hosts we employe *P. pastoris* and *Rhodobacter sphaeroides*. Mainly three compounds were used in the screening assay namely (+)-valencene, trans-nootkatol and (+)-nootkatone. The screening assay was also tested in the absence of microbial hosts applying a series of pure volatile compounds that did include structures other than terpenoids. The sesquiterpene (+)-valencene naturally occurs in citrus fruits such as oranges. It is used as flavor and fragrance compound in industry. Additionally, hydroxylation of (+)-(+)-valencene gives rise to nootkatone, which is found in grapefruit and is a highly sought-after sesquiterpenoid. The intermediate in the reaction from (+)-valencene to nootkatone is trans-nootkatol (Figure 1).

5 Materials and methods

5.1 General methods

5.1.1 Gel electrophoresis

To separate DNA fragments, gel electrophoresis was performed using agarose gels containing ethidium bromide and agarose dissolved in 1xTAE buffer. Analytical gels contained 0.8% agarose and were run at 120 V for 45 min. Preparative gels contained 1% agarose and were run at 90 V for 90 min. In the case of preparative gels, matching bands were cut out under UV light and purified via DNA gel purification (5.1.2 DNA Gel Purification).

5.1.2 DNA gel purification

Bands were cut out and weighed. Afterwards, purification was performed according to kit manual using "GeneJET PCR Purification Kit" (Thermo Scientific).[17] The DNA was eluted from the column by applying 40 μl of ddH_2O prewarmed to 65°C and stored at -20°C. Concentration was determined via NanoDrop measurement using ddH_2O as blank.

5.1.3 DNA restriction

To perform a control restriction cut, 300 ng of purified plasmid DNA was mixed with 1 μL of restriction enzyme(s), 1 μL of recommended buffer and the corresponding amount of ddH_2O to a final volume of 10 μL. The reaction mix was incubated for 30 min (FastDigest, Thermo Scientific) to 60 min (standard restriction enzymes) at 37°C. For a preparative restriction cut, 3 μg of purified plasmid DNA or 25 μL of a 50 μL PCR reaction were mixed with 3 μL of restriction enzyme(s) and appropriate buffer at the recommended concentration. The reaction mix was incubated for at least 2 h at 37°C (if not recommended otherwise).

5.1.4 DNA ligation

For ligation, vector backbone and insert were used at a 1:3 molar ratio. Hundred ng of linearized and dephosphorylated vector DNA was mixed with the calculated amount of insert and 2 μL of T4 DNA ligase buffer as well as 5 U of T4 DNA ligase. The volume was adjusted to 20 μL with ddH_2O. The reactions were incubated either for 2 h at room temperature or overnight at 16°C. The ligase was then heat-inactivated for 10 min at 65°C. To calculate the corresponding amount of insert to 100 ng of vector backbone, a ligation calculator tool ($http://www.insilico.uni-duesseldorf.de/Lig_Input.html$) was used. For desalting, the reaction mix was put on a 0.025 μM Millipore filter floating on ddH_2O for 30 min. The desalted DNA was transferred to sterile Eppendorf tubes and either immediately used for electrotransformation or stored at -20°C.

5.1.5 *E. coli* electrocompetent cells

First, overnight cultures were started inoculating 30 mL of LB media with single colonies for incubating at 37°C and 220 rpm. Then, 5 mL of the overnight culture were used to inoculate 500 mL of LB media in 2 L baffled flasks. The cultures were incubated at 37°C and 170 rpm until an OD600 between 0.7 and 0.9 was reached. The cells were put on ice for 30 min before harvesting. The cultures were centrifuged in sterile, pre-cooled 500 mL centrifugation bottles for 15 min at 2000 g and 4°C. The supernatant was discarded and the cells were resuspended in 500 mL of pre-cooled ddH_2O and centrifuged for 15 min at 2000 g and 4°C. This washing step was repeated once. Then, the cells were resuspended in 35 mL of pre-cooled, sterile 10% glycerol and centrifuged for 15 min at 4000 g and 4°C. The supernatant was discarded and the pellets were resuspended in 1 mL of cold and sterile 10% glycerol. Aliquots of 80 μL were taken and transferred into Eppendorf tubes and were either put on ice for immediate use or frozen in liquid N_2 for storage at -80°C.

5.1.6 Electrotransformation into *E. coli*

Eighty μL or 50 μl of electrocompetent *E. coli* cells were mixed with 1 μL of ligated and desalted plasmid DNA in pre-cooled electroporation cuvettes. After 2 min of incubation on ice, the cells were pulsed with the "EC2" program for 5-6 ms at 2.5 kV and 1 mL of SOC media was added immediately. The cells were then incubated in a thermomixer at 37°C. After 1 h, 100 μL of cell suspension were plated onto LB plates containing antibiotics for selection. The rest of the cell suspension was centrifuged, resuspended in 100 μL media and plated as well. The plates were incubated at 37°C overnight. In the case of a conjugation (see 5.6.3 Conjugation) 100 μl of the cell suspension were added to 4.9 ml of LB media with antibiotics and were incubated overnight at 37°C and 100 rpm.

5.1.7 Plasmid purification

To isolate and purify plasmid DNA from *E. coli* or *R. sphaeroides*, the "GeneJET Plasmid Miniprep Kit" (ThermoFisher Scientific) was used.[18] Plasmid isolation was carried out according to the manual. In the end, the DNA was eluted in 50 μL of ddH_2O. For mini-preparations with *R. sphaeroides*, the protocol was slightly changed. When resuspending the cells in the resuspension solution, 1 min vortexing improved the mini-preparation quantity and quality. Lysis was performed by adding the 250 μl of lysis solution, inverting 4-6 times, subsequent 5 min incubation and, then, another 4-6 times of inverting the tube. Plasmid DNA was eluted by 5 min incubation in 25 μl of ddH_2O and 5 min centrifugation at 16,000 rpm.

5.2 Screening assay

5.2.1 Production of the screening films

The glass substrate (7 cm x 10 cm) was first rinsed with methylene chloride, acetone and water. Afterwards, the substrate was placed into "piranha" acid (H_2SO_4(95%):H_2O_2(30%) = 7:3 (v/v)) for 30 min to remove organic residues and then neutralized with distilled water. For the film preparation trimethylsilyl-cellulose (TMSC; DS: 0.8-3.0) and nile red were dissolved in the organic solvent (chloroform, toluene, tetrahydrofuran, dichloromethane, acetone, butanone), filtered (pore size: 0.45 – 3 μm) and afterwards spin-coated onto the glass substrate. The obtained film thickness (20 nm – 3 μm) depended on the concentration of the TMSC (0.1 – 5 wt%) respectively nile red (0.1 wt%), amount of solution (3 – 12 ml) and the parameters of the spin-coating (speed: 500 – 7000 rpm; acceleration: 100 – 4000 rpm/s; time: 10 – 300 s). This step was performed by Mathias Hobisch and Michael Süßenbacher.

5.2.2 The screening film in practice

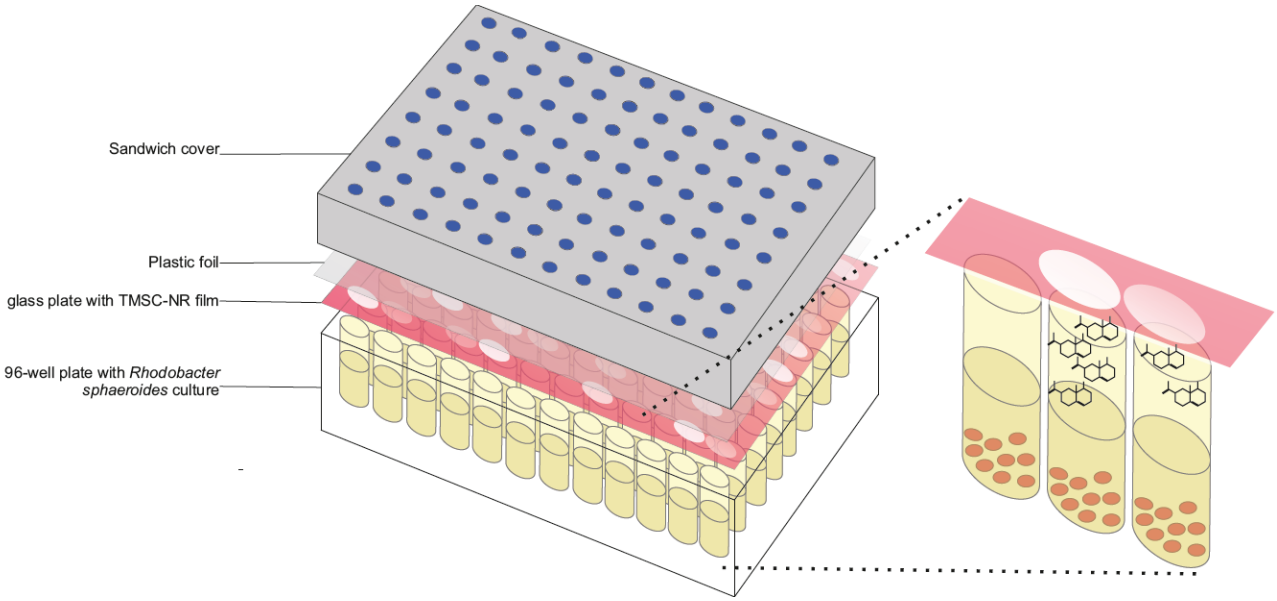

Figure 2: **Screening assay.** The principle setup of the screening assay. The screening film was positioned over the DWP and fixed with tape. A plastic foil was used to protect the glass plate. The sandwich cover/metal lid was positioned over the whole setup to apply pressure and seal the plate. The more, for example, (+)-valencene was produced the stronger the color shift. Image created by Sandra Moser.

After spin-coating the nile red films were dried and stored until use protected from light . Films can be stored for 1 month. Longer storage is not advised as films might start to lose color and, thus, screening capacity. The films on the glass plates support fit on hDWP and DWP. Right before experiments, plates were predried at 100°C for 45 min and cooled down before screening. All films seen in this work had a nile red concentration of 0.1% spin-coated onto the glass plate. To generate evaluable data, the start point of incubation and the duration of incubation for the screening film can be freely choosen. The longest period of incubation was 5 h. A longer incubation period usually

led to tearing of the TMSC film. It was suggested that the humidity has a strong influence on the incubation duration (Sandra Moser, personal communication). The maximum incubation time has to be significantly shorter than 5 h if the humidity exceeds. The general setup (Figure 2) included the DWP with the microbial cultures, the screening film, a plastic foil and a metal lid. The screening film was placed on the DWP with the TMSC side facing downside. On two opposite sides the glass plate was fixed with tape. Otherwise the TMSC film got damaged. On top of the glass plate a foil was placed to prevent the build up of a vacuum between the glass plate and the metal lid. The metal lid has little holes and rubber inside. The metal lid creates microaerobic conditions and prevents the evaporation of water in the wells. Finally, the metal lid was placed over the plastic foil. In combination with the System Duetz (EnzyScreen) and the lid it is possible to establish pressure from the upside. This pressure forced the glass plate onto the DWP and sealed the wells. The sealing was determined as a critical step and worked better with hDWP. This was probably because DWP were often autoclaved and the surfaces were uneven. The hDWP from EnzyScreen were never autoclaved, but UV sterilized for 90 min. Afterwards, they were packed in aluminium foil that was rinsed in ethanol.

5.3 Compound-only experiment

It was of interest to search for different compounds that can be detected with the screening assay to document broad applicability of the assay. This was done in hDWP at 28°C and 320 rpm for 1 h in the CERTOMAT BS-1 shaker. Screening films were predried at 100°C for 45 min as above. In each hDWP plate 60 wells were used for positioning. Samples were positioned only in a way that they were apart from each other by at least one well. Per substance three wells were measured. Each tested well contained 200 μl Fresenius water plus 5 μl of the compound - if not other mentioned. Each methanol well contained 200 μl of methanol only. Controls per plate were either 200 μl ddH_2O or 200 μl ddH_2O + 5 μl or 25 μl ethanol. The amount of ethanol serving as a control was depending on how much compound dissolved in ethanol was pipetted on each of the plates. Since the compounds are highly volatile, repetitive film developments were performed applying only two columns of volatile compounds in each round to avoid premature evaporation. After pipetting two columns the film was placed over the hDWP and fixed with adhesive tape. Plastic foil was applied over the screening film and the metal lid was fixed with tape. Incubation took place in the System Duetz.

5.4 Bioinformatical methods

After screening the microbial culture, the screening film had changed its color depending on the amount and chemical properties of the volatile compounds. Subsequently, the empty side of the glass support was cleaned with isopropanol and special lint-free tissue. For scanning a HP Scanjet 4370 was used. The scanner was cleaned in regular time intervals with 70% ethanol. The screening film was placed on the glass scanning plate with the TMSC side facing down. Therefore, the screening plate should be moved as little as possible. Three sheets of A4 paper were placed over the screening film to create a white background while scanning. The lid was closed and the scanning was started. Automatically the HP scanning program HP Scansoftware 4.0 popped up. Resolution was set to 300 dpi or later 600 dpi. A preview scan was performed and only the region of interest was selected. After finishing the scanning process the program switched automatically to the HP Image Zone 5.3. In this application the images were saved in the .tiff-format. Although the screening pattern stayed visible for weeks - until the screening films lost their color - best results were achieved by scanning the screening film right after screening. On average, the film could be scanned until a week after the screening and still gave useful results.

The created tiff-images were afterwards analyzed in ImageJ 1.50d with the Fiji distribution. Before getting started in ImageJ Edit - Options - Conversions was opened and it was verified that Weighted RGB conversions is unchecked. Otherwise, the single colors during image conversions to grayscale are not treated the same way. At first the images were flipped horizontally. Subsequently, the MicroArray Profile plugin was called. This plugin was developed by Bob Dougherty and Wayne Rasband (Copyright (c) 2005, 2012 OptiNav, Inc.).[19] Region of interest (ROI) shape inside the plugin was set to "Rectangles". With a resolution of 300 dpi the region of interest was set to 60x60 pixel per well and with 600 dpi resolution images the region of interest was set to 120x120 pixel per well. The button “Measure RT” opened another window called "Results". Here the measured parameters were shown. These data sets were saved and the evaluation of the data sets was followed in Microsoft Excel 2010. The saved data set file from ImagJ can be opened via Excel. It contains the values for each well from left to right and top to bottom. The calculated integrated density was used for evaluation during the project. This resulted in values below 10. A different approach was the use of the mean gray value (declared as “Mean” in the table). The mean gray value varied between 0 and 255. Both methods showed the exactly same results while only the values on the y-axis changed. For triplicate and higher sample number measurements a standard deviation was calculated. For only duplicate measurements, the difference from the mean value was calculated. The Excel file contained not only the data evaluation, but always a screenshot of the evaluated screening film and the distribution pattern of strains in the DWP.

5.5 Modification of screening film images for publications

The images of the screening films were well visible on computer screens, but as practical experience showed they were not reliable for presentations or publications. Beamer quality, printer quality, image saturation or contrast might be weak and the audience/the reader would not be able to follow the results. Therefore, all screening films were modified to improve their visibility. For RGB, red channel, green channel and blue channel images the modification was done via a macro (Figure 3). The upper and lower display range was adjusted (Image - Adjust - Brightness/Contrast...). RGB images were adjusted to 150 and 246. Blue channel images were adjusted to 200 and 240. Green channel images were adjusted to 175 and 240. Red red channel images were adjusted to 190 and 255. Detailed information about the display range modification of other images is given in the related caption.

*TSA Publication Macro.txt

```
/*Valentin Steinwender, January 06, 2017*/
dir=getDirectory("image");
imgName=getTitle();
baseNameEnd=indexOf(imgName, ".tif");
baseName=substring(imgName, 0, baseNameEnd);
run("Flip Horizontally");
run("Split Channels");
selectWindow(imgName + " (blue)");
setMinAndMax(200, 240);
saveAs("png", dir + baseName + "_editedBlue.png");
close();
selectWindow(imgName + " (green)");
setMinAndMax(175, 240);
saveAs("png", dir + baseName + "_editedGreen.png");
close();
selectWindow(imgName + " (red)");
setMinAndMax(190, 255);
saveAs("png", dir + baseName + "_editedRed.png");
close();
open(imgName);
run("Flip Horizontally");
setMinAndMax(150, 246);
saveAs("png", dir + baseName + "_edited.png");
close();
```

Figure 3: **Java code for image modification.** Display range was adjusted as following: For RGB images to 150 and 246, for blue channel images to 200 and 240, for green channel images to 175 and 240, and for red channel images to 190 and 255. These changes were not used in the evaluation process. These manipulations only served for better depiction in presentations.

5.6 Biological example with *R. sphaeroides*

5.6.1 The screening assay and *R. sphaeroides*

To perform the screening assay on *R. sphaeroides* strains a preculture was inoculated. This preculture was incubated for 65 - 72 h at 320 rpm and 28°C. For the preculture, 500 μl of RS102 medium per well containing 100 μg/ml neomycin were used. Strains were taken from LB-Kan plates. The main culture was either started in hDWP or DWP. In hDWP, 140 μl of RS102 containing 100 μg/ml neomycin was pipetted per well and inoculation was performed via a 96-position pin stamp from the preculture. Cultivation conditions were 28°C, 50 mm orbit at 320 rpm in the CERTOMAT BS-1 shaker with a humidity of 30-40%. After 18 h of cultivation the screening was performed for 70 min. In DWP, 400 μl of RS102 containing 100 μg/ml neomycin were added per well and inoculated via a 96-position pin stamp from the preculture. Cultivation conditions were 28°C, 50 mm orbit at 320 rpm in the CERTOMAT BS-1 shaker with a humidity of 30-40%. After 17 h of cultivation the screening was performed for 5 h. If the cultivation was done in the Kuhner Climo-Shaker ISF1-XP, the conditions were 300 rpm, 28°C, 50 mm orbit and humidity was constantly under 40%.

5.6.2 Creation of *Pppa*-mutant library and transformation into *E. coli* S17-1

To find *R. sphaeroides* strains with an improved (+)-valencene production, we created a mutant library for the *Pppa* promoter driving (+)-valencene synthase expression and screened 1000 clones for improved (+)-valencene production. The *Pppa* region localized between EcoRI and NdeI restriction sites had a length of 88 bp and is placed in the plasmid p-m-Pppa-trx-ValCO Q492K L566S-mpmii alt (further called "pmeV", Figure 5). In the first, step a 1085 bp fragment was amplified from the p-m-Pppa-trx-ValCO Q492K L566S-mpmii alt plasmid using primer Fw_UpPppaBglII and Rev_DownPppaNcoI (Figure 20) with the Phusion polymerase. The resulting 1085 bp fragment was then blunt end cloned into the pJET1.2/blunt cloning vector (Figure 4). This vector was called "pJET1085". In the next step, the mutagenic PCR was performed with the „GeneMorph II Random Mutagenesis Kit" (Agilent Technologies). There were three stages for generation of a suitable library of mutagenized *Pppa* fragments. At first, a test mutagenic PCR was performed to determine the mutagenesis efficiency. Through the analysis of the test mutagenic PCR two template amounts were determined to create a most suitable library. The first amount to create a fragment library was 5 ng template (Fragment I). The second amount to create a fragment library was 0.5 ng template (Fragment II). The primers Fw_PppaMut and Rev_PppaMut were used for the PCR protocol (Figure 1). After the PCR, the fragment libraries were separated on a 1.5% agarose gel at 100 V. The corresponding bands were cut out and purified. Nanodrop measurements yielded a concentration of 47.2 ng/μl for fragment library I and 64.3 ng/μl for fragment library II. The purified fragment libraries were cut with the fast digest restriction enzymes NdeI and EcoRI for 45 min at 37°C. In the following ligation the two different *Pppa* libraries were EcoRI/NdeI introduced into the pJET1085 vector replacing the original *Pppa* fragment. Each fragment library, i.e. 11.8 ng/μl of fragment I and 16.1 ng/μl of fragment II was ligated with 81.9 ng of linearized pJET1085 at room temperature for 2 h. Afterwards, an inactivation step at 65°C for 10 min and desalting

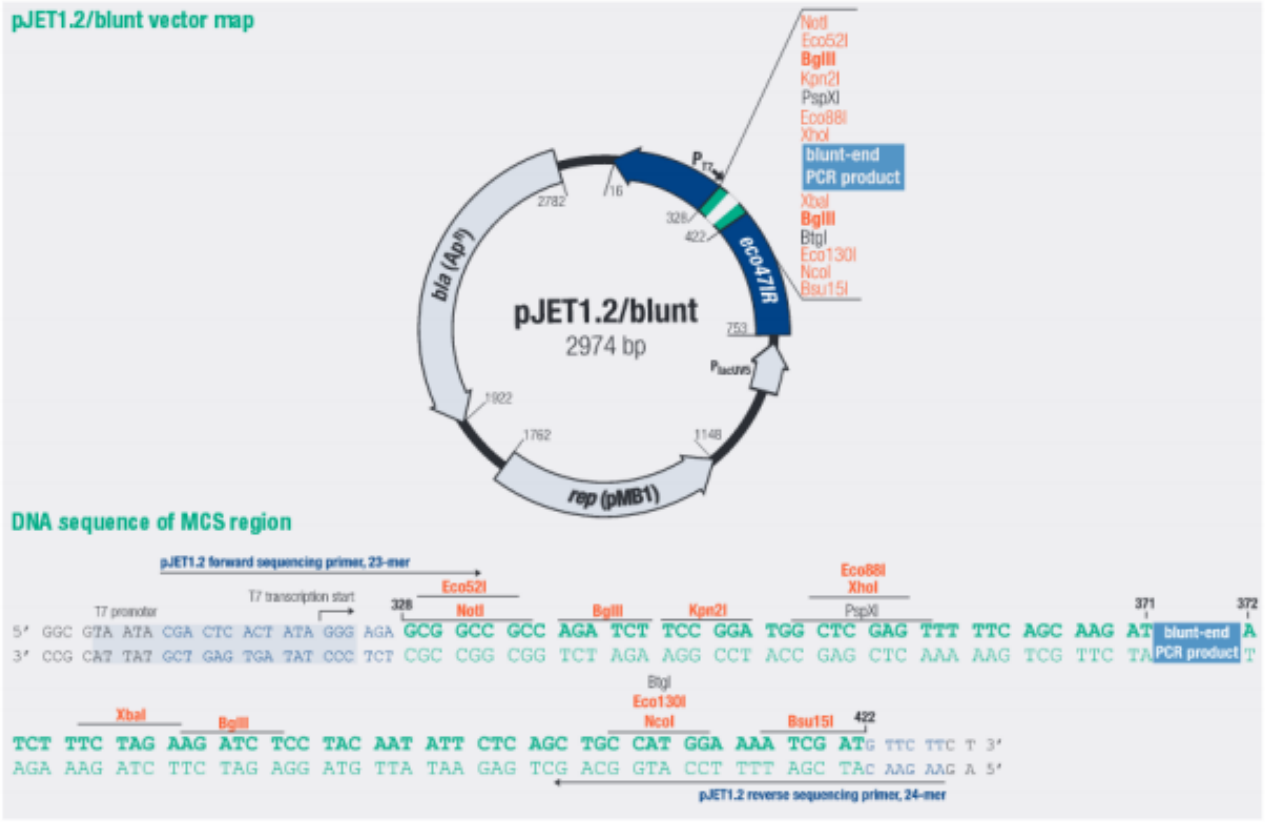

Figure 4: **Map and features of pJET1.2/blunt cloning vector.**

step for 20 min were performed. The ligated samples were then transformed into *E. coli* TOP10F' cells. Eighty μl of competent *E. coli* TOP10F' were transformed with 8 μl of each ligation sample. Transformants were regenerated at 37°C for 60 min, and subsequently plated on LB + 100 mg/L ampicillin plates for plasmid amplification. The day after, they were sent for sequencing with the sequencing primer Fw_UPtrxValC and Rev_SeqValC_1.

Since the sequencing results of experiments based on fragment I and fragment II libraries were not satisfying the needs, another round of mutagenesis was performed with 0.1 ng (fragment III), 0.025 ng (fragment IV) of template sequence and 0.64 ng of fragment II library template sequence (fragment V). The procedure for the mutagenesis of these three *Pppa* mutant libraries was the same as for the previous two libraries apart from the PCR protocol that was slightly changed (Figure 2). The ligation was performed with 17 ng of fragment III, 22 ng of fragment IV and 25 ng of fragment V libraries with each 98 ng of linearized pJET1085 as above.

Ten selected transformants per library were then streaked out for sequencing. The plasmids of the ten streaked clones were isolated via mini-preparation on the next day and sent for sequencing with the primer Fw_UPtrxValC and Rev_SeqValC_1.

After the determination of the mutation rate, the 1085 bp fragments were cut out of the pJET1085 libraries with the appropriate mutation rates (fragment III and fragment V libraries) by using the restriction enzymes SpeI and SgrDI in sequential reactions. At first SpeI digest took place for 2 h at 37°C. Then, SgrDI was added with the right amount of Tango buffer and the digest was continued overnight at 37°C. The plasmid p-m-Pppa-trx-ValCO Q492K L566S-mpmii alt (vector)

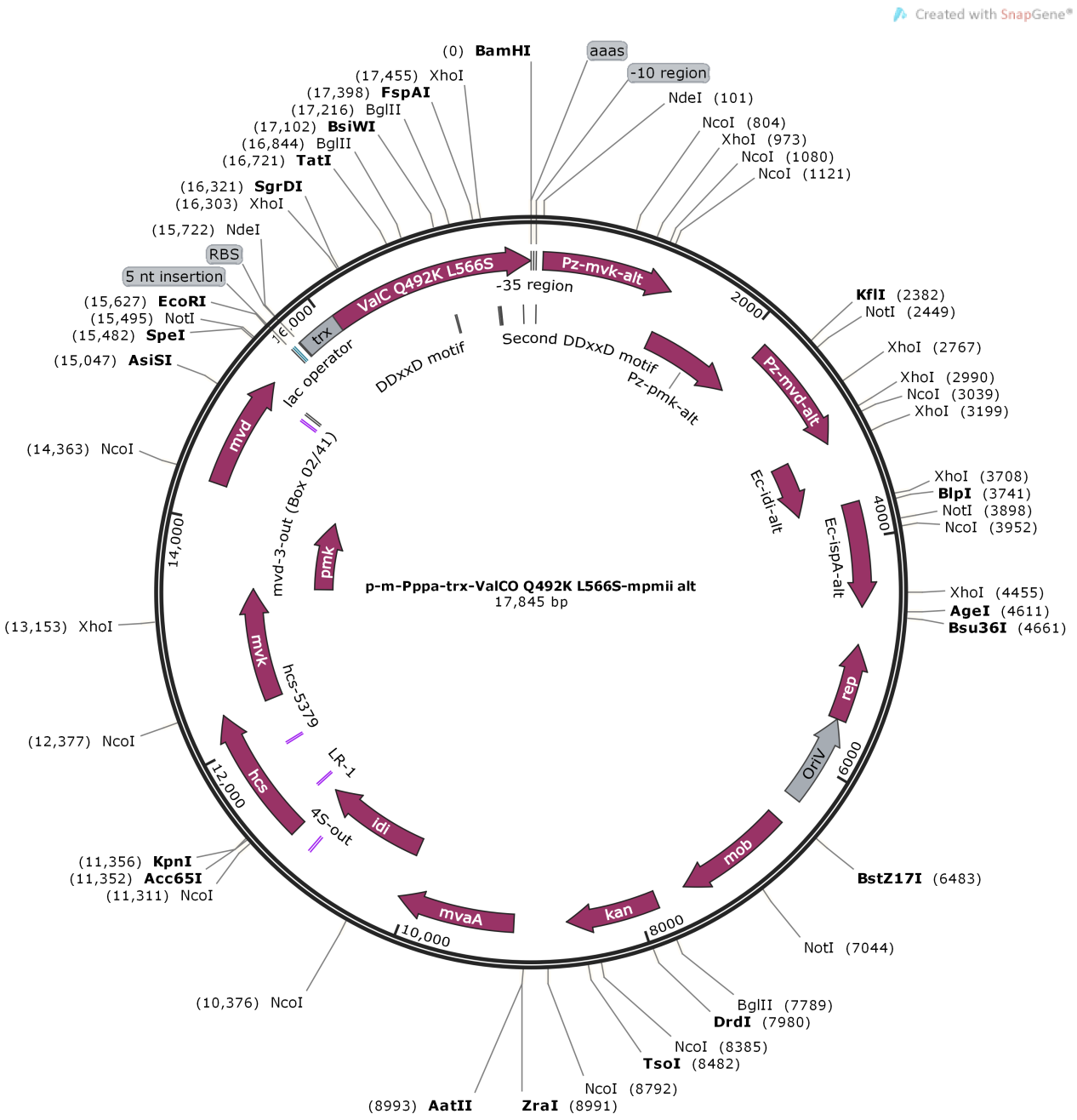

Figure 5: **Wild type plasmid (p-m-Pppa-trx-ValCO Q492K L566S-mpmii alt) used to create the *Pppa* libraries.** The *Pppa* promoter is driving the (+)-valencene synthase (trx-ValC Q492K L566S) expression. Additionally, the plasmid containes the genes of the mevalonate pathway and the backbone with a kanamycin resistance cassette.

Table 1: **PCR protocol for library fragments I and II.**

	Time	Temperature
Initial denaturation	2 min	95 °C
35 Cycles	30 sec	95 °C
	30 sec	56 °C
	1 min	72 °C
Final Extension	10 min	72 °C
Cooling	Open end	4 °C

Table 2: **PCR protocol for library fragments III, IV and V.**

	Time	Temperature
Initial denaturation	2 min	95 °C
40 Cycles	30 sec	95 °C
	30 sec	56 °C
	1 min	72 °C
Final Extension	10 min	72 °C
Cooling	Open end	4 °C

digest was performed with 20 μl of pmeV (140 ng/μl), 3 μl Tango-Buffer, 2 μl SpeI and 5 μl ddH2O. Afterwards, additionally 4 μl of Tango buffer and 2 μl SgrDI were added. The fragment III and fragment V library digest was performed with 25 μl of fragment III (86.1 ng/μl) or Fragment V (136.5 ng/μl), 3 μl Tango-Buffer, 2 μl SpeI. Afterwards, additionally 4 μl Tango buffer and 2 μl SgrDI were added. Digested vector and the fragment libraries were purified over a 0.7% agarose gel at 100 V. After purification, the *Pppa* libraries were ligated into the linearized pmeV vector. This ligation was performed at 16°C over night for maximal efficiency. Subsequently, T4 DNA ligase was inactivated at 65°C for 10 min and the samples were then desalted for 25 min. Ligation of Fragment III and Fragment V into p-m-Pppa-trx-ValCO Q492K L566S-mpmii alt contained 2 μl of T4 DNA ligase Buffer, 1 μl T4 Ligase, 10 μl pmeV and 3 μl of fragment III or 5 μl of fragment V libraries.

Two libraries with different mutation rates for the *Pppa* promoter were generated in the p-m-Pppa-trx-ValCO Q492K L566S-mpmii alt plasmid (Figure 3). These libraries were then transformed into *E. coli* S17-1 competent cells. This was necessary for the conjugation into *R. sphaeroides*. In our case, since the results of the initial conjugation experiments were very insufficient, the plasmid was transformed into *E. coli* TOP10F' for amplification. After a mini-preparation of the *E. coli* TOP10F' libraries, the plasmid were transformed into *E. coli* S17-1 competent cells for conjugation once more.

Table 3: **Summary of the created libraries.** The libraries III and V were chosen for transformation, conjugation and subsequent screening.

Library	Amount of template sequence for PCR (ng)	Analyzed clones	Number of clones with mutations	Average mutations in *Pppa*	% clones without mutation
Test	30	15	1 mutation: 2 clones	**0.13**	87%
I	5	11	1 mutation: 2 clones	**0.18**	82%
II	0.5	11	3 mutations: 1 clone 1 mutation: 1 clone	**0.36**	82%
III	0.1	10	2 mutations: 1 clone 1 mutation: 3 clones	**0.4**	60%
IV	0.025	10	3 mutations: 1 clone 2 mutations: 1 clone 1 mutation: 1 clone	**0.6**	70%
V (sequential PCR)	0.5 (PCR product II)	10	4 mutations: 1 clone 2 mutations: 2 clones 1 mutation: 2 clones	**1**	50%

5.6.3 Conjugation

Transformation of *R. spaeroides* was performed via conjugative transfer of the plasmid from an *E. coli* S17-1 strain. Prior to the conjugation the *E. coli* S17-1 strain was transformed with the plasmid of interest following the standard transformation protocol (5.1.6). On the first day, 2 mL of RS102 medium were inoculated with a loop of the desired *R. sphaeroides* strain(s) in a 15 mL Greiner tube and were grown for 24 h at 30°C. On the second day, 15 mL of RÄ medium were inoculated with 100, 250 and 500 μl of the overnight culture in 250 mL flasks and were incubated for 24 h at 30°C. The *E. coli* S17-1 strain was transformed with the plasmid of interest and also grown overnight at 37°C in 10 ml LB-Kan media in Greiner tubes. On the third day, a tense, but not filamentous, *Rhodobacter* culture of 450 μl was mixed with 1 μl of *E. coli* S17-1 culture. As a negative control, one sample without *E. coli* S17-1 was cultivated. Samples were centrifuged for 5 min at 7000 rpm and resuspended with 450 μl of fresh RÄ medium. Once more the samples were centrifuged for 5 min at 7000 rpm and resuspended in 30 μL of RÄ medium. Afterwards, the 20 μl of samples were spotted on a PY plate (see 8.2.2) and incubated for 4 - 5 h at 30°C. The spots were then resuspended with a loop in 300 μL of RÄ medium. Samples were diluted 1:30 and 1:300, and 100 μl plated on RÄ agar + 3.5 μg/ml tellurite. Incubation took place for several days at 30°C.

5.6.4 Potassium tellurite as a selection reagent

For the evaluation of potassium tellurite as a potent selection marker in the design of a high-throughput screening method, several tellurite concentrations were tested. This was necessary, because the tellurite concentrations used by other research groups varied, and there was the need to optimize for the used strains and medium. Three rounds of conjugation were performed; two took place on RÄ-neomycin-agar and one on RS102-neomycin-agar. Every conjugation followed the standard protocol (Chapter 5.6.3). For conjugation, the wild type plasmid p-m-Pppa-trx-ValCO Q492K L566S-mpmii alt was used to compare signal intensities in the assay. The RÄ and RS102 plates were produced with 14 g/L agar-agar. After autoclaving the remaining ingredients were mixed, including the potassium tellurite. The potassium tellurite was pre-warmed to a temperature of 65°C. In a 50 ml Greiner tube 50 ml of media were mixed with different concentrations of potassium tellurite. In the first round concentrations of 0 μg/ml, 10 μg/ml, 50 μg/ml and 100 μg/ml potassium tellurite were used. After the interpretation of the results, concentrations were adapted and another round of conjugation took place with concentrations of 0 μg/ml, 1 μg/ml, 2.5 μg/ml, 5 μg/ml, 7.5 μg/ml and 10 μg/ml potassium tellurite. For the RS102 medium, concentrations of 50 μg/ml, 75 μg/ml, 100 μg/ml and 125 μg/ml were used.

5.6.5 Dodecane cultivation in 24-well deep well plates

The 24-well DWP cultivation was performed for selected *R. sphaeroides* strains. Cultivation took place at 28°C and 280 rpm in a shaker with an orbit of 25 mm. The plates were sealed with AeraSeal foil to ensure equal oxygen transfer. Each well was filled with a multichannel pipette with 1.2 ml

of RS102 containing 100 μg/ml neomycin. Inoculation was performed via toothpicks from LB-Kan plates. After inoculation, 250 μl of n-dodecane were added per well. Each plate contained the control strains *R. sphaeroides* #88 and #100 in triplicates. The conjugants were also measured in triplets. All strains were equally distributed over the plate. After 72 h of cultivation, the plates were centrifuged at 4000 rpm for 10 min. Subsequently, 30 μl of the n-dodecane phase was withdrawn per well and diluted in the same volume of n-dodecane. Afterwards, samples were measured via GC-FID (Chapter 5.8).

5.6.6 Dodecane cultivation in 96-well deep well plates

The 96-well DWP cultivation was performed for selected *R. sphaeroides* strains. Cultivation took place at 28°C and 320 rpm in a shaker with an orbit of 50 mm. The plates were cultivated with the metal lid for equal microaerobic conditions. Each well was filled with a multichannel pipette with 400 μl RS102 containing 100 μg/ml neomycin. Inoculation was performed via pinning with a 96-well pinning stamp from a preculture. The preculture has been started three days earlier from glycerol stocks in 300 μl of RS102 containing 100 μg/ml neomycin in 96-well deep well plates. After inoculation 100 μl of n-dodecane was added. After 72 h of cultivation the n-dodecane phase was measured via GC-FID (Chapter 5.8). Therefore, the deep well plate was centrifuged at 4000 rpm for 10 minutes. The (+)-valencene content of the *R. sphaeroides* control strains #88, #100 and the promising conjugants V8-C3 V2-F6, V4-D9, V6-D10, V6-D9, V10-G7, V2-G5, V2-D5 and V3-B5 was quantified. Each strain was measured 6 times. All strains were equally distributed over the plate.

5.6.7 Dodecane cultivation in flasks

The flask cultivation was performed for selected *R. sphaeroides* strains. Cultivation took place at 28°C and 130 rpm in a shaker with an orbit of 25 mm. Hundred ml baffled flasks (containing 4 baffles at the side) were used with an aluminum cap instead of just aluminium foil and tissue. The flasks were filled via 25 ml pipettes with 18 ml of RS102 containing 100 μg/ml neomycin. The inoculation followed with 150 μl of preculture. The preculture had been started two days earlier from glycerol stocks in 5 ml RS102 containing 100 μg/ml neomycin in 50 ml Greiner tubes. After inoculation OD600 measurement was performed to ensure a starting OD of about 0.1. The OD-measurement was followed by addition of 2 ml of n-dodecane to each flask (about 10% of total volume). After 72 h of cultivation the dodecane phase was analyzed via GC-FID (Chapter 5.8). Therefore, the volume in the flasks was transferred to 50 ml Greiner tubes and centrifuged at 4000 rpm for 10 min. The (+)-valencene content of the *R. sphaeroides* control strains #88, #100 and the promising conjugants V2-G5, V4-D9 and V10-G7 was quantified. Each strain was measured 4 times.

5.7 Biological example with *Pichia pastoris*

5.7.1 Terpenoid concentration change over time in *Pichia pastoris* constructs containing the *AOX1* promoter

For a comparison between the signal received in the screening assay for *P. pastoris* and the actual amount of compounds produced, it was necessary to perform a GC-FID analysis. To map the production curve over time, five different strains were cultivated in DWP in 250 µl/well BMGY for 48 h. The strains were picked from YPD plates with toothpicks. At 48 h the first induction was performed with 250 µl/well BMMY containing 2% methanol (final methanol concentration of 1% per well) and 100 µl of n-dodecane were added per well. After 48 h every 12 h the samples of one DWP were drawn and the remaining plates were induced with 50 µl/well BMMY to reach overall methanol concentration per well of 1%. After the first induction the measurements were continued for 72 h. Overall, 6 time points were analyzed. Each time point consisted of one 96-well deep well plate containing 4 replicates of each five strains plus negative controls distributed over the whole plate. Before drawing the samples 50 µl of n-dodecane were added per well and centrifugation at 4000 rpm, 20 °C for 10 min followed. Subsequently, 50 µl of dodecane phase were withdrawn, transferred into GC-vials, sealed and stored at -20°C until GC-FID analysis two days later. The selected strains were *Pichia pastoris* CBS7435 (WT), ValS, HCV, HCVA, HCVA/tHMG. [20]

5.7.2 Screening for different *AOX1* strains

The results of the GC-FID measurement of the *AOX1* strains was the basis for the screening. As in the GC-FID measurement, a DWP was used with 250 µl/well BMGY, that were inoculated with colonies from YPD plates. Every sample was measured 10 times. The DWPs were incubated for 48 h in the 28°C temperature controlled room at 320 rpm. After 48 h, the first induction took place by adding 250 µl/well BMMY containing 2% methanol (final methanol concentration of 1% per well), and incubation was continued. After 60 h the second induction was performed with 50 µl/well BMMY and 10% methanol (final methanol concentration of 1% per well). The screening film was pre-heated for 45 min at 100°C right before the screening. For the screening, the DWP was transferred to the CERTOMAT BS-1 shaker with an orbit of 50 mm at 320 rpm and 28°C. During the positioning of the screening film the plastic lid was replaced by a metal lid. At 62 h of cultivation time the screening procedure was started at a humidity of 46%. After 5 h (time point: 67 h), the screening was stopped at a humidity of 39%. Subsequently, the film was scanned.

5.7.3 *P. pastoris* electrocompetent cells

First, precultures were started by inoculating 5 mL of BMGY media with a single colony and incubating at 28°C and 100 rpm for 48 h. Then, 50 mL of BMGY media were inoculated to a start OD600 of 0.2 and were cultivated for about 4 h at 28°C and 100 rpm to a final OD600 of 0.8-1.0. The cells were harvested by centrifugation for 5 min at 1000 rpm, the supernatant was discarded and the pellet was resuspended in 9 mL of sterile BEDS solution before adding 1 mL of 1 M DTT. The cell solution was incubated at 28°C and 100 rpm for 10 min, and then centrifuged for 5 min

at 1000 rpm. The supernatant was discarded and the pellet was resuspended in 1 mL of BEDS solution. The electrocompetent cells were stored on ice and used immediately for transformation.

5.7.4 Electrotransformation of pGAPZ A-ValC_opt_v2rc into *P. pastoris*

The plasmid to be transformed was pGAPZ A-ValC-opt-v2rc. About 1.7 μg of plasmid were linearized by adding 2 μl of the enzyme XmaJI (AvrII) and digesting at 37°C for 2 h. The reaction was stopped at 80°C for 20 min. Afterwards 6 μl (about 500 ng DNA) were transformed into 80 μl of competent *P. pastoris* cells in pre-cooled electroporation cuvettes. After incubation for 2 min on ice, the cells were pulsed with the "Pic" program for 4-6 ms at 1500 V, 200 Ω and 25 μF. Immediately after transformation, 500 μL of sterile 1 M sorbitol and 500 μl of sterile YPD were added. The cells were regenerated for 2 h at 28°C at 300 rpm shaking. Hundred μL of the cell suspension were plated onto YPD plates containing 100 μg/ml zeocin for selection. The rest of the cell suspension was centrifuged, resuspended in approximately 100 μL medium and plated as well. The plates were incubated at 28°C for 72 h.

5.7.5 Screening in hDWP for best *GAP*-transformants

A preculture was started in a DWP with 400 μl of YPD per well. Randomly, 20 transformants were picked from the transformation plate(Chapter 5.7.4)and inoculated as duplets. The second time the preculture was inoculated with 6 transformants and controls in quadruplicates. The preculture was incubated at 320 rpm in the 28°C temperature controlled room for three days. A hDWP was filled with 140 μl of YPD per well and the preculture was transferred with a 96-position pin stamp. The hDWP was sealed with the metal lid for equal oxygen distribution. Incubation was performed at 28°C, 300 rpm and a humidity between 35-40% in the kuhner shaker with an orbit of 50 mm. After 18 h, the screening was started. The film was predried at 100°C for 45 min. Humidity during the screening stayed constant in the Kuhner shaker. The screening ended after 4 h (time point: 22 h). Subsequently, the film was scanned.

5.7.6 GC-FID measurement for *GAP*-transformants

In parallel a DWP containing 450 μl YPD per well was inoculated from the same preculture as above ("5.7.5"). Subsequently, 100 μl/well of n-dodecane were added. Incubation took place in the Kuhner shaker at 28°C room and 300 rpm for 72 h. At 72 h the DWP was centrifuged at 4000 rpm, 20°C for 10 min. Forty μl n-dodecane were carefully withdrawn and placed in GC-vials for GC-FID measurement (Chapter 5.8).

5.8 GC-FID measurement

The preparation of the samples was as described previous. Terpenoid levels in the n-dodecane phases were directly quantified by GC-FID using external standards. A HP-5 column (crosslinked 5 % Ph-Me Siloxane; 10 m x 0.10 mm x 0.10 μm) on a Hewlett-Packard 6890 GC equipped with a flame ionization detector (FID) was used. Sample aliquots of 1 μL were injected in split mode (split ratio 30:1) at 250°C injector temperature and 320°C detector temperature with hydrogen as carrier gas and a flow rate set to 0.4 mL/min in constant flow mode (49 cm/s linear velocity). The oven temperature program was as follows: 100°C for 1 min, 20°C/min ramp to 250°C, and 45°C/min ramp to 280°C (0.5 min). The use of a high-speed/high-resolution column reduced the total run time to 9 min per sample, at full chromatographic resolution.[20]

6 Results and discussion

A general requirement for our screening assay was to show its practicability in an actual high/medium-throughput strain engineering example (6.3 Biological Example: *Rhodobacter sphaeroides*). The evaluation process was investigated in detail to improve the resolution of the screening assay (6.2 Evaluation Improvement). Furthermore, we decided that there were three ways for broadening the applicability of the screening assay. One way was to show that it can be used with multiple microorganisms and genetic setups (6.5 Biological Example: *Pichia pastoris* and the *AOX1* promoter, 6.4 Biological Example: *Pichia pastoris* and the GAP promoter). The second was to show that it can be used to detect a variety of substances (6.1 Compound-only Experiment). A third way was to show that the assay worked without the presence of microorganisms (6.1 Compound-only Experiment).

6.1 Compound-only experiment

The ultimate goal of this experiment was to focus on which substances create a signal in our screening assay. Therefore, the system was reduced to its simplest setup. According to our working hypothesis, the system needed a hydrophilic environment and small hydrophobic molecules that have the tendency to escape this environment. The hydrophilic environment was created by ddH_2O in excess (200 μl per well). Small hydrophobic molecules can come from several compound classes. The decision was made to use monoterpenoids, sequiterpenoids, and some aldehydes and alcohols that are used in the flavor&fragrance industry. These compounds have quite low molecular weight and the tendency to evaporate, below their intrinsic boiling point, from aqueous milieu. These compounds do not remain in the bulk mass of the liquid, because of the lack of intermolecular forces. Since it was not known which compounds would give a signal in the assay, or how strong the signal might be, we omitted the standardization of substance concentrations. The experiment followed an easy question: Does a given substance create a signal in the screening assay? The screening was performed in hDWP since they proved to have the best sealing. However, the step of actual fixing the screening film to the hDWP proved to be a critical step, that can lead to contamination of neighboring wells. Hence the used wells for this experiment were all separated from each other by at least one empty well to eliminate the possibility of diffusion/cross-contamination.

The results of these experiments looked very promising. On every plate all controls were negative. Also, it should be mentioned that the intensities were different for the three color channels for the unused assay: the red channel showed high intensity (bright), the blue and green channel showed low intensity (dark). Valencene was the compound we had the most experience with. Therefore, we used the behavior of valencene as a reference in the interpretation of the results. With increasing valencene concentration the intensity of the red channel decreased. At the same time the intensity of the green and the blue channel increased. The intensity increase was about the same in both channels.

The first plate (Figure 6) shows the behavior of trans-cinnamaldehyd, cinnamyl-alcohol, (+)-valencene, cis-nootkatol and nootkatone. Trans-cinnamaldehyde gave a medium signal intensity with an increase in red and green. The blue channel nearly did not change. The increase of the red

channel was quite unusual compared to valencene. In contrast, cinnamyl alcohol showed a decrease in red, but an increase in blue and green. Signal intensity was medium again. The trend was similar to that of valencene. Valencene created a strong signal with a decrease in red and an increase in blue and green. Valencene seems to interact quite strong with nile red. For trans-cinnamaldehyde and cinnamyl alcohol five times more volume of the compounds were used and it created a signal of about half the intensity. Trans-nootkatol did not give a signal. When bringing the trans-nootkatol in contact with the water a crystallization-like reaction was observed. Therefore, it cannot be stated that trans-nootkatol does not give a signal in the assay. It may be that nearly all molecules crystallized and thus did not evaporate. In the case of nootkatone the signal was weak, although 10 μl were used instead of 5 μl like for valencene. Red and green signal channels decreased, but blue increased.

The second plate (Figure 7) shows the behavior of (E)-nerolidol, (1R,2S,5R)-(-)-menthol, farnesol and (E)-beta-farnesene. The substance (E)-nerolidol showed a decrease of signal intensity in the red channel and an increase in the blue and green channel. The signal intensity was strong. Incubation with (1R,2S,5R)-(-)-menthol led also to a decrease of intensity in the red channel and an increase in blue and green channels. The signal intensity was as well strong. For farnesol the signal intensity was weak. Other than with valencene the red and the green channel were decreasing and only the blue channel showed an increase. In comparison with farnesol (E)-beta-farnesene showed a strong signal. As with valencene the green and blue channel increased and the red channel decreased. The wells around (E)-beta-farnesene were also contaminated, because the clouds of this substance were pressed into these wells when the screening film was applied. The different behavior of (E)-beta-farnesene compared to farnesol may be explained by the different polarity of the compounds.

The third plate (Figure 8) shows the behavior of methanol, (1S)-(-)-beta-pinene, (S)-(+)carvone and linalool. The 200 μl of methanol created a strong signal with a decrease of red channel and an increase of blue and green channels. This is expected, since methanol is used as a solvent. But this result does not necessarily mean that experiments that use in any kind methanol are not suitable for the assay. How to circumvent methanol attributing to the screening signal is described in another chapter (Chapter 5.7.2 Screening for different *AOX1* strains). (1S)-(-)-beta-pinene showed a strong signal which was similar to valencene samples. Red channel intensity decreased while blue and green channel intensity increased. Incubation with (S)-(+)-carvone showed a signal similar to a valencene signal. The red channel intensity decreased and blue and green channel increased. The same pattern was obtained for linalool intensity decreased as well in red channel, but pixel values in the green and blue channel were elevated.

Table 4: **Compounds, concentration and signal intensity in the compound-only experiment.** Fresenius water and ethanol were used as negative controls. Ethanol was used as a solvent for nootkatol, menthol and piperonal.

Compound	Incubation conditions	Signal intensity
Aqua bidestilled Fresenius (ddH_2O) Fresenius Kabi Austria	200 μl ddH_2O	-
Ethanol absolut AnalaR NORMAPUR Purity: 99.9% VWR Chemicals	200 μl ddH_2O + 5 μl or 25 μl (Figure 9) Compound	-
trans-Cinnamaldehyde Purity: 99% Sigma Aldrich (C80687)	200 μl ddH_2O + 25 μl Compound	++
Cinnamyl alcohol Purity: 98% Sigma Aldrich (108197)	200 μl ddH_2O + 25 μl Compound	++
Valencene Purity: 70% Isobionics	200 μl ddH_2O + 5 μl Compound	+++
cis-Nootkatol Purity: 98% Isobionics	200 μl ddH_2O + 5 μl Solution (dissolved in Ethanol absolute; 3,05 M)	-
Nootkatone Purity: 70-80% Isobionics	200 μl ddH_2O + 10 μl Compound	+
(E)-Nerolidol Purity: 97.2% DSM Nutritional Products (LJ 32808B049)	200 μl ddH_2O + 5 μl Compound	+++
(1R,2S,5R)-(-)-Menthol Purity: >99% DSM Nutritional Products (Fluka 63660)	200 μl ddH_2O + 5 μl Solution (dissolved in Ethanol absolute; 1,66 M)	+++
Farnesol Purity: $\geq$95% Sigma Aldrich (43348)	200 μl ddH_2O + 5 μl Compound	+
(E)-beta-Farnesene Purity: - Bedoukian Research	200 μl ddH_2O + 5 μl Compound	+++
Methanol Purity: 99.9% Carl Roth (7342.1)	200 μl Compound	+++
(1S)-(-)-beta-Pinene Purity: -	200 μl ddH_2O + 5 μl Compound	+++

Table 5: **Compounds, concentration and signal intensity in the compound-only experiment.** Fresenius water and ethanol were used as negative controls. Ethanol was used as a solvent for nootkatol, menthol and piperonal.

Compound	Incubation conditions	Signal intensity
(S)-(+)-Carvone Purity: 96% Sigma Aldrich (435759)	200 μl ddH_2O + 5 μl Compound	+++
Linalool Purity: 97% Acros Organics (125151000)	200 μl ddH_2O + 5 μl Compound	+++
Myrcene Purity: $\geq$90%	200 μl ddH_2O + 5 μl Compound	+++
Piperonal Purity: 99% Sigma Aldrich (P49104)	200 μl ddH_2O + 25 μl Solution (dissolved in Ethanol absolut; 0,75 M)	++
(S)-(-)-Limonene Purity: 96% Sigma Aldrich (218367)	200 μl ddH_2O + 5 μl Compound	+++

The fourth plate (Figure 9) shows the behavior of myrcene, piperonal, (S)-(-)-limonene. All three compounds showed a valencene-like result. Signals increased in the blue and green channel while a decrease in the red channel for myrcene, piperonal, (S)-(-)-limonene was observed. Myrcene caused massive contamination, which became visible just after fixing the screening film. This experiment showed that from 16 different compounds that were tested, 15 gave a positive signal on the screening film (Table 4, Table 5). The negative controls used on every plate were always negative. When valencene was taken as a reference, it was concluded that not all tested substances behaved the same way when interacting with the screening film. These results indicated that different color changes might occur by screening for different compounds particularly when observing the red, blue and green channels. This unexpected and remarkable fact may be of special interest for the future studies. With this screening assay one may differentiate between different compounds. Potentially it may be achievable in one single well. And not only valencene can be detected, but a variety of volatile compounds could be detected as well. The obtained results also prove that the screening assay might be used for non-biotechnological applications such as special medical compound detection and environmental assays for greenhouse gases.

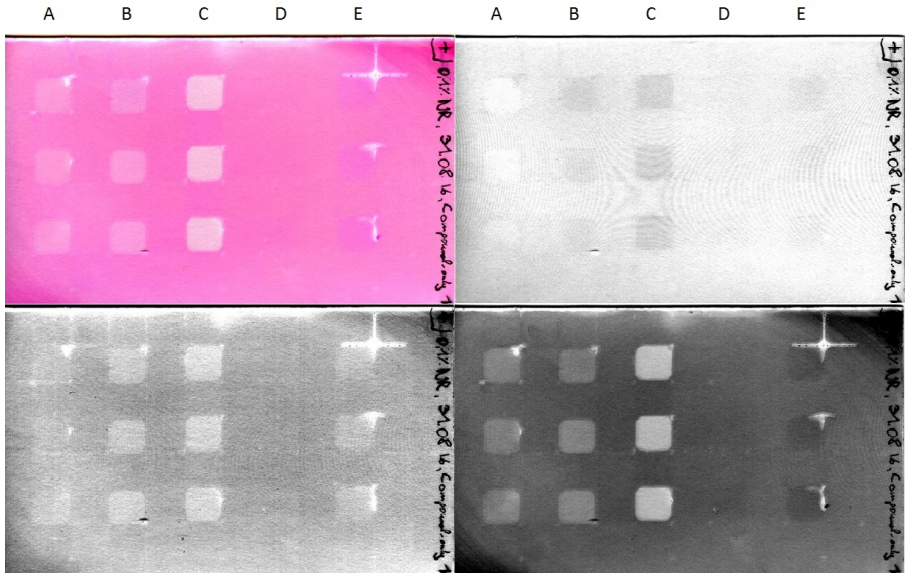

Figure 6: **Plate 1: Measurement of trans-cinnamaldehyd (A), cinnamyl alcohol (B), valencene (C), cis-nootkatol (D), nootkatone (E).** Single column contains triplicates of the compound. As controls ddH_2O and ddH_2O plus ethanol were applied and remained negative. Left Top: RGB picture; Right Top: Red channel; Left Bottom: Blue channel; Right Bottom: Green channel. Detailed information about the compounds in Table 4, 5.

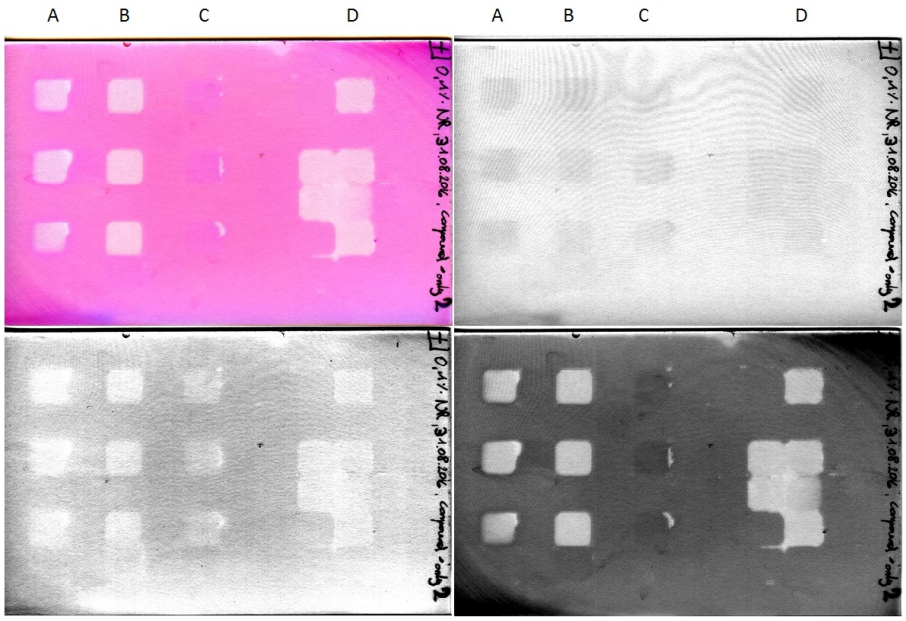

Figure 7: **Plate 2: Measurement of (E)-nerolidol (A), (1R,2S,5R)-(-)-menthol (B), farnesol (C), (E)-beta -farnesene (D).** Legend see Figure 6.

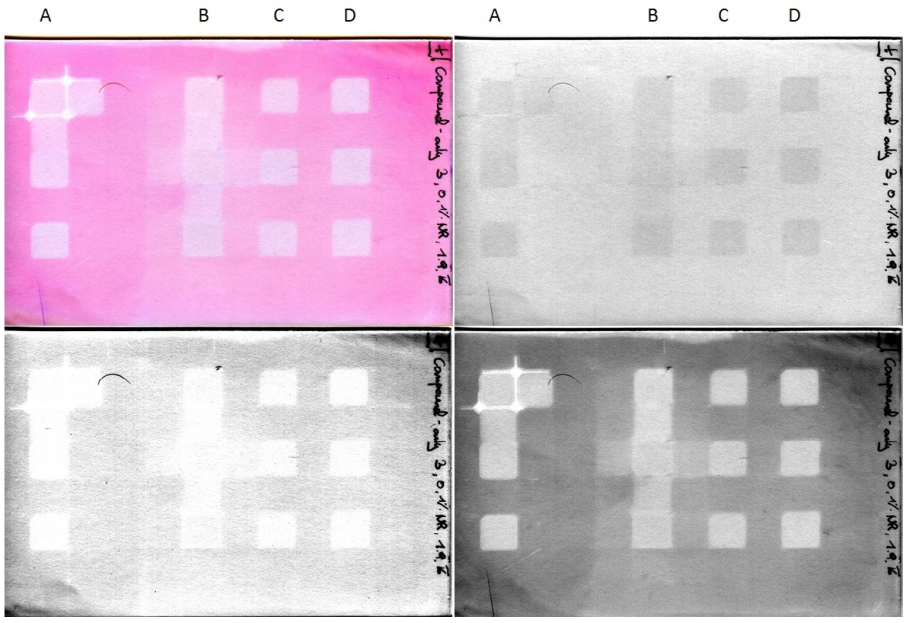

Figure 8: **Plate 3: Measurement of methanol (A), (1S)-(-)-beta -pinene (B), (S)-(+)-carvone (C), linalool (D).** Legend see Figure 6.

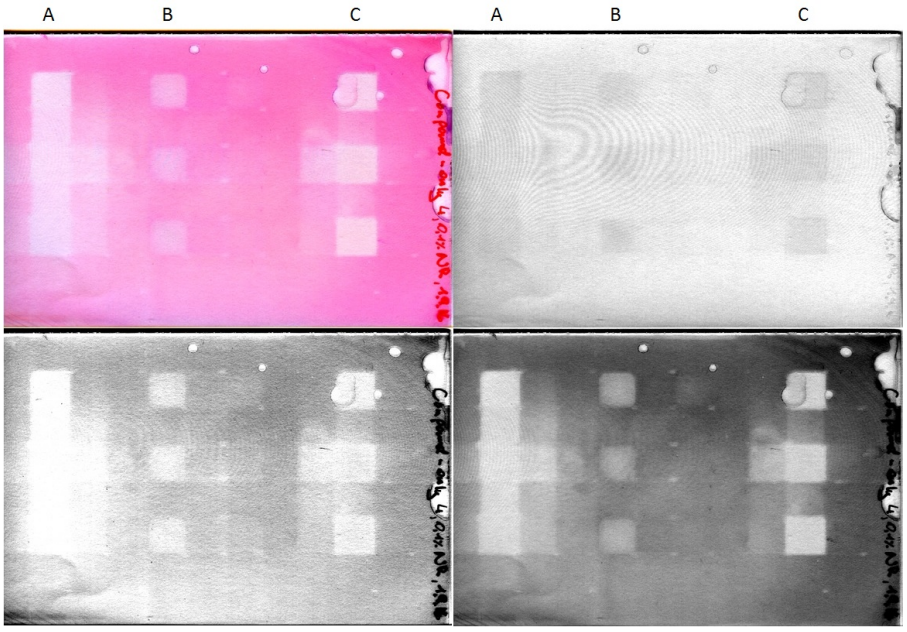

Figure 9: **Plate 4: Measurement of myrcene (A), piperonal (B), (S)-(-)-limonene (C).** Legend see Figure 6.

6.2 Evaluation improvement

The improvement of the screening assay offered two different approaches for optimization. On the one hand, there is a lot of chemical engineering that can be done to increase the resolution of the screening assay. On the other hand, we did not fully understand the bioinformatical approach to evaluate our samples. This chapter focuses on the improvement of the evaluation method.

In this evaluation method the RGB color space was used. In general, RGB color space states that every pixel consists of the three colors red, green and blue. These three colors are mixed with each other in different amounts so that every color that is visible for the human eye can be created. Each three colors can be assigned a value between 0 and 255. For example if red = 255, blue = 0 and green =0, one sees a strong red color. Brightness and darkness are regulated by the size of these values. If the value for red would be 40 and blue and green are 0, the red would be dark. If all the colors have the same value, then the observed image color would be white. If all the colors have a value of 0, then the image would be completely dark. The higher all values get, the brighter the picture would be. A transformation into a black and white image could be done by averaging the three values. This is the basic concept of our evaluation method.

With this information it was possible to take a two dimensional image of the screening film that has an x-axis (length) and a y-axis (width) and add a third dimension to every pixel in the image (Figure 10). The third dimension is the pixel value for each pixel (average of the three values or one single color value). The RGB surface plot showed that average value for pixels increased for developed wells. Additionally the developed wells changed color from red to white. As explained previously white means that all three colors have the same value. The representative example (Figure 10) shows an RGB image that also showed a successful RGB channel evaluation.

A general requirement for the development of the screening assay was an optical readout. Next to this requirement, an easy setup should be possible without expensive equipment. The use of a flat bed scanner combined these two requirements. As an output, this device creates an RGB image. Different file formats are available for this image type, but only the .tiff-file format saves the images without data compression and data loss. The tiff-format is the highest image standard used for printing. Therefore, we do not suggest to change the image format. The scanning resolution was set to 300 dpi (dots per inch). Later it was increased in the following stages of the project to 600 dpi. By doubling the resolution small improvements in image quality were seen. The interference effect may become a little bit weaker and the additional data storage space was manageable due to low cost of hard drives. Statistical significance can be improved through resolution increase, since the pixel measured per well changes by a factor of four, if the resolution is doubled. For the evaluation and depiction of data the integrated density was used. The integrated density uses the mean gray value of a certain region (one well) and multiplies it with the area of interest (inch x inch). This methods creates values that are positive numbers under 10 for our setup. For example at 300 dpi a 60x60 pixel square fits one well. If 300 pixels are 1 inch, then 60 pixels are 0.2 inch. The square will therefore, have an area of (0.2 x 0.2) 0.04 inch^2. Therefore the mean gray value is multiplied by factor of 0.04 to generate the integrated density. Another approach generates exactly

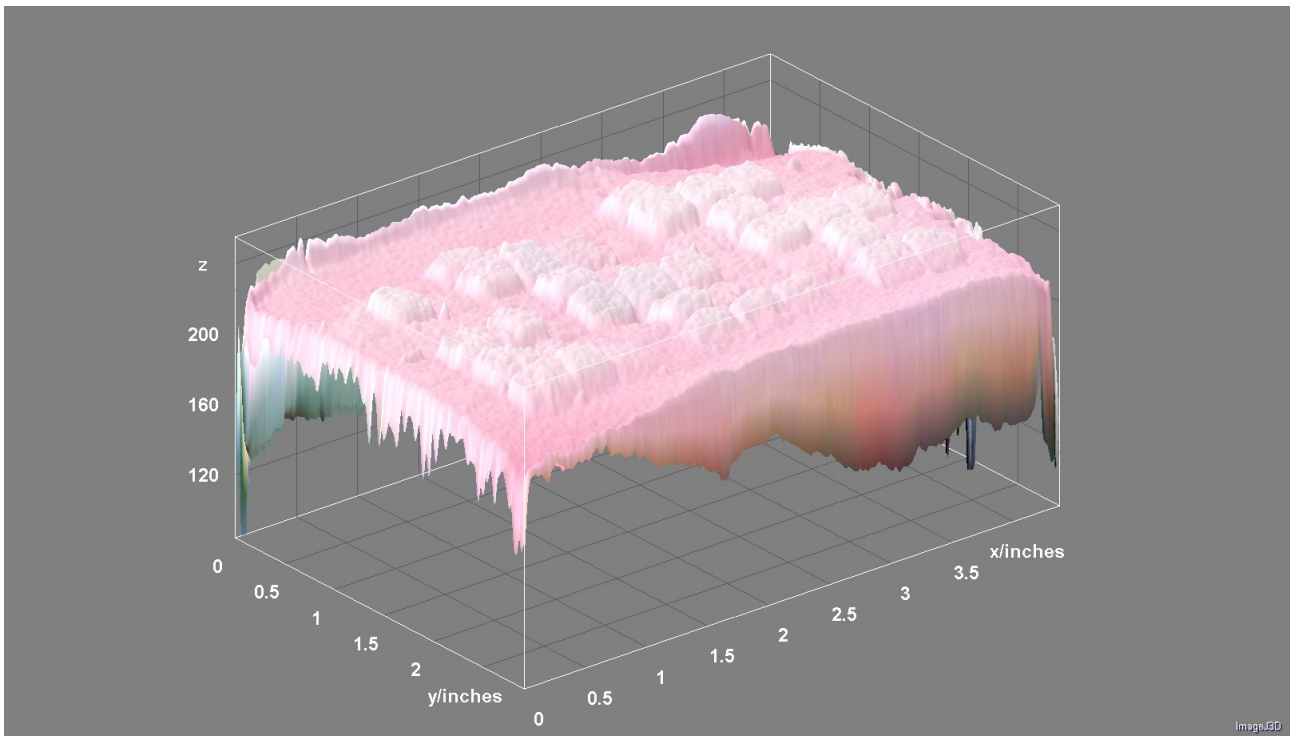

Figure 10: **Surface plot of a screening film.** The x-axis and y-axis show the two dimensional scan of the screening plate in inches. The two dimensional image was supplemented by a third dimension. This third dimension represents the pixel value for each pixel. These values vary between 0 and 255. This representation shows the RGB channel of GAP transformants rescreening (Figure 44). This RGB image was also successfully evaluated.

the same results, but changes the x-axis scale, is using just the mean gray value. It turned out that behind the term "Mean" in the result table in ImageJ the mean gray value of a certain area was hidden. It is the mean of all pixel values in a marked region and can vary between 0 and 255, because every single pixel value is described in this range. The change in mean gray value is the change that is seen between an developed and an undeveloped well. In this work, most of the graphs are depicted with the integrated density on the y-axis. Another critical point was the color balance.

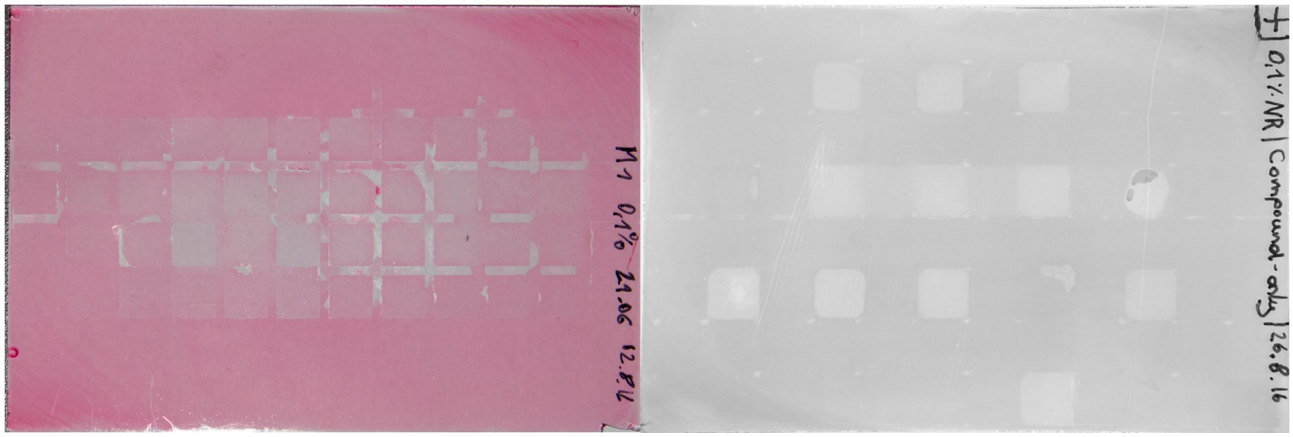

Figure 11: **Alternative devices.** Left: DSLR image. Right: G:BOX (Syngene) image.

Color balance is an adjustment affecting the whole image in which the intensities of the three colors are balanced. Especially, it focuses on the adjustment of neutral colors. For example that white

looks really like white in an image and not like there is a red hue mixed in it. Often, white pixels are used as an anchor in the image and all the other colorful pixels are rearranged around this value. In this project, an average end customer scanner - HP Scanjet 4370 - was used. These kind of scanners often use an automatic function to do the color balance (automatic white balance, AWB). However, in order to perform a densitometric analysis with stable results it is important to disable the AWB. Otherwise, each scanned screening film might have differently rearranged pixel intensities. The HP Scanjet 4370 did not have any options to clearly disable AWB, yet we disabled all color, dust and "Moire effect" correction options. More sophisticated scanners should have white balance options. Furthermore, there should also be a calibration option, to detect exposure differences over the scanned area and to suppress these variances via a calibration profile. This option was also not available for us.

A complete different approach to improve the evaluation was the change of platform from scanner to high-level DSLR and lense equipment (Figure 11). Although the resolution increased, the color depth decreased and the image evaluation failed. This problem has also been discussed in an article for library archives.[21] The scanner created a more saturated image with more differences in color change. A possible explanation could be that the distance between sensor and screening film is shorter, therefore less light is scattered and more information is captured.

Another platform change was a switch to the G:Box from Syngene (Figure 11). Although the images seemed solid with this device, the G:Box lacked a Bayer filter to create RGB images. This is a disadvantage compared to the scanner, because the blue, green and red color channels can be used for signal improvement. Since fluorescence measurements are usually very sensitive this might be an alternative for the future with the right detection device.

In the future it might be possible to change the production process of the screening assay. Maybe the carrier material can be changed from glass to one-way plastic or the whole system might change to limber foils or paper. Paper might also be printed and coupled with a dye like described by Große et al..[22]

6.2.1 Approach 1: RGB color evaluation

During the first stage of the screening development the RGB color evaluation was performed (Figure 12). An RGB image was created by scanning the screening film. The scanning resolution was usually 300 dpi. A densitometric analysis was performed by measuring the overall pixel values and integrating them over the area of interest (one well: 60x60 pixels at 300 dpi). The results of using this method varied quite strongly. In some cases this approach worked well. In other cases the evaluation failed, although signals were visible (Figure 12). In the last example, clear signals were recognizable by the human eye. In the contrary, the image evaluation did not show differences in the integrated density between the wells. This can be seen in the table and the diagram (Figure 12). Standard deviations of the graph were also quite high.

A possible explanation for this phenomenon could be the splitting of the color channels. The first hypothesis was that the color of nile red is seen as red in the film and loses its color when exposed to hydrophobic compounds. Color channel splitting revealed that the red, green and blue channel

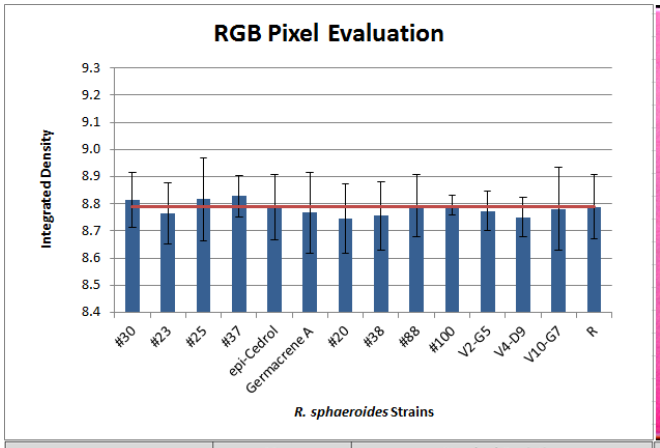

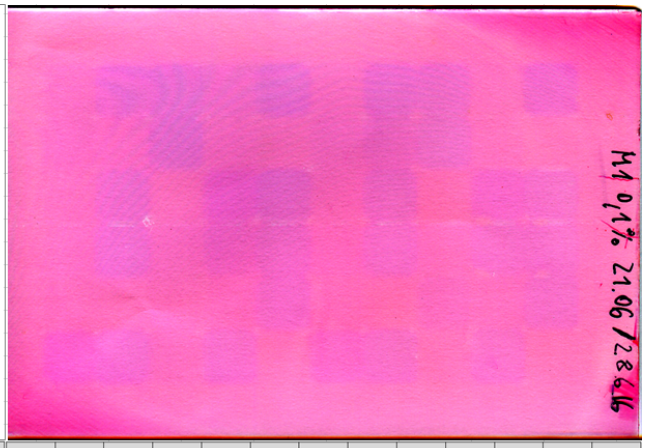

	Mean	Standard Deviation
#30	8.814	0.101
#23	8.765	0.112
#25	8.817	0.153
#37	8.828	0.077
epi-Cedrol	8.786	0.120
Germacrene A	8.767	0.148
#20	8.745	0.127
#38	8.756	0.126
#88	8.793	0.116
#100	8.794	0.036
V2-G5	8.774	0.072
V4-D9	8.751	0.072
V10-G7	8.781	0.152
R	8.789	0.118

	1	2	3	4	5	6	7	8	9	10	11	12
A	-	-	-	-	-	-	-	-	-	-	-	-
B	-	#30	#20	V2-G5	#37	#100	#30	#20	V2-G5	#37	#100	-
C	-	#23	#38	V4-D9	epi-Cedrol	R	#23	#38	V4-D9	epi-Cedrol	R	-
D	-	#25	#88	R	Germacrene A	V10-G7	#25	#88	R	Germacrene A	V10-G7	-
E	-	#37	#100	#30	#20	V2-G5	#37	#100	#30	#20	V2-G5	-
F	-	epi-Cedrol	R	#23	#38	V4-D9	epi-Cedrol	R	#23	#38	V4-D9	-
G	-	Germacrene A	V10-G7	#25	#88	R	Germacrene A	V10-G7	#25	#88	R	-
H	-	-	-	-	-	-	-	-	-	-	-	-

Figure 12: **RGB pixel evaluation.** Left Top: Diagram showing the mean integrated density for all measured strains; Right Top: Scanned RGB image of the screening film; Left Bottom: Results of the densitometric measurement applied on the scanned RGB image. Every strain was measured 4 times; Right Bottom: Distribution of strains in the DWP and on the screening film.

did not behave in the same way. The red channel image changed by decoloring. Concomitantly, the green and blue channel pixel values increased. In the next chapter the advantages of channel splitting and possible approaches to circumvent this problem will be discussed (6.2.2 Approach 2: Single color channel evaluation). In this case, it was observed that RGB evaluation sometimes fails, because the color reduction in the red channel is compensated by an increase of blue and green pixel values. Although pixel values change the overall sum of all channels stays the same. And the overall sum of pixel values of the three color channel is the measured value by the RGB screening evaluation.

One improvement for the RGB pixel evaluation contributed the "Subtract Background" function (Figure 13). The "Subtract Background" function is based on the concept of the "rolling ball" algorithm and aims to remove smooth continuous backgrounds/uneven illuminated backgrounds in images. A 2D picture was added by a third dimension (height), which was the value of each pixel over the whole image (see Figure 10). The working principle of this algorithm can be imagined as a ball with a fixed radius (in pixel), that is rolling over the bottom side of this surface. The background to be subtracted is the hull of the volume reachable by the ball. The ball radius should be set to at least the size of the largest object that is not part of the background for each pixel. [23] This method has been used on some images in the earlier phase of the project. The best results were achieved with a radius of 50 pixels, although the largest object we measured was at least 60 pixels.

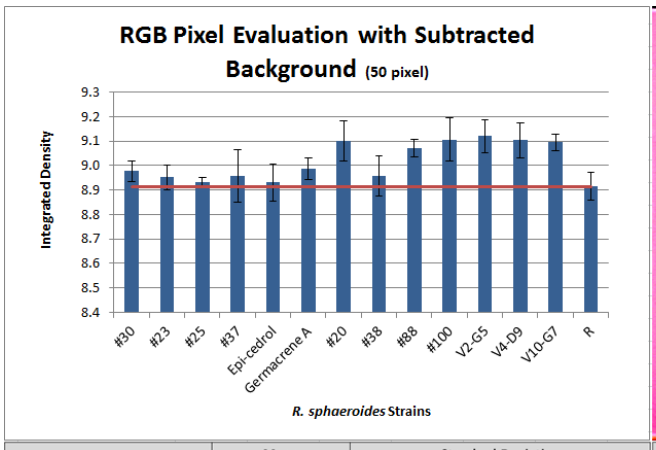

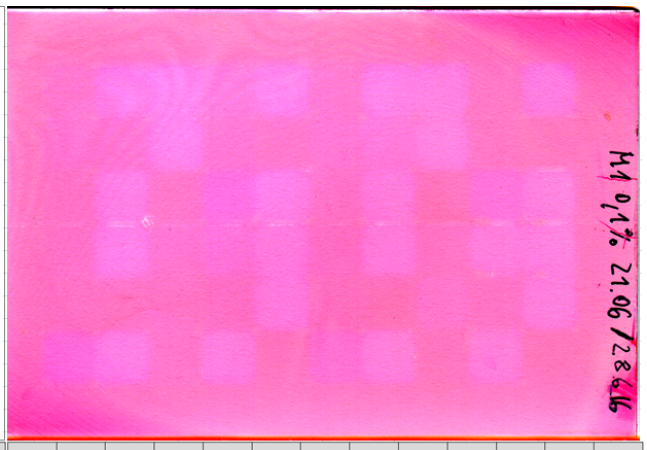

	Mean	Standard Deviation
#30	8.978	0.043
#23	8.952	0.052
#25	8.932	0.019
#37	8.959	0.107
epi-Cedrol	8.931	0.075
Germacrene A	8.987	0.044
#20	9.100	0.081
#38	8.957	0.081
#88	9.071	0.034
#100	9.106	0.088
V2-G5	9.121	0.068
V4-D9	9.104	0.073
V10-G7	9.095	0.032
R	8.914	0.057

	1	2	3	4	5	6	7	8	9	10	11	12
A	-	-	-	-	-	-	-	-	-	-	-	-
B	-	#30	#20	V2-G5	#37	#100	#30	#20	V2-G5	#37	#100	-
C	-	#23	#38	V4-D9	epi-Cedrol	R	#23	#38	V4-D9	epi-Cedrol	R	-
D	-	#25	#88	R	Germacrene A	V10-G7	#25	#88	R	Germacrene A	V10-G7	-
E	-	#37	#100	#30	#20	V2-G5	#37	#100	#30	#20	V2-G5	-
F	-	epi-Cedrol	R	#23	#38	V4-D9	epi-Cedrol	R	#23	#38	V4-D9	-
G	-	Germacrene A	V10-G7	#25	#88	R	Germacrene A	V10-G7	#25	#88	R	-
H	-	-	-	-	-	-	-	-	-	-	-	-

Figure 13: **RGB pixel evaluation with subtracted background.** Left Top: Diagram showing the mean integrated density for all measured strains after applying the Subtract Background function with 50 pixels; Right Top: Scanned RGB image of the screening film with applied Subtract Background function with 50 pixels; Left Bottom: Results of the densitometric measurement applied on the scanned RGB image with Subtract Background function at 50 pixels. Every strain was assessed 4 times; Right Bottom: Distribution of strains in the DWP and on the screening film.

We also realized that interference effects vanished above a certain radius. The evaluation without the subtracted background (Figure 12) did not show any difference between the production levels of (+)-valencene. By using the "Subtract Background" function with a radius of 50 pixels (Figure 13) the results changed. Now the relation between the strains looked like expected from the GC results. Although the "Subtract Background" function led to improved results, the algorithm changes the image in a non-linear way, which meant that each pixel was not changed by the same factor and the following evaluation was therefore biased. Generally speaking, this function does not change every scanned film the same way and, therefore, it does not lead to reproducible results. This is a clear disadvantage and forced us to search for new evaluation approaches.

6.2.2 Approach 2: single color channel evaluation

Since the RGB evaluation showed some disadvantages, two other approaches were developed. By splitting the color channels of the RGB image, we showed that there were additional changes in the blue and the green color space. When the film was incubated for example with (+)-valencene, the intensity of red signal decreased over time. In the meantime the intensity of green and blue signals increased over time. That result was observed upon increasing amount of (+)-valencene over time. As a result of this observation we wondered whether this approach could be used for improved evaluation. Therefore all three color channels were analyzed separately. The images from three different color channel (Figure 16, 15, 14) originate all from the same screening film that was also used for the RGB evaluation (Figures 12, 13). The "Subtract Background" function was not applied on images, since it would create a drift. The different color channels represented light at different wavelengths in the range of visible light.

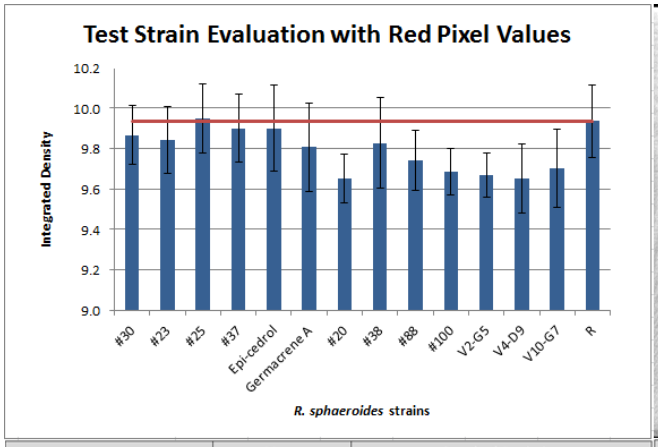

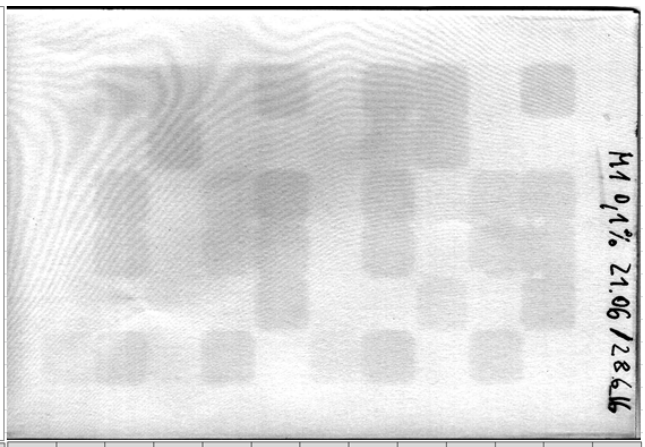

	Mean	Standard Deviation
#30	9.867	0.145
#23	9.843	0.165
#25	9.949	0.171
#37	9.900	0.169
epi-Cedrol	9.900	0.212
Germacrene A	9.806	0.219
#20	9.651	0.119
#38	9.828	0.223
#88	9.743	0.150
#100	9.685	0.115
V2-G5	9.668	0.110
V4-D9	9.654	0.170
V10-G7	9.701	0.195
R	9.935	0.178

	1	2	3	4	5	6	7	8	9	10	11	12
A	-	-	-	-	-	-	-	-	-	-	-	-
B	-	#30	#20	V2-G5	#37	#100	#30	#20	V2-G5	#37	#100	-
C	-	#23	#38	V4-D9	epi-Cedrol	R	#23	#38	V4-D9	epi-Cedrol	R	-
D	-	#25	#88	R	Germacrene A	V10-G7	#25	#88	R	Germacrene A	V10-G7	-
E	-	#37	#100	#30	#20	V2-G5	#37	#100	#30	#20	V2-G5	-
F	-	epi-Cedrol	R	#23	#38	V4-D9	epi-Cedrol	R	#23	#38	V4-D9	-
G	-	Germacrene A	V10-G7	#25	#88	R	Germacrene A	V10-G7	#25	#88	R	-
H	-	-	-	-	-	-	-	-	-	-	-	-

Figure 14: **Red color channel evaluation.** Left Top: Diagram shows the mean integrated density for all measured strains in the red color channel; Right Top: Red color channel image of the screening film; Left Bottom: Results of the densitometric measurement. Every strain was measured 4 times; Right Bottom: Distribution of strains in the DWP and on the screening film.

For the red color channel the results are inverted as compared to the blue, green and RGB images (Figure 14). Since the red color was eventually fading, the intensity in the red color channel was expected to decrease. In other words, the more (+)-valencene was produced, the lower the integrated density in this channel. A comparison of the mean integrated densities in the diagram showed that values - relative to each other - behave like expected. But the standard deviation was high and the interference effect was very dominant in this channel. Although the trend of the mean values

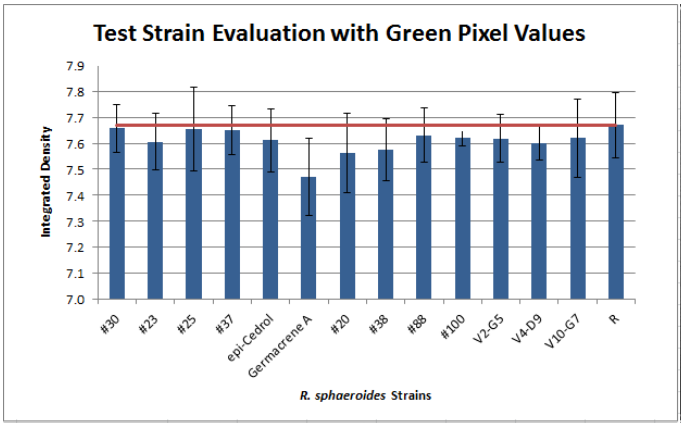

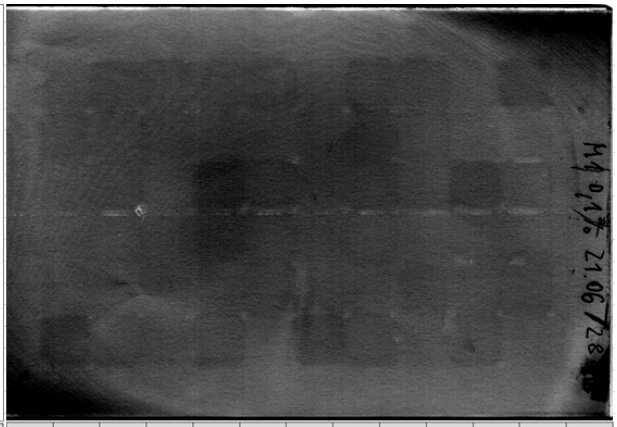

	Mean	Standard Deviation
#30	7.657	0.092
#23	7.605	0.109
#25	7.656	0.160
#37	7.649	0.093
epi-Cedrol	7.611	0.122
Germacrene A	7.471	0.147
#20	7.563	0.152
#38	7.577	0.119
#88	7.631	0.106
#100	7.619	0.031
V2-G5	7.618	0.091
V4-D9	7.601	0.064
V10-G7	7.620	0.150
R	7.669	0.124

	1	2	3	4	5	6	7	8	9	10	11	12
A	-	-	-	-	-	-	-	-	-	-	-	-
B	-	#30	#20	V2-G5	#37	#100	#30	#20	V2-G5	#37	#100	-
C	-	#23	#38	V4-D9	epi-Cedrol	R	#23	#38	V4-D9	epi-Cedrol	R	-
D	-	#25	#88	R	Germacrene A	V10-G7	#25	#88	R	Germacrene A	V10-G7	-
E	-	#37	#100	#30	#20	V2-G5	#37	#100	#30	#20	V2-G5	-
F	-	epi-Cedrol	R	#23	#38	V4-D9	epi-Cedrol	R	#23	#38	V4-D9	-
G	-	Germacrene A	V10-G7	#25	#88	R	Germacrene A	V10-G7	#25	#88	R	-
H	-	-	-	-	-	-	-	-	-	-	-	-

Figure 15: **Green color channel evaluation.** Left Top: Diagram shows the mean integrated density for all measured strains in the green color channel; Right Top: Green color channel image of the screening film; Left Bottom: Results of the densitometric measurement. Every strain was measured 4 times; Right Bottom: Distribution of strains in the DWP and on the screening film.

matched the expectations, it was hard to make conclusions because of the high standard deviations. Furthermore, it should be noted that the interference effect (see 6.2.4) has been always the strongest in the red channel. The screening film is mainly of red color and, therefore, the strongest interference effects were observed with this color channel causing constructive and destructive areas. The green color channel showed positive signals, since the green pixel values were increasing the more (+)-valencene was present. This has been a general observation during this project. However, the green color channel (Figure 15) was not suitable for evaluation. It showed even a decrease in intensity. In other experiments, the green color channel looked promising, but this might also depend on incubation time or (+)-valencene amount. In general this channel behaves in an unexpected way. Sometimes the signal evaluation was the best of all three channels, other times it was not possible to gather information about the (+)-valencene production. Another reason that makes the green channel interesting is that the interference effect was weak compared to the red channel.

The blue color channel again gave positive values. The general observation was that the pixel values for blue channel increased over time. However the blue channel evaluation (Figure 16) showed the expected correlation between the strains with quite low standard deviations. Additionally the interference effect was weak in the blue channel. This channel seemed to be stable and suitable for our evaluation procedure to measure the different production levels of (+)-valencene. Therefore, most of the experiments on this project were analyzed in the blue channel. After we had found out the reason causing the interference effect, we were also able to eliminate it's consequences. The

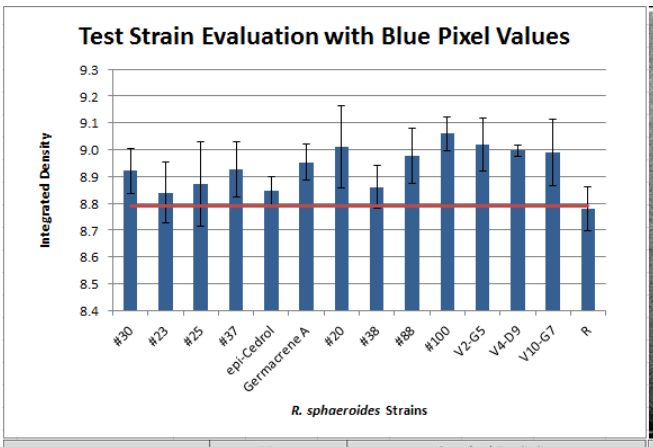

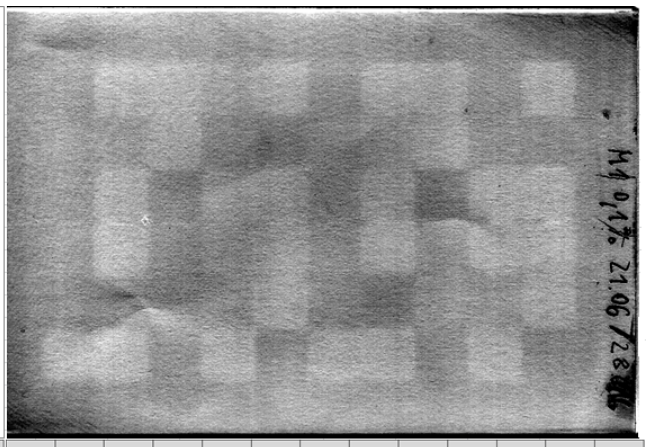

	Mean	Standard Deviation
#30	8.921	0.085
#23	8.840	0.114
#25	8.873	0.158
#37	8.928	0.104
epi-Cedrol	8.845	0.054
Germacrene A	8.953	0.067
#20	9.011	0.155
#38	8.862	0.080
#88	8.976	0.103
#100	9.059	0.063
V2-G5	9.019	0.097
V4-D9	8.997	0.021
V10-G7	8.990	0.124
R	8.780	0.081

	1	2	3	4	5	6	7	8	9	10	11	12
A	-	-	-	-	-	-	-	-	-	-	-	-
B	-	#30	#20	V2-G5	#37	#100	#30	#20	V2-G5	#37	#100	-
C	-	#23	#38	V4-D9	epi-Cedrol	R	#23	#38	V4-D9	epi-Cedrol	R	-
D	-	#25	#88	R	Germacrene A	V10-G7	#25	#88	R	Germacrene A	V10-G7	-
E	-	#37	#100	#30	#20	V2-G5	#37	#100	#30	#20	V2-G5	-
F	-	epi-Cedrol	R	#23	#38	V4-D9	epi-Cedrol	R	#23	#38	V4-D9	-
G	-	Germacrene A	V10-G7	#25	#88	R	Germacrene A	V10-G7	#25	#88	R	-
H	-	-	-	-	-	-	-	-	-	-	-	-

Figure 16: **Blue color channel evaluation.** Left Top: Diagram shows the mean integrated density for all measured strains in the blue color channel; Right Top: Blue color channel image of the screening film; Left Bottom: Results of the densitometric measurement. Every strain was measured 4 times; Right Bottom: Distribution of strains in the DWP and on the screening film.

rescreening of the *P. pastoris* transformants did not show an interference effect due to the plastic foil between scanner and glass plate (Figure 17). Avoiding the interference effect was necessary to reduce possible background noise in the image.

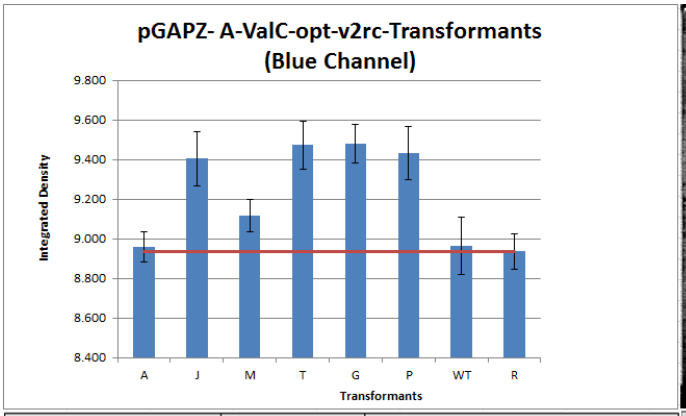

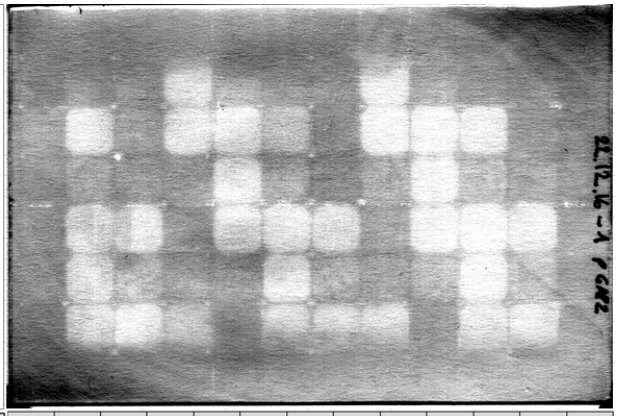

	Mean	Standard Deviation
A	8.962	0.076
J	9.406	0.138
M	9.118	0.082
T	9.475	0.120
G	9.480	0.097
P	9.435	0.134
WT	8.965	0.143
R	8.936	0.088

	1	2	3	4	5	6	7	8	9	10	11	12
A	-	-	-	-	-	-	-	-	-	-	-	-
B	-	A	WT	G	M	A	WT	G	M	A	WT	-
C	-	J	R	P	T	J	R	P	T	J	R	-
D	-	M	A	WT	G	M	A	WT	G	M	A	-
E	-	T	J	R	P	T	J	R	P	T	J	-
F	-	G	M	A	WT	G	M	A	WT	G	M	-
G	-	P	T	J	R	P	T	J	R	P	T	-
H	-	-	-	-	-	-	-	-	-	-	-	-

Figure 17: **Blue color channel evaluation for *P. pastoris*.** Left Top: Diagram shows the mean integrated density for measured *P. pastoris* transformants in the blue color channel; Right Top: Blue color channel image of the screening film; Left Bottom: Results of the densitometric measurement. Every strain was measured 4 times; Right Bottom: Distribution of strains in the DWP and on the screening film.

6.2.3 Approach 3: subtracting the picture of the unscreened film from the developed film

The approach of subtracting the image before from the image after the screening can also improve our evaluation process, hence all of the noise before the screening (concentration gradient, moisture gradient, etc...) and during the scanning (light/exposure gradient, etc.) would be subtracted in theory. Only the changes between the beginning and end of screening would remain in the picture and would constitute the ideal screening readout.

To achieve that a film was first scanned at t0, i.e. between the 45 min, 100 °C predrying and the screening. After the screening, the film was scanned again (Figure 18). These two images were then subtracted from each other via the image calculator in ImageJ. The image in this example showed turquoise wells, when (+)-valencene was produced. If necessary the pixel values can be multiplied by a factor of choice for creating a brighter image, which would be better recognized by the human eye. In some cases, this was necessary to apply the grid in ImageJ for densitometric measurement. This multiplication is a linear procedure for every pixel, but it was important not to saturate the pixels. If some of the pixels became saturated (pixels would reach values over 255) the process would get non-linear.

Comparing the blue channel evaluation (Figure 17) and the image subtraction evaluation (Figure 18) the results seemed similar. In the blue channel evaluation the standard deviation for the wild type strain was higher, but the mean value was more comparable to the media. In the case of the image subtraction the wild type strain had a trend to give a stronger signal than the media.

The image subtraction was also a suitable evaluation process. Maybe, this process will become even more important, when working on the chemical engineering of the screening film.

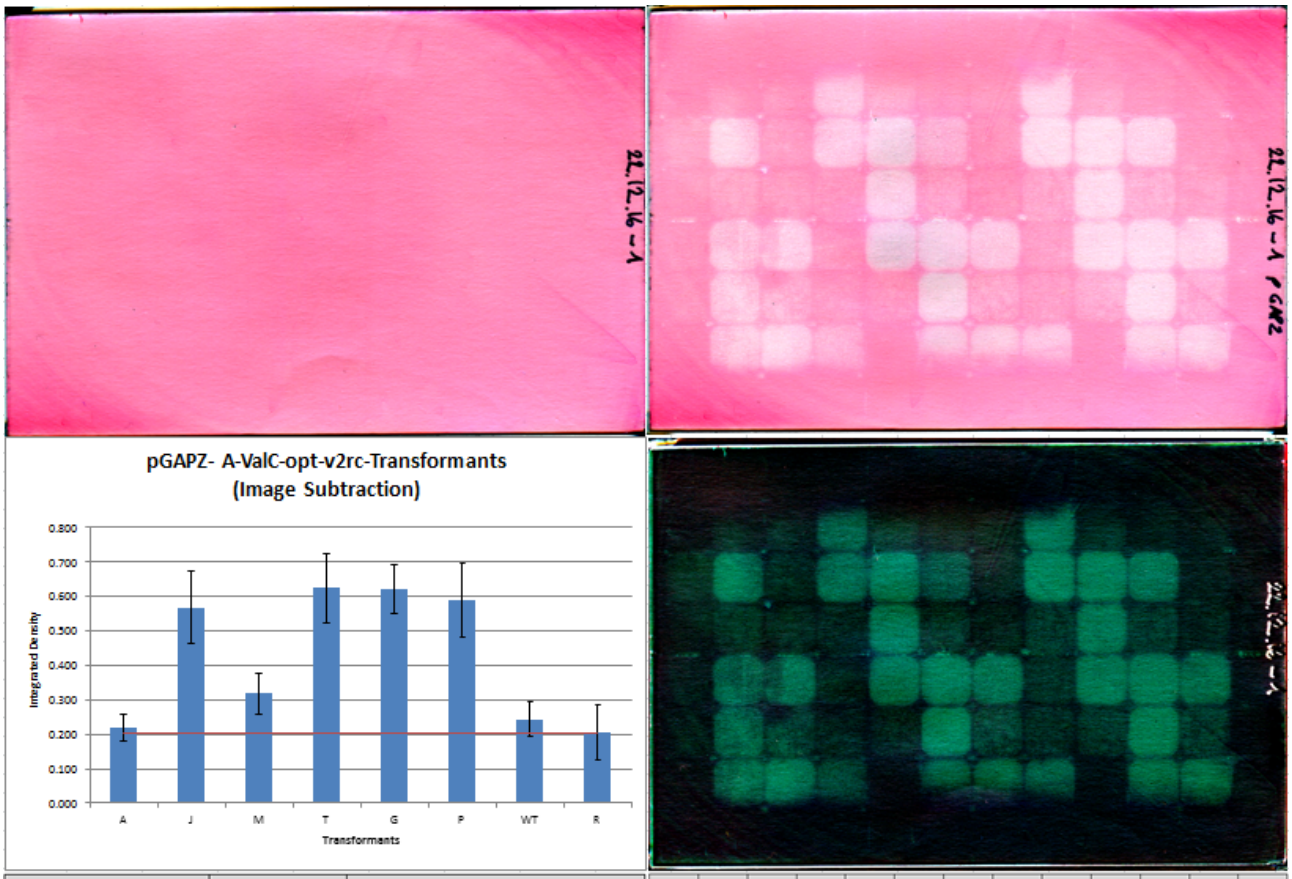

	Mean	Standard Deviation
A	0.219	0.040
J	0.567	0.104
M	0.318	0.059
T	0.623	0.099
G	0.619	0.071
P	0.587	0.107
WT	0.243	0.052
R	0.204	0.080

	1	2	3	4	5	6	7	8	9	10	11	12
A	-	-	-	-	-	-	-	-	-	-	-	-
B	-	A	WT	G	M	A	WT	G	M	A	WT	-
C	-	J	R	P	T	J	R	P	T	J	R	-
D	-	M	A	WT	G	M	A	WT	G	M	A	-
E	-	T	J	R	P	T	J	R	P	T	J	-
F	-	G	M	A	WT	G	M	A	WT	G	M	-
G	-	P	T	J	R	P	T	J	R	P	T	-
H	-	-	-	-	-	-	-	-	-	-	-	-

Figure 18: **pGAPZ image subtraction evaluation.** Left Top: image of the screening film after predrying, but before screening - t0 ; Right Top: image of the screening film after screening; Left Center: Diagram showing the mean integrated density for all measured strains after subtracting the two images from each other; Right Center: The result of subtracting the two image from each other. The Brightness and Contrast option in ImagJ was set to 0-64 for better depiction; Left Bottom: Results of the densitometric measurement applied on the subtracted image. Every strain was measured 4 times; Right Bottom: Distribution of strains in the DWP and on the screening film.

6.2.4 Interference effect

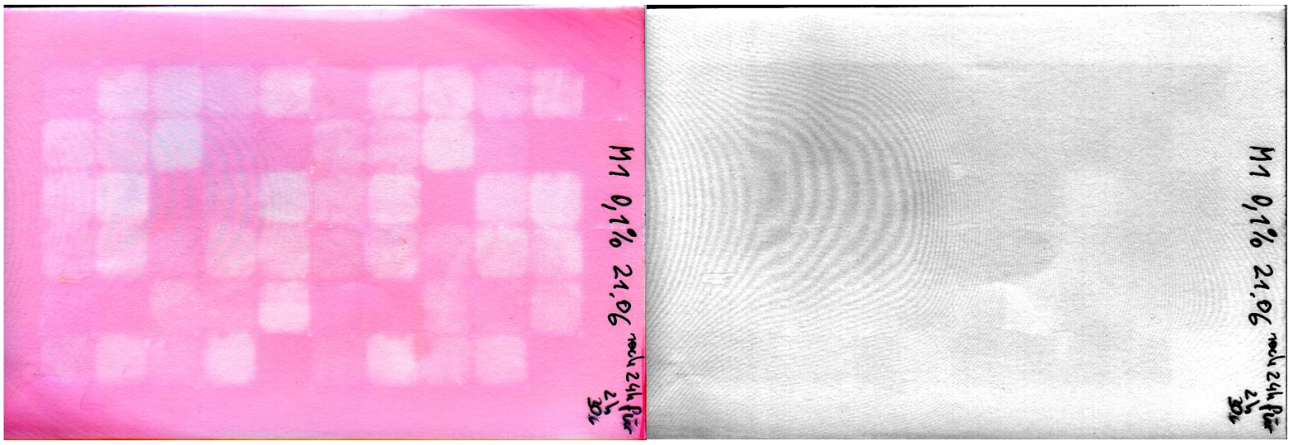

Figure 19: **Example for the interference effect.**

As we developed the screening assay and worked on the bioinformatical aspect, we concluded that artifacts can be seen in the scanned screening films. When we analyzed the older screening films, we observed that these artifacts had always been present during development. After these observations, several questions arose. We wondered if the visibility of structures originated from high contrast sensitivity, high dynamic range and combinatorial abilities of the human eye. An ImageJ analysis showed that these artifact are integral part of the pixel values and, therefore, affect the evaluation process. Thus human eye-brain imagination or interpretation could be ruled out. A common effect during scanning is called "Moire effect", which is created by low scanning resolution and is well known in the art design industry while working with scanners. It is created by two non-identical patterns that overlap with each other. Our hypothesis was that the glass plate had a fine regular crystal pattern and it interfered for example with the sensor pattern. Also in photography interference with the fine regular structures of the light sensor is known. Since the used scanner was a flat bed scanner, it seemed easy to imagine that a fixed pixel on a scanner sensor gets light in different angles by the moving lighting bar. At some point or angle positive or negative interference takes place. An imaginary example would be when the lightning bar is directly over the corresponding point on the paper. The light stream hits the paper surface in a 90° angle and gets reflected in the same direction. This could be a situation where interference occurs. Quite some effort was spent to inhibit or circumvent the Moire effect, but all actions failed. One particular experiment consisted of a gradual increase of scanning resolution (Figure 20). The screening film was not moved and the flat bed scanner was not opened during the experiment. The scanning took place at the following resolution-values: 150, 200, 300, 600, 1200 and 2400 dpi. With the increasing resolution values the "Moire effect" should decrease, but our data did not show a reduction. Alternative approaches such as to photographing the screening film with a DSLR camera or in the GBox were successful in preventing the interference effect (Figure 11). Furthermore, these interference patterns have been seen once by the naked human eye (out of hundreds of screened films). Another finding was that the interference effect was never reproducible . Even if the same film was lifted from the scanner surface

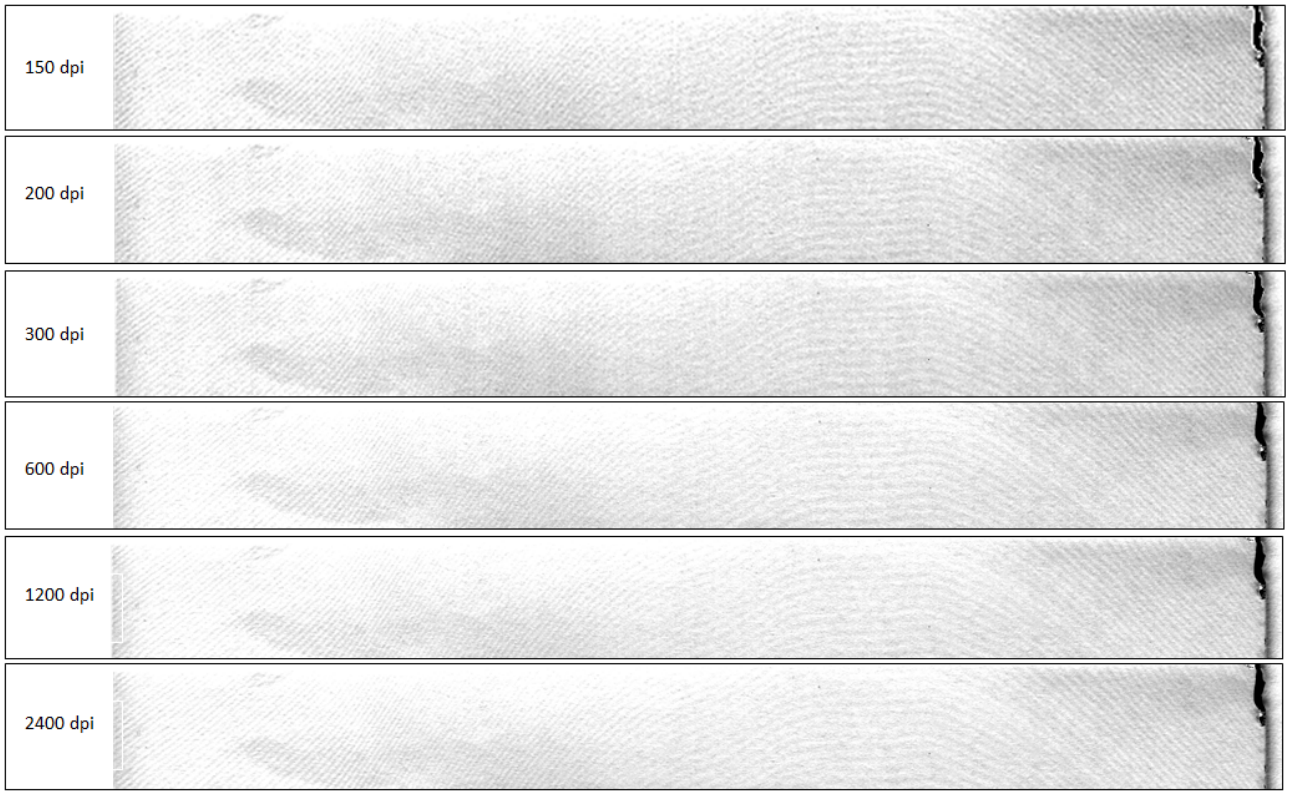

Figure 20: **Interference effect at different resolutions.** The screening film was scanned at resolution of 150, 200, 300, 600, 1200 and 2400 dpi without opening the scanner. Images depicted show the red color channel, because in this channel the interference effect was always expressed the strongest. If the "Moire effect" causes the interference effect, the effect should decrease with increasing resolution. This is not shown by the data.

and placed at the exactly same position again, the scan showed a different interference pattern. Over time this led to the presumption that the interference pattern was not caused by the "Moire effect". Since the "Moire effect" has not been seen by photographing the screening film, the focus fell on the two touching glass plates. Žan Caf-Feldin discovered an article about archiving of glas plates - used as storage for old pictures instead of film - that suggested a "Newton ring effect".[21] Although the "Newton ring effect" is a phenomenon that is created by light between a flat and an adjacent touching spherical surface, it was tested. Reports suggested to use plastic foil to interrupt the effect. By using plastic foil from laboratory trash bags our interference effect was successfully abrogated. The rescreening of *GAP* transformants (Figure 44) was the only experiment conducted with plastic foils in this thesis.

6.3 Biological example: *Rhodobacter sphaeroides*

6.3.1 The use of tellurite as a selection reagent

During conjugation the *E. coli* and *R. sphaeroides* cultures get mixed to bring the cells in contact with each other and enable plasmid transfer. First trials showed that screening cultures were still highly contaminated with *E. coli* cells. Although after conjugation RÄ plates are used to inhibit growth of *E. coli* cells, apparently the malic acid did not completely starve the *E. coli* cells to death. Probably they just remained in a dormancy state and started to grow again after being transferred to complex media. The company partner had used multiple streaking out and subsequent colony PCR to evaluate positive conjugants. Since the conventional microbial approach of streaking

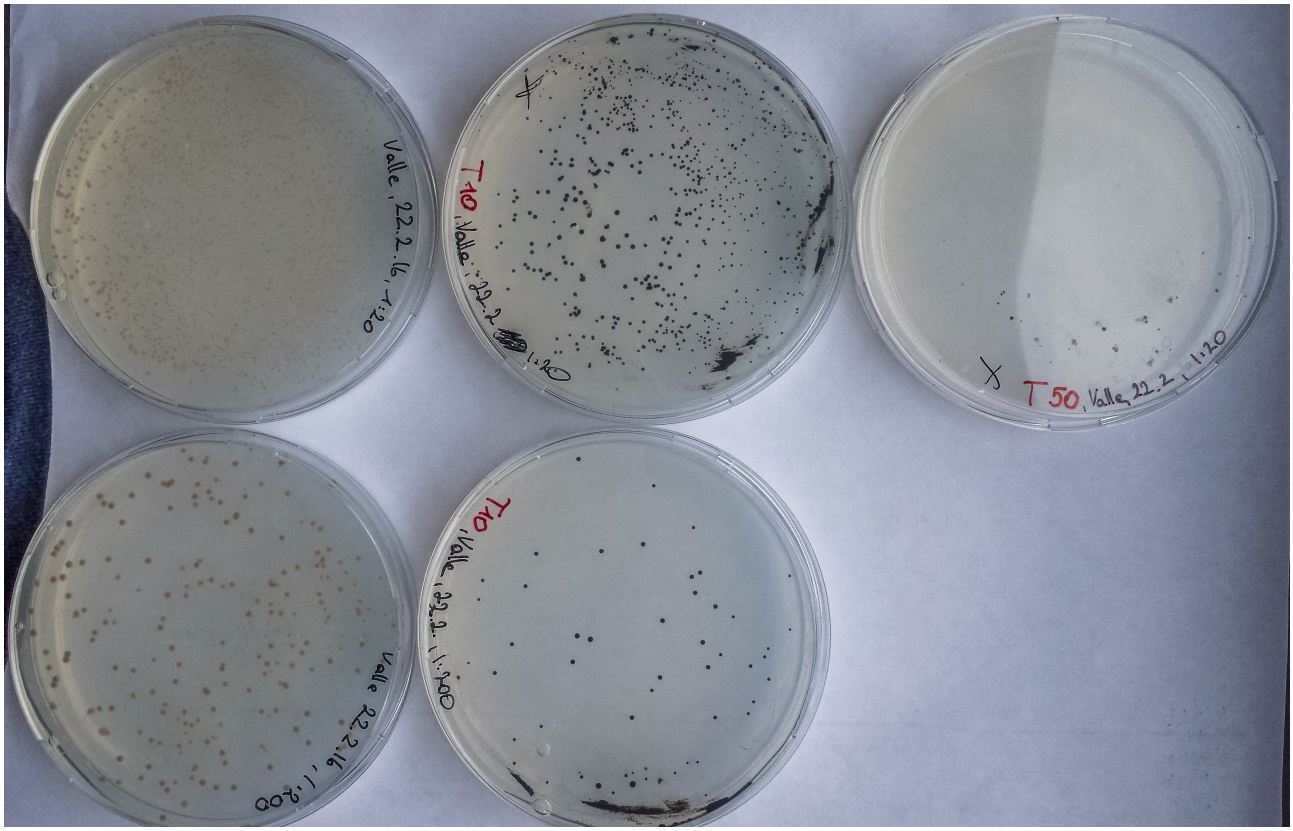

Figure 21: **Tellurite as a selection reagent.** Conjugations done on RÄ plates with different amounts of potassium tellurite. On the left, colonies on RÄ plate without potassium tellurite. In the center, colonies on RÄ plates with 10 μg/ml potassium tellurite. On the right, RÄ plate with 50 μg/ml potassium tellurite.

out is not suitable for high-throughput screening approaches, we followed the suggestion of our company partner to use potassium tellurite. Tellurite is toxic for eukaryotes and most prokaryotes, but some microbes of the class *Proteobacteria* developed a resistance mechanism including *Rhodobacter sphäroides*. These organisms survive at tellurite concentration at which *E. coli* cannot sustain its viability. For most procaryotes a concentration of 1 μg/ml is toxic. The concentrations for sufficient selection of *R. sphaeroides* varied strongly in literature depending on media composition, growth conditions and *R. sphaeroides* strain. For *R. sphaeroides* a tellurite resistence of up to 1 mg/ml was reported.[24][25][26] For that reason different potassium tellurite concentrations were tried out in

combination with the *R. sphaeroides* strain #22, during conjugation with WT plasmid p-m-Pppa-trx-ValCO Q492K L566S-mpmii alt creating strain #88. Therefore, RÄ plates with a concentration of 10, 50 and 100 μg/ml potassium tellurite and standard neomycin concentration were prepared (Figure 21). A standard conjugation was performed with *E. coli* S17-1 cells carrying the wildtype

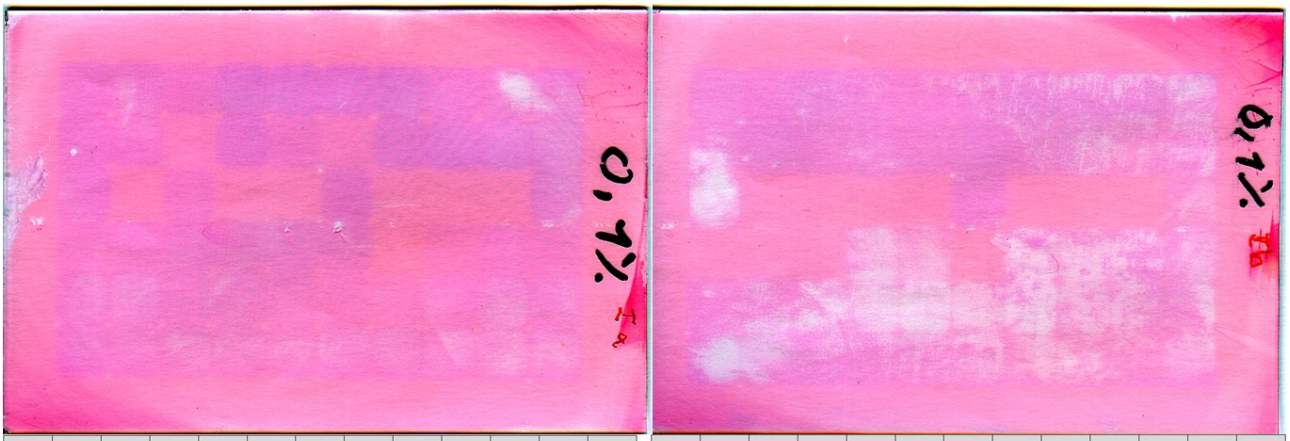

	1	2	3	4	5	6	7	8	9	10	11	12
A	-	-	-	-	-	-	-	-	-	-	-	-
B	-	T1	T1	T1	T1	T1	T1	T1	T1	T1	T1	-
C	-	T1	T1	T1	T1	T1	T1	T1	T1	T1	T1	-
D	-	#88	R	T0	T0	T0	#88	R	T0	T0	#88	-
E	-	T10	T10	T10	T10	T10	T10	T10	T10	T10	T10	-
F	-	T2.5	T2.5	T2.5	T2.5	T2.5	T2.5	T2.5	T2.5	T2.5	T2.5	-
G	-	T2.5	T2.5	T2.5	T2.5	T2.5	T2.5	T2.5	T2.5	T2.5	T2.5	-
H	-	-	-	-	-	-	-	-	-	-	-	-

	1	2	3	4	5	6	7	8	9	10	11	12
A	-	-	-	-	-	-	-	-	-	-	-	-
B	-	T5	T5	T5	T5	T5	T5	T5	T5	T5	T5	-
C	-	T5	T5	T5	T5	T5	T5	T5	T5	T5	T5	-
D	-	#88	R	T0	T0	T0	#88	R	T0	T0	#88	-
E	-	T10	T10	T10	T10	T10	T10	T10	T10	T10	T10	-
F	-	T7.5	T7.5	T7.5	T7.5	T7.5	T7.5	T7.5	T7.5	T7.5	T7.5	-
G	-	T7.5	T7.5	T7.5	T7.5	T7.5	T7.5	T7.5	T7.5	T7.5	T7.5	-
H	-	-	-	-	-	-	-	-	-	-	-	-

Figure 22: **Testing potassium tellurite as an selection agent.** Top: Images of two screening films, that have been used for screening of *R. sphaeroides* pmeV conjugants after incubation on RÄ plates with different tellurite concentrations. Bottom: Shows distribution over plate. T(N_0), N_0 refering to the tellurite concentration in μg/ml.

plasmid. The conjugant mixture was plated on the tellurite plates as well as on control plate without potassium tellurite. Cell growth was significantly reduced on the tellurite plates. Tellurite also caused a change in colony color. The usual color of *R. sphaeroides* is a light orange to brown. When incubated in the presence of tellurite colonies became black. This color change comes from the reduction of TeO_3^{2-} to elemental Te, which is black.[27] These colonies were then transferred to DWP and screened. The controls without tellurite showed stable growth. However, (+)-valencene signals were not visible because of *E. coli* contamination. The conjugation on RS102 with different amounts of potassium tellurite did not select for *Rhodobacter*. Again contamination was seen. The RÄ medium with potassium tellurite concentrations over 10 μg/ml showed growth, but a lot of conjugants did not show a signal in the screening assay. Therefore, the tellurite concentration was decreased. Conjugants grown on a tellurite concentration of 10 μg/ml showed weak growth. Yet only 22 % of screening positions gave signals. Colonies picked from the 50 μg/ml tellurite plate did not grow on RS102 + Kan. Concentrations of potassium tellurite were lowered to 1 μg/ml, 2.5 μg/ml, 5 μg/ml, 7.5 μg/ml and 10 μg/ml (as a control) and conjugants were screened again. Additional conjugation was performed without potassium tellurite (Figure 22). This experiment

showed that at a concentration of 1 μg/ml only two positions of 20 did not give a screening signal. Probably, the concentration of potassium tellurite started to get too low. For 10 positions over two plates without tellurite as a selection marker one position gave a signal. With a potassium tellurite concentration of 2.5 μg/ml, 5 μg/ml and 7.5 μg/ml all wells (of 20 wells inoculated) showed signals. At a concentration of 10 μg/ml tellurite conjugants started to fail in delivering signals again. One possible explanation is that the potassium tellurite concentration got to high even for *R. sphaeroides*. Five positions out of ten on two plates did not give a signal. While media controls did not show a signal, the control strain #88 created a signal. Apparently, a potassium tellurite concentration between 2.5 μg/ml and 7.5 μg/ml suited our conjugation conditions best. For the conjugation of the libraries a potassium tellurite concentration of 3.5 μg/ml was chosen.

6.3.2 Screening for promising conjugants

After the first struggles in conjugation we managed to solve the *E. coli* contamination issue. The conjugation of the two libraries III and V were performed successfully. *Rhodobacter sphaeroides* colonies were picked and placed into DWP to grow the precultures. Then, these plates were used to inoculate the screening cultures by a 48-position pin stamp for duplicate measurements. For the hDWP and *Rhodobacter sphaeroides* with the (+)-valencene synthase under the control of the *Pppa* promoter a screening interval from 18 h to 19 h (60-70 min) was figured out to work best. For the mutation of the *Pppa* promoter, a library size of 1200 conjugants was supposed to cover all the possible mutations.

Shortly after the conjugation, when the first screenings were performed, we noticed that many conjugants did not show a signal in the screening assay at all. Yet, the growth of the cultures was comparable to the cultures that created signals. About 80% of the picked conjugants did not create signals on the screening films. This meant that apparently these negative conjugants did not produce (+)-valencene or only did produce it in small quantities. At 80% negative conjugants the library size shrank to about 200 conjugants (20%) that could be measured with the screening films. Although the library size was small, we decided to continue with the screening, since the preceding selection problem had taken a long time to solve. In the first round of screening, 80% of the wells gave negative screening results. Many positive conjugants were rescreened though. The rescreening comprised 96 *Pppa* mutants. Due to an unwanted change in resolution caused by a third party, the films of the rescreening were scanned at a resolution of 200 dpi only. Screening and rescreening were performed at a time, when the full spectrum of possibilities for evaluation was unknown. Then, the RGB evaluation (Chapter 12) was the standard evaluation method. These two factors contributed more uncertainty to the screening results here. Compared to the standard now, at the time of writing this thesis, the resolution is 600 dpi. A resolution of 200 dpi means 1600 pixel measured per well. At a resolution of 600 dpi, 14 400 pixel are measured. With a resolution of 600 dpi nine times more information is captured. Additionally, the RGB evaluation delivered not the most reliable results. Therefore, the films were evaluated later again by using the green or blue color channel. The RGB evaluation was used to choose promising conjugants. The images for the rescreening were supplemented with the evaluation of the green/blue channel to approach the more recent standard and furthermore, this helped us interpreting the results. On every plate the strains #88 and #100 were inoculated to have reference points. The strain #100 produces about 10% more (+)-valencene than #88 (GC results). Since the screening assay showed so many conjugants that possibly outperformed #88, not all promising conjugants were tested.

Plate 1 (Figure 23) showed the expected relation between #88 and #100. All conjugants showed a mean (+)-valencene production that was higher than #88 in the RGB channel. But the standard deviation overlapped most of the time with the one of #88. Because of the tendency of high production in the RGB channel all conjugants were transferred to the 24-well plate cultivation. The green channel evaluation later showed that only a few of these conjugants generated high mean values and the screening with this film was not optimal, because of the high standard deviations.

Plate 2 (Figure 24) did not show a strong trend of #88 and #100. Again conjugants showed a high mean (+)-valencene production that was often higher than #88 in the RGB channel. Because of the tendency of high production in the RGB channel almost all conjugants were transferred to the 24-well plate cultivation. The green channel evaluation later on showed also high mean values for many conjugants, all were overlapping with the standard deviation of #88.

Plate 3 (Figure 25) showed the expected relation of #88 and #100 with marked difference. All conjugants showed a higher mean (+)-valencene production than #88 in the RGB channel. Because of the tendency of high signals in the RGB channel, many conjugants were picked to be cultivated in 24-well plates. The blue channel evaluation later showed that only a few of these conjugants generated high mean values (V10-F5, III1-C4, III1-B10).

Plate 4 (Figure 26) showed insignificant differences between #88 and #100. Some conjugants showed a high mean (+)-valencene production that was higher than #88 in the RGB channel. The four conjugants that reached the signal intensity of #100 were transferred to the 24-well plate cultivation. The green channel evaluation later showed similar results, but the mean values were in general lower. None of the conjugants were markedly more productive than #88.

Plate 5 (Figure 27) showed the expected trend of #88 and #100 signals. Many conjugants showed a high mean (+)-valencene production that was higher than #88 in the RGB channel. Four conjugants with high signal intensity were chosen for 24-well plate cultivation. The green channel evaluation later showed different results. The seven strains on the right side of the graph (III7-D10, III8-C9, III8-E3, III8-D9, III8-F11, III8-C11, III8-E6) performed still quite well.

Plate 6 (Figure 28) showed the expected relation of #88 and #100 signals. Again, many conjugants showed a high mean (+)-valencene production that was higher than #88 in the RGB channel. Four conjugants with high signal intensity were transferred to the 24-well plate cultivation. The green channel evaluation later on showed that none of them outperformed #88.

Overall, it can be stated that the results in the RGB channel and the green/blue channel evaluations were substantially different. In general the conjugants had lower integrated densities in the green/blue channel than in the RGB channel. In the green/blue channel only four conjugants (V10-F5, III8-D9, III8-F11, III8-C11) significantly outperformed the wild type strain #88. The RGB screening showed many promising conjugants. An explanation for these results might be the RGB evaluation in combination with the low resolution of the images. Another possibility is an exposure/concentration gradient (in one color channel) over the film from the middle (brighter) to the outer wells (darker), since all the controls were positioned in outer wells, but all around the plate. Overall, 54 conjugants were selected for 24-well plate cultivation.

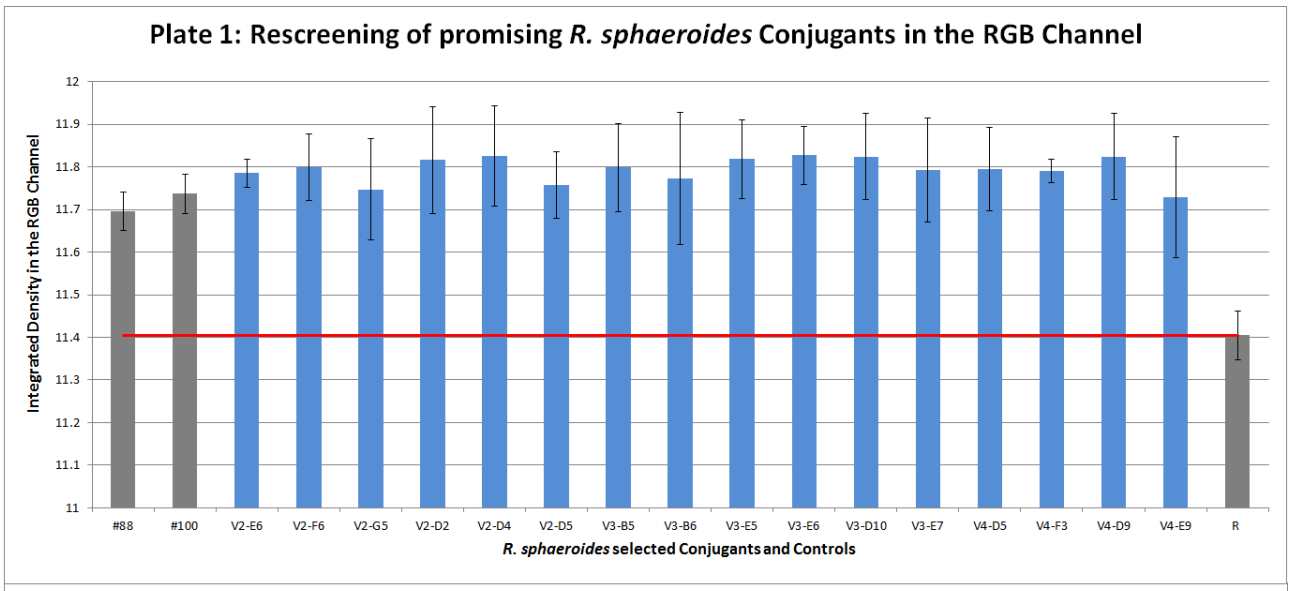

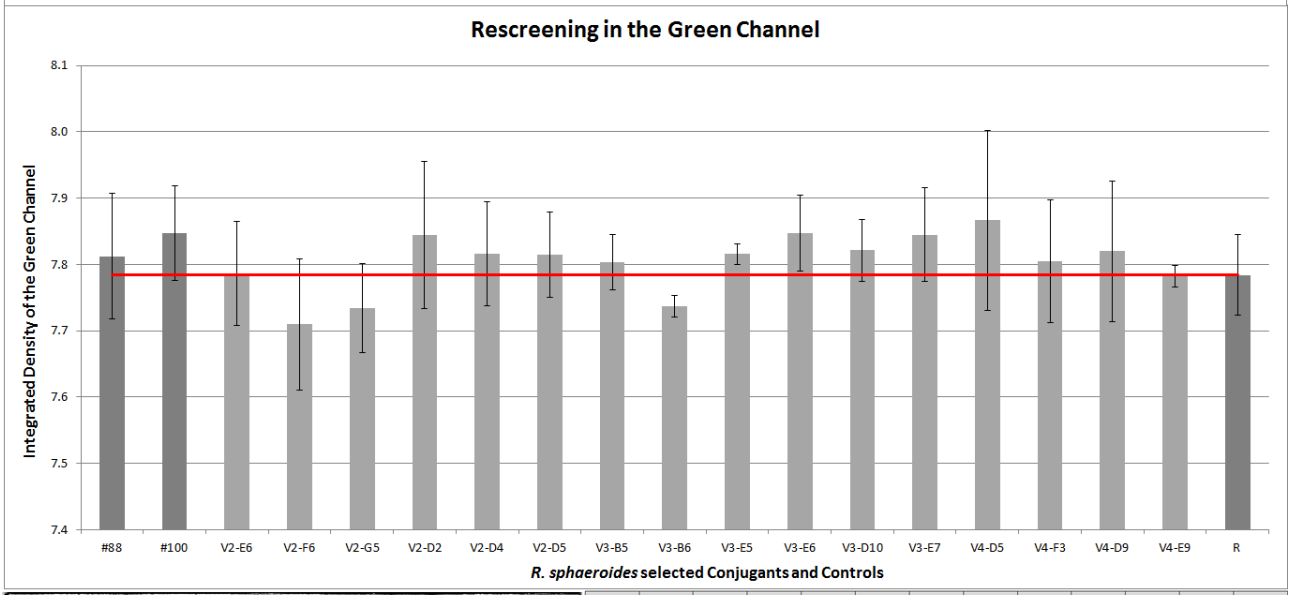

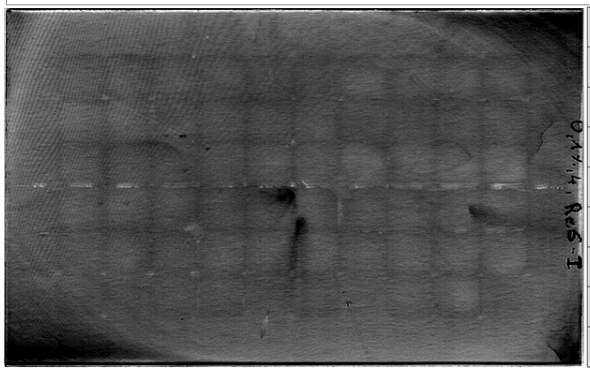

	1	2	3	4	5	6	7	8	9	10	11	12
A	-	-	-	-	-	-	-	-	-	-	-	-
B	-	#88	#100	V2-E6	V2-F6	V2-G5	#88	#100	V3-E5	V3-E6	V3-D10	-
C	-	V2-D2	V2-D4	V2-D5	V3-B5	V3-B6	V3-E7	V4-D5	V4-F3	V4-D9	V4-E9	-
D	-	V2-E6	V2-F6	V2-G5	V2-D2	V2-D4	V3-E5	V3-E6	V3-D10	V3-E7	V4-D5	-
E	-	V2-D5	V3-B5	V3-B6	V2-E6	V2-F6	V4-F3	V4-D9	V4-E9	V3-E5	V3-E6	-
F	-	V2-G5	V2-D2	V2-D4	V2-D5	V3-B5	V3-D10	V3-E7	V4-D5	V4-F3	V4-D9	-
G	-	V3-B6	R	#88	#100	R	V4-E9	R	#88	#100	R	-
H	-	-	-	-	-	-	-	-	-	-	-	-

Figure 23: **Rescreening of selected conjugants.** Top: RGB evaluation of 200 dpi image. R refers to media. Middle: Green channel evaluation of the same image. Bottom left: Image in the green channel. Bottom right: Distribution over the plate. Mean values and standard deviation of triplicates are given.

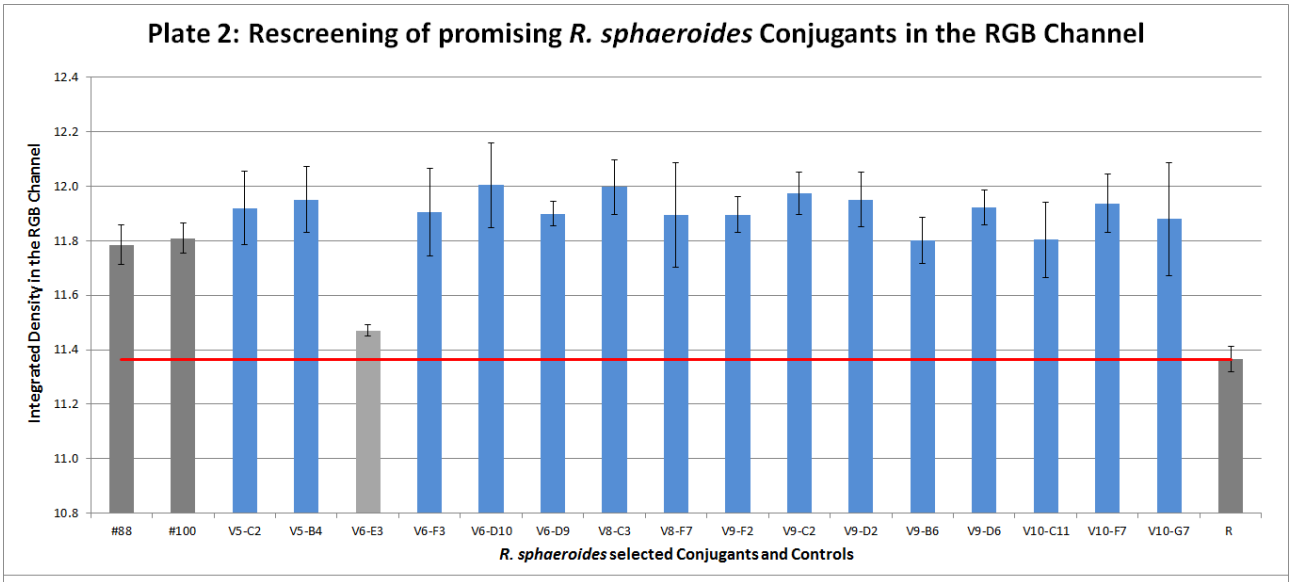

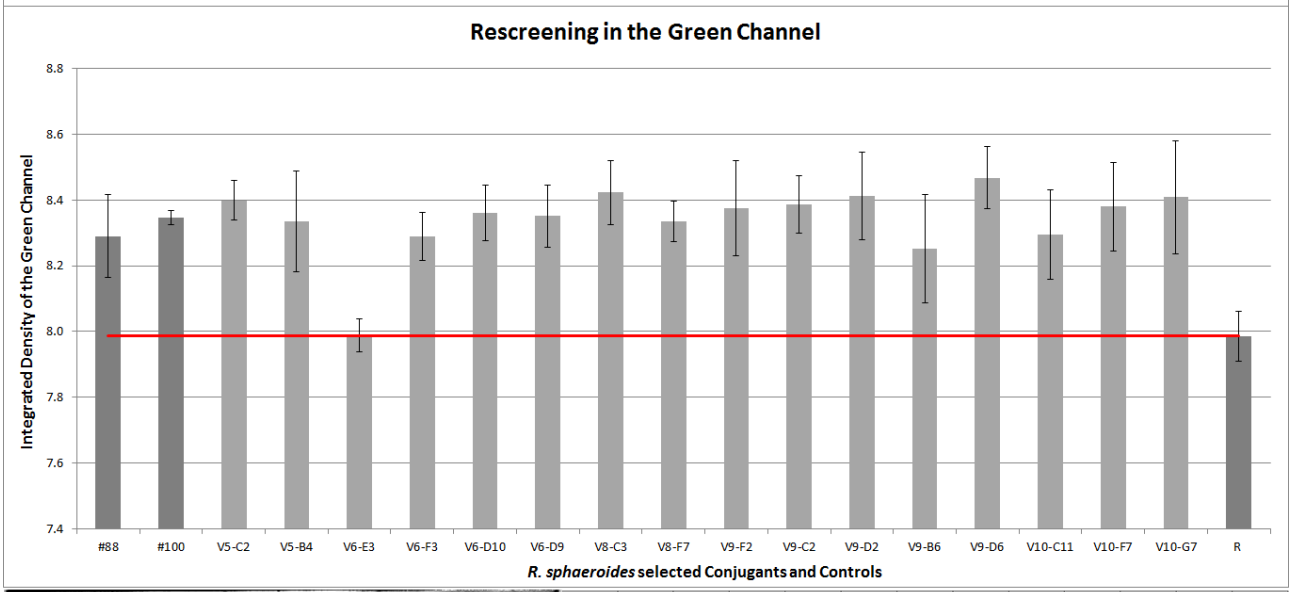

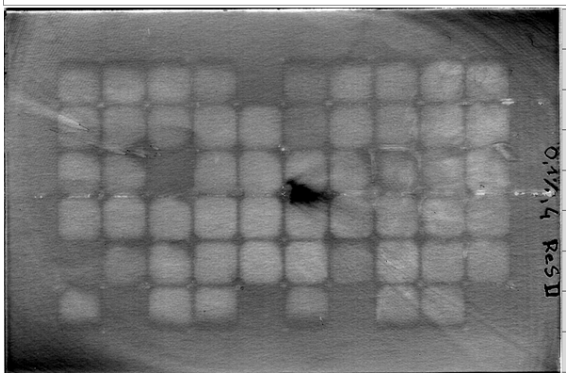

	1	2	3	4	5	6	7	8	9	10	11	12
A	-	-	-	-	-	-	-	-	-	-	-	-
B	-	#88	#100	V5-C2	V5-B4	V6-E3	#88	#100	V9-F2	V9-C2	V9-D2	-
C	-	V6-F3	V6-D10	V6-D9	V8-C3	V8-F7	V9-B6	V9-D6	V10-C11	V10-F7	V10-G7	-
D	-	V5-C2	V5-B4	V6-E3	V6-F3	V6-D10	V9-F2	V9-C2	V9-D2	V9-B6	V9-D6	-
E	-	V6-D9	V8-C3	V8-F7	V5-C2	V5-B4	V10-C11	V10-F7	V10-G7	V9-F2	V9-C2	-
F	-	V6-E3	V6-F3	V6-D10	V6-D9	V8-C3	V9-D2	V9-B6	V9-D6	V10-C11	V10-F7	-
G	-	V8-F7	R	#88	#100	R	V10-G7	R	#88	#100	R	-
H	-	-	-	-	-	-	-	-	-	-	-	-

Figure 24: **Rescreening of selected conjugants.** Top: RGB evaluation of 200 dpi image. R refers to media. Middle: Green channel evaluation of the same image. Bottom left: Image in the green channel. Bottom right: Distribution over the plate.Mean values and standard deviation of triplicates are given.

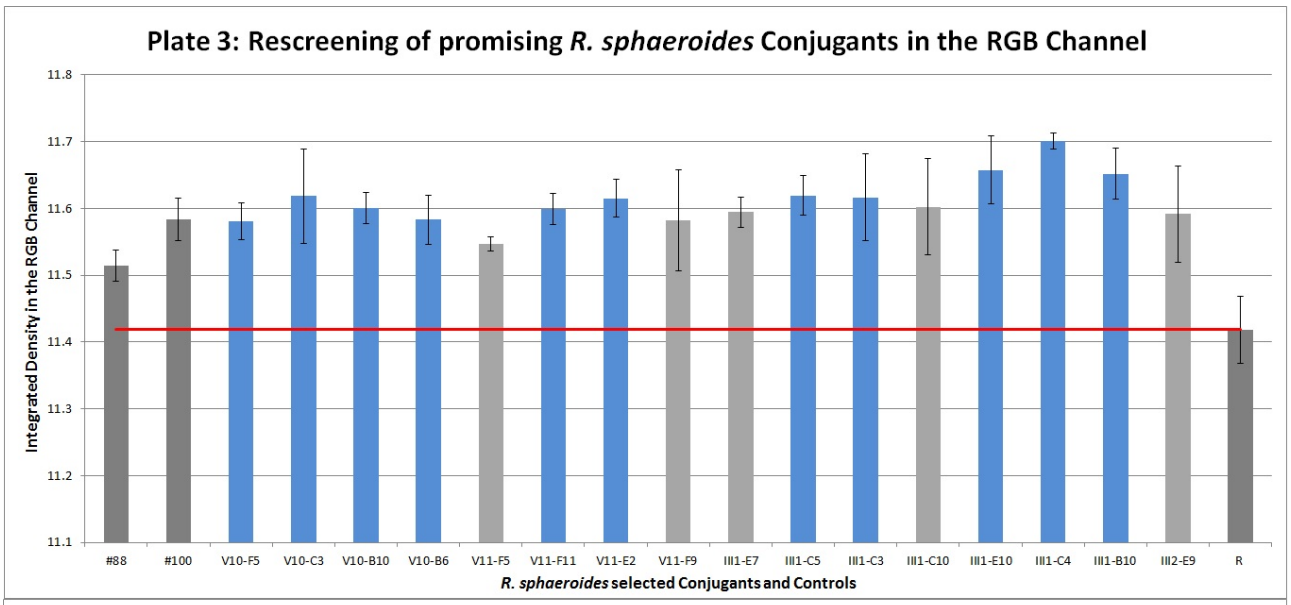

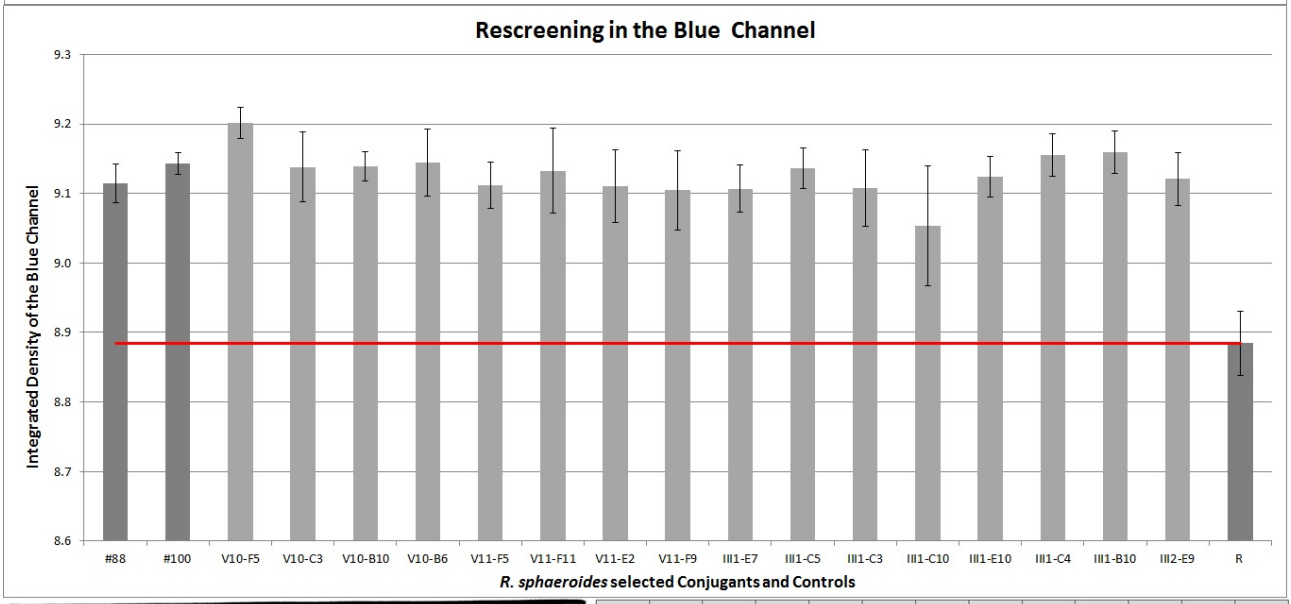

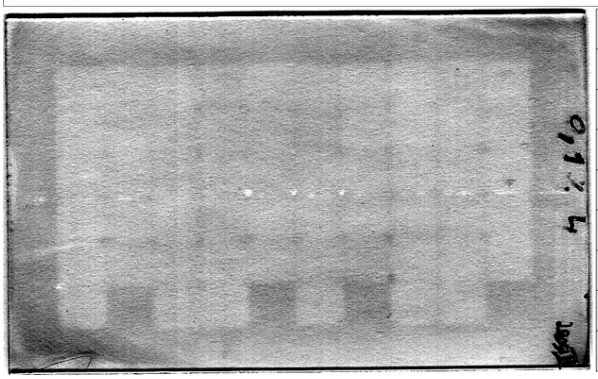

	1	2	3	4	5	6	7	8	9	10	11	12
A	-	-	-	-	-	-	-	-	-	-	-	-
B	-	#88	#100	V10-F5	V10-C3	V10-B10	#88	#100	V10-F5 (X)	III1-C5	III1-C3	-
C	-	V10-B6	V11-F5	V11-F11	V11-E2	V11-F9	III1-C10	III1-E10	III1-C4	III1-B10	III2-E9	-
D	-	V10-F5	V10-C3	V10-B10	V10-B6	V11-F5	III1-E7	III1-C5	III1-C3	III1-C10	III1-E10	-
E	-	V11-F11	V11-E2	V11-F9	III1-E7 (X)	V10-C3	III1-C4	III1-B10	III2-E9	III1-E7	III1-C5	-
F	-	V10-B10	V10-B6	V11-F5	V11-F11	V11-E2	III1-C3	III1-C10	III1-E10	III1-C4	III1-B10	-
G	-	V11-F9	R	#88	#100	R	III2-E9	R	#88	#100	R	-
H	-	-	-	-	-	-	-	-	-	-	-	-

Figure 25: **Rescreening of selected conjugants.** Top: RGB evaluation of 200 dpi image. R refers to media. Middle: Green channel evaluation of the same image. Bottom left: Image in the green channel. Bottom right: Distribution over the plate. Mean values and standard deviation of triplicates are given.

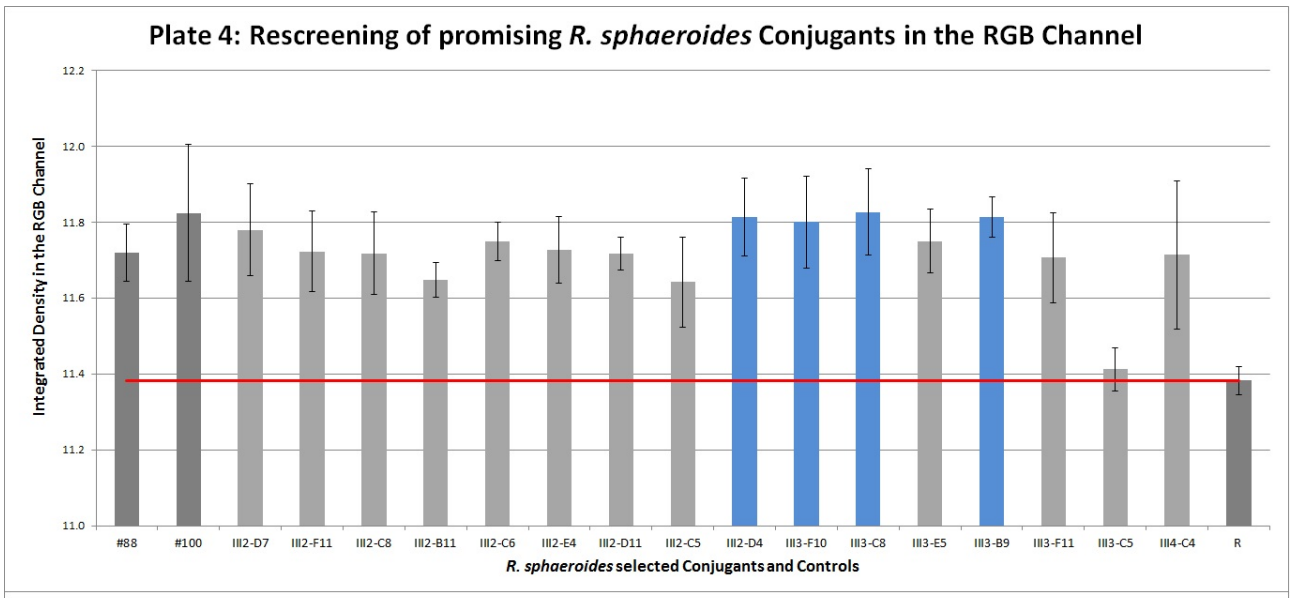

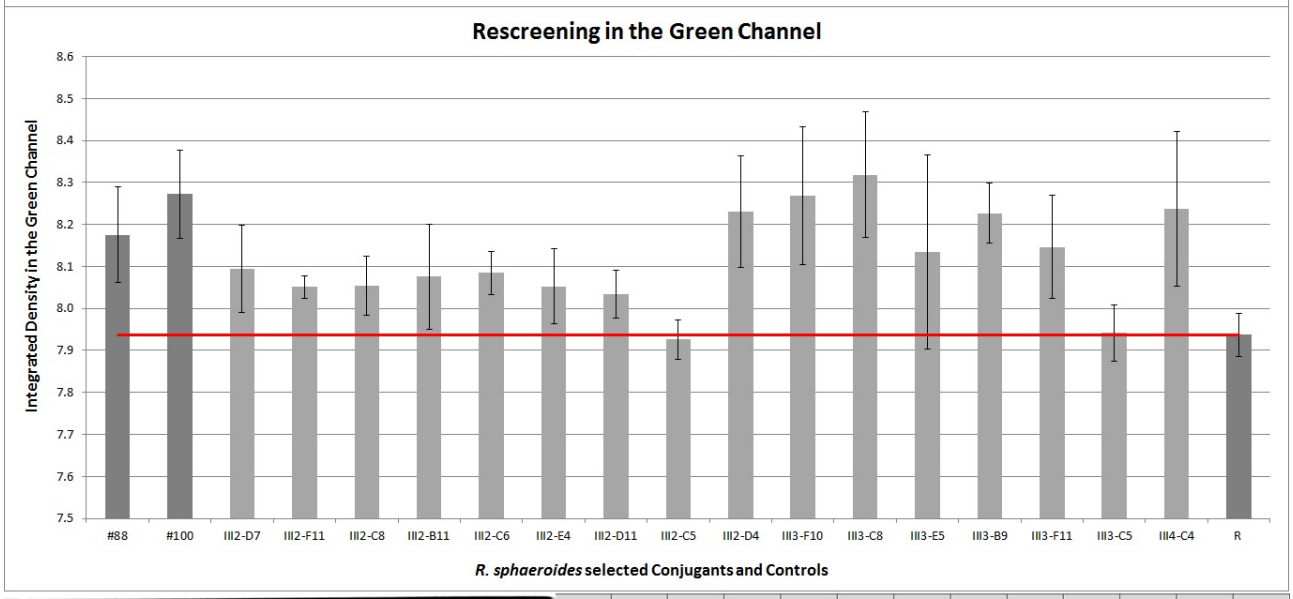

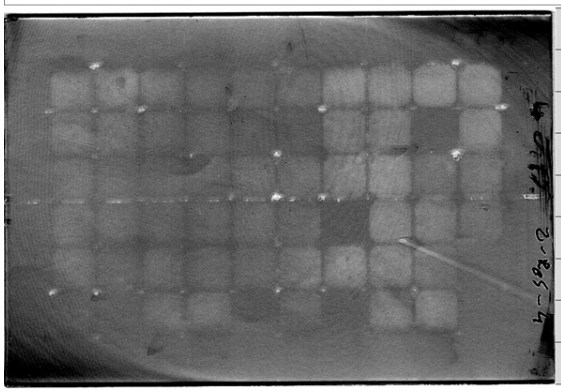

	1	2	3	4	5	6	7	8	9	10	11	12
A	-	-	-	-	-	-	-	-	-	-	-	-
B	-	#88	#100	III2-D7	III2-F11	III2-C8	#88	#100	III2-D4	III3-F10	III3-C8	-
C	-	III2-B11	III2-C6	III2-E4	III2-D11	III2-C5	III3-E5	III3-B9	III3-F11	III3-C5	III4-C4	-
D	-	III2-D7	III2-F11	III2-C8	III2-B11	III2-C6	III2-D4	III3-F10	III3-C8	III3-E5	III3-B9	-
E	-	III2-E4	III2-D11	III2-C5	III2-D7	III2-F11	III3-F11	III3-C5	III4-C4	III2-D4	III3-F10	-
F	-	III2-C8	III2-B11	III2-C6	III2-E4	III2-D11	III3-C8	III3-E5	III3-B9	III3-F11	III3-C5	-
G	-	III2-C5	R	#88	#100	R	III4-C4	R	#88	#100	R	-
H	-	-	-	-	-	-	-	-	-	-	-	-

Figure 26: **Rescreening of selected conjugants.** Top: RGB evaluation of 200 dpi image. R refers to media. Middle: Green channel evaluation of the same image. Bottom left: Image in the green channel. Bottom right: Distribution over the plate. Mean values and standard deviation of triplicates are given.

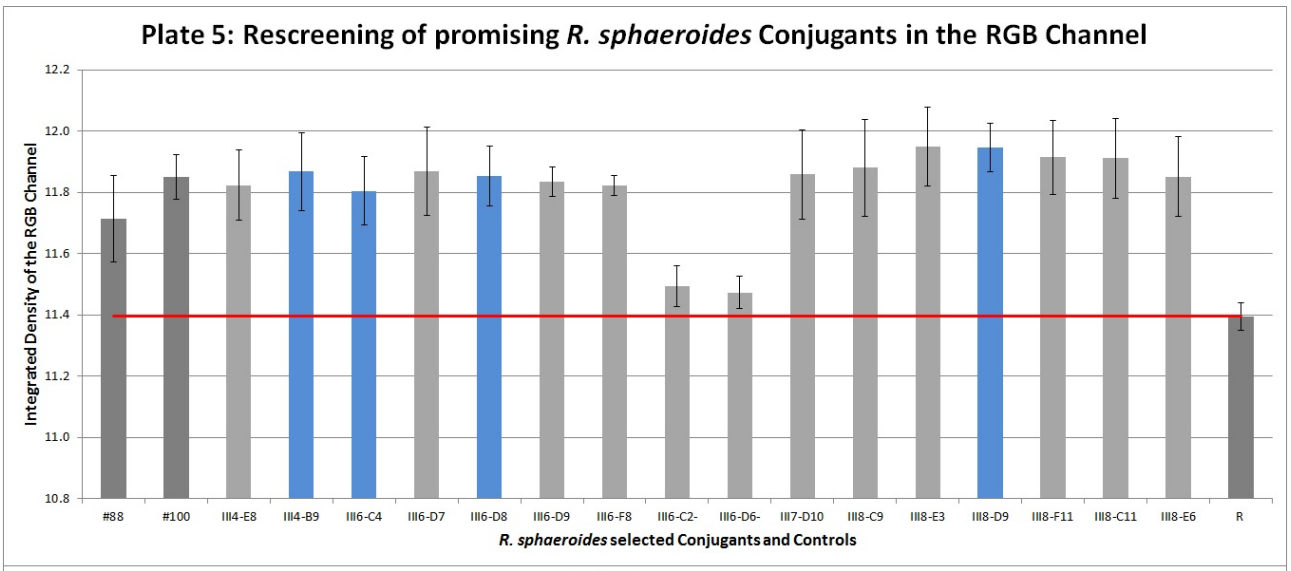

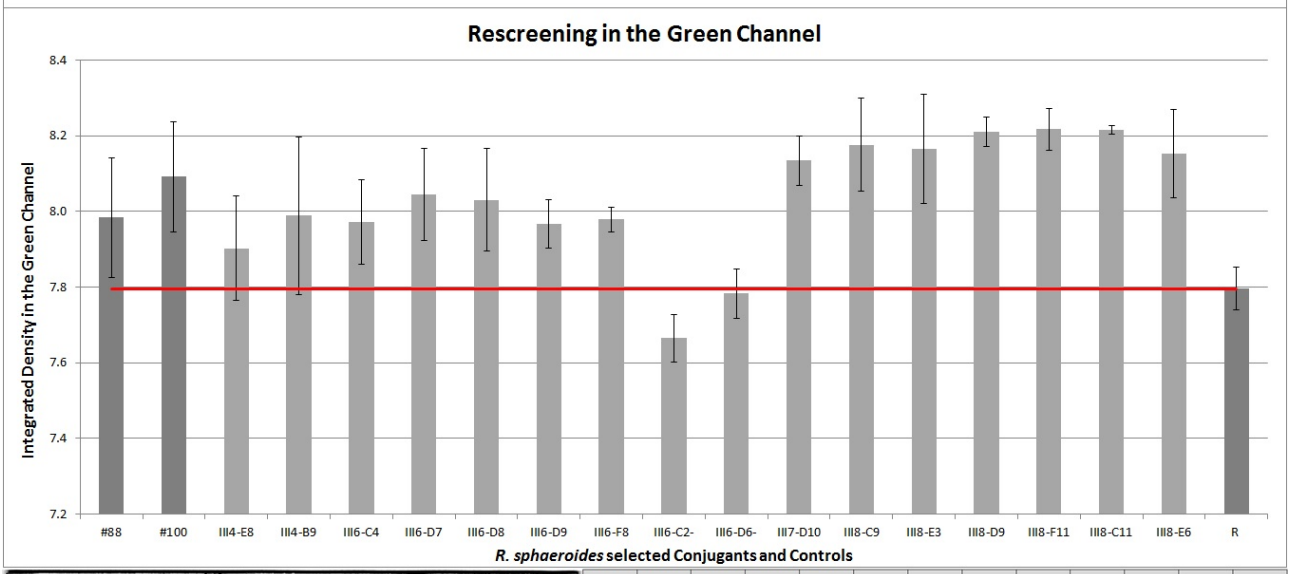

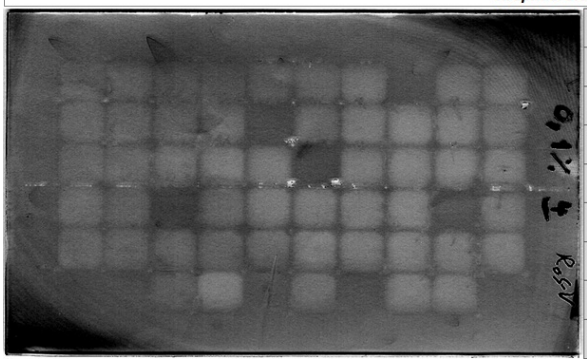

	1	2	3	4	5	6	7	8	9	10	11	12
A	-	-	-	-	-	-	-	-	-	-	-	-
B	-	#88	#100	III4-E8	III4-B9	III6-C4	#88	#100	III6-D6-	III7-D10	III8-C9	-
C	-	III6-D7	III6-D8	III6-D9	III6-F8	III6-C2-	III8-E3	III8-D9	III8-F11	III8-C11	III8-E6	-
D	-	III4-E8	III4-B9	III6-C4	III6-D7	III6-D8	III6-D6-	III7-D10	III8-C9	III8-E3	III8-D9	-
E	-	III6-D9	III6-F8	III6-C2-	III4-E8	III4-B9	III8-F11	III8-C11	III8-E6	III6-D6-	III7-D10	-
F	-	III6-C4	III6-D7	III6-D8	III6-D9	III6-F8	III8-C9	III8-E3	III8-D9	III8-F11	III8-C11	-
G	-	III6-C2-	R	#88	#100	R	III8-E6	R	#88	#100	R	-
H	-	-	-	-	-	-	-	-	-	-	-	-

Figure 27: **Rescreening of selected conjugants.** Top: RGB evaluation of 200 dpi image. R refers to media. Middle: Green channel evaluation of the same image. Bottom left: Image in the green channel. Bottom right: Distribution over the plate. Mean values and standard deviation of triplicates are given.

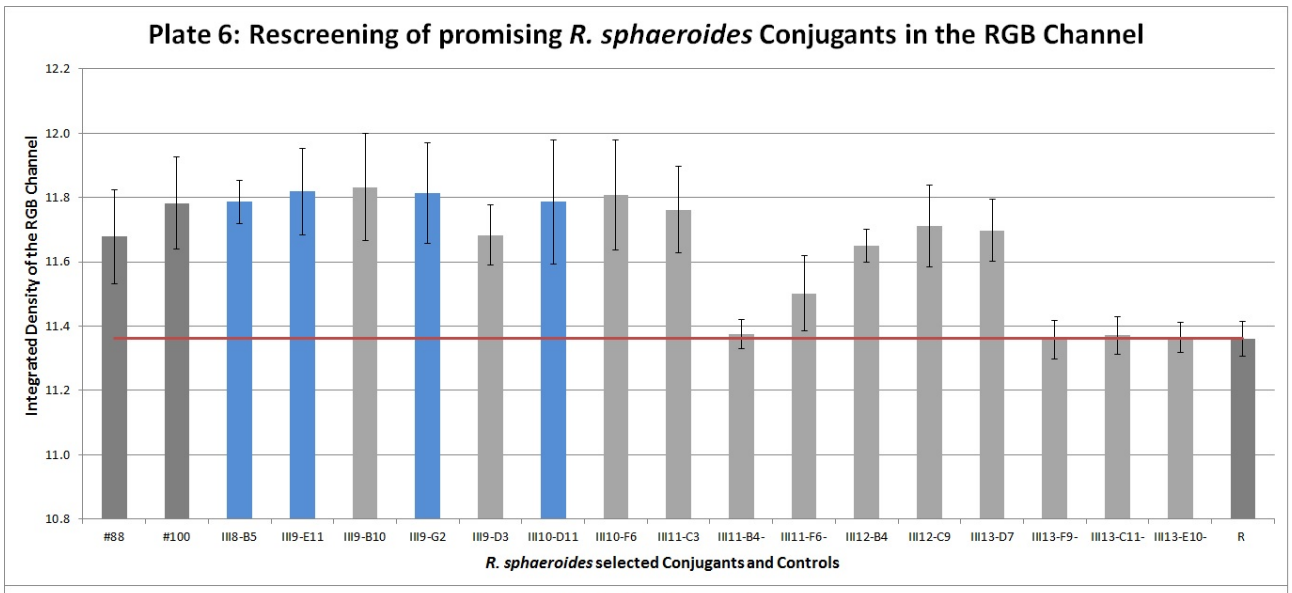

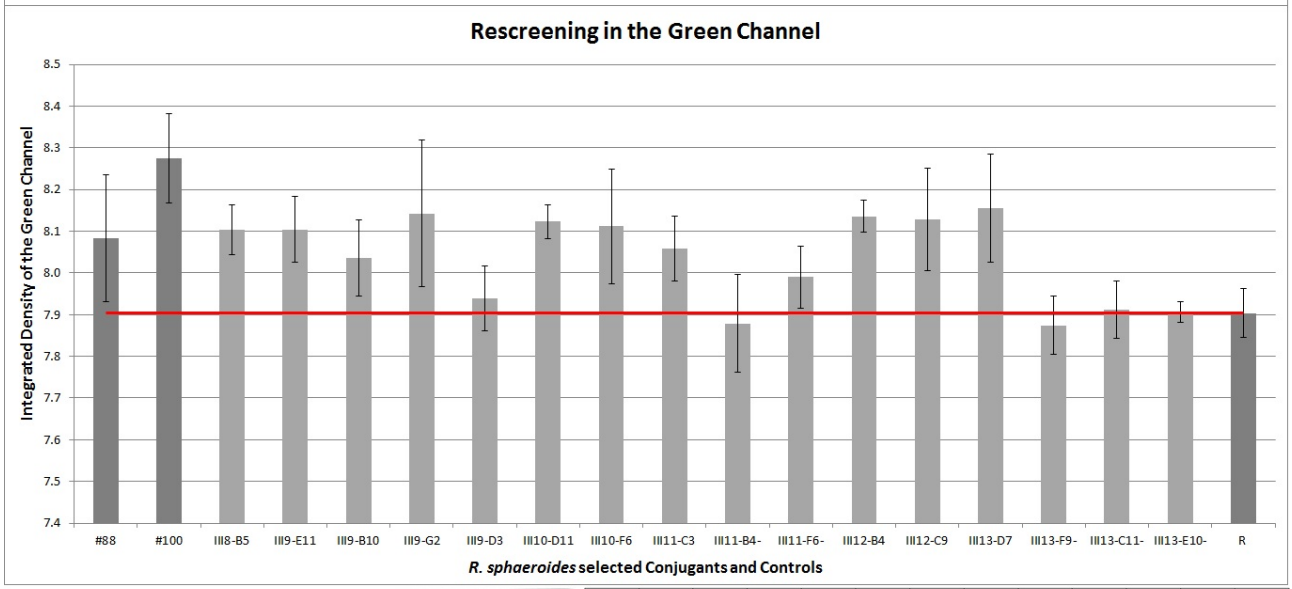

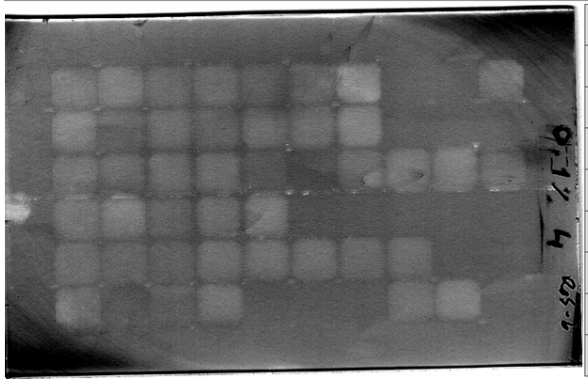

	1	2	3	4	5	6	7	8	9	10	11	12
A	-	-	-	-	-	-	-	-	-	-	-	-
B	-	#88	#100	III8-B5	III9-E11	III9-B10	#88	#100	III11-B4-	III11-F6-	III12-B4	-
C	-	III9-G2	III9-D3	III10-D11	III10-F6	III11-C3	III12-C9	III13-D7	III13-F9-	III13-C11-	III13-E10-	-
D	-	III8-B5	III9-E11	III9-B10	III9-G2	III9-D3	III11-B4-	III11-F6-	III12-B4	III12-C9	III13-D7	-
E	-	III10-D11	III10-F6	III11-C3	III8-B5	III9-E11	III13-F9-	III13-C11-	III13-E10-	III11-B4-	III11-F6-	-
F	-	III9-B10	III9-G2	III9-D3	III10-D11	III10-F6	III12-B4	III12-C9	III13-D7	III13-F9-	III13-C11-	-
G	-	III11-C3	R	#88	#100	R	III13-E10-	R	#88	#100	R (X)	-
H	-	-	-	-	-	-	-	-	-	-	-	-

Figure 28: **Rescreening of selected conjugants.** Top: RGB evaluation of 200 dpi image. R refers to media. Middle: Green channel evaluation of the same image. Bottom left: Image in the green channel. Bottom right: Distribution over the plate. Mean values and standard deviation of triplicates are given.

6.3.3 Promising conjugants in 24-well DWP cultivation

After using the newly developed screening assay to select promising *Pppa* promoter mutants, the most promising conjugants were cultivated in 24-well deep well plates and their (+)-valencene levels were determined via GC-FID to monitor (+)-valencene production. The switch from 96-well DWP to 24-well DWP created a difference in cultivation conditions and, therefore, showed us if the desired improvement was only seen in 96-well DWP or also in 24-well DWP. We aimed to find *Pppa* promoter mutants that show a general improvement ideally under all cultivation conditions, since this should improve the strain capacities in bioreactor as well. Cultivation with n-dodecane was performed not only to measure (+)-valencene levels, but it was also used in commercial production systems. Since the rescreening showed a lot of promising strains, nine 24-well DWPs were cultivated. Every conjugant and control strain was analyzed in triplicates. The distribution over the plates were homogenous as possible. Two positions of each strain were on the outer wells, one position was in an inner well. Previous cultivation with n-dodecane and subsequent GC-FID analysis never showed problems with the used media. Therefore, media controls were carried out on these plates. Instead of the media control one additional conjugant was cultivated per plate. As references the *Rhodobacter sphaeroids* #88 - carrying the wild type plasmid - and the #100, which produces around 10% more (+)-valencene than #88, were used. In general, the results had quite high standard deviations. This was probably due to the fact that the cultures had not been OD normalized. Nevertheless, standard curves for the calculation of (+)-valencene concentrations showed all a very high significance value.

Figure 29 shows low standard deviation, but the expected ratio between #88 and #100 was not that clear visible. The mean value of strains was 2706 ng/μl (#88), 2765 ng/μl (#100), 2603 ng/μl (V2-E6), 2739 ng/μl (V2-F6), 2514 ng/μl (V4-F3), 2497 ng/μl (V2-D2), 2557 ng/μl (V2-D4) and 2642 ng/μl (V3-E6). All conjugants showed a behavior that was similar or a little lower than the two reference strains.

Figure 30 shows higher standard deviations than Plate A, but the expected difference between #88 and #100 was visible. Mean values of strains were 2251 ng/μl (#88), 2634 ng/μl (#100), 2628 ng/μl (V4-D9), 2326 ng/μl (V6-D10), 2424 ng/μl (V8-C3), 2459 ng/μl (V6-D9), 1957 ng/μl (V9-C2) and 753 ng/μl (V5-B4). Most of the strains performed in the range of #88 or lower. The strain V4-D9 showed a (+)-valencene production that was comparable to #100, but was statistically not significantly different from #88.

Figure 31 shows the expected ratio between #88 and #100 signals, even though there was no statistically difference. The mean values of strains were 2142 ng/μl (#88), 2366 ng/μl (#100), 1325 ng/μl (V9-D2), 1913 ng/μl (V9-D6), 1988 ng/μl (III2-D4), 2101 ng/μl (III3-F10), 1272 ng/μl (III3-C8) and 1450 ng/μl (III3-B9). All conjugants show lower or markedly lower production levels than #88.

Figure 32 shows the expected ratio between #88 and #100, but were not significantly distinguishable. The mean values of strains were 2459 ng/μl (#88), 2673 ng/μl (#100), 1977 ng/μl (V10-F5), 1546 ng/μl (V10-C3), 1449 ng/μl (V10-B6), 1189 ng/μl (V11-F11), 2171 ng/μl (V11-E2) and 2139 ng/μl (III1-C5). All conjugants were significantly lower than #100 and #88.

Figure 33 shows the expected ratio between #88 and #100, but the standard deviation of #100

was very high. The mean value of strains were 2260 ng/μl (#88), 2602 ng/μl (#100), 2130 ng/μl (III3-C3), 1731 ng/μl (III1-E10), 1913 ng/μl (III1-C4), 1984 ng/μl (III1-B10), 2136 ng/μl (III4-B9) and 2042 ng/μl (III6-C4). Comparing the results with #88 all conjugants showed equal or lower production.

Figure 34 shows the expected ratio between #88 and #100. The mean values of strains were 2384 ng/μl (#88), 2577 ng/μl (#100), 2232 ng/μl (III6-D8), 2131 ng/μl (III8-D9), 2365 ng/μl (III8-B5), 2238 ng/μl (III9-E11), 2079 ng/μl (III9-G2) and 2002 ng/μl (III10-D11). None of the conjugants did exceed the standard deviation range of #88 and all valencene concentrations were significantly lower than the control strain #100.

Figure 35 shows the expected ratio between #88 and #100, but the standard deviation of #100 was very high. The mean values of strains were 2580 ng/μl (#88), 2961 ng/μl (#100), 2543 ng/μl (V10-B10), 2468 ng/μl (V5-C2), 2566 ng/μl (V6-F3), 2352 ng/μl (V8-F7), 2140 ng/μl (V9-F2) and 2433 ng/μl (V9-B6). There were no conjugants that outperformed the reference strain #88.

Figure 36 shows the expected ratio between #88 and #100. The mean values of the strains were 2398 ng/μl (#88), 2875 ng/μl (#100), 2335 ng/μl (V10-C10), 2359 ng/μl (V10-F7), 3052 ng/μl (V10-G7), 2970 ng/μl (V2-G5), 2696 ng/μl (V2-D5) and 2781 ng/μl (V3-B5). Two *Pppa* mutants had high standard deviations and were chosen for 96-well DWP cultivation. Further two conjugants were significantly better than #88 and were chosen for 96-well DWP cultivation. Two conjugants showed the same level of (+)-valencene production as #88.

Figure 37 shows the expected ratio between #88 and #100, but standard deviation for #88 was very high. The mean values of the strains were 2337 ng/μl (#88), 2949 ng/μl (#100), 1993 ng/μl (V3-B6), 2301 ng/μl (V3-E5), 2484 ng/μl (V3-D10), 2389 ng/μl (V3-E7), 2637 ng/μl (V4-D5) and 2602 ng/μl (V4-E9). All conjugants were in the range of #88, but none of the conjugants reached the level of #100.

Overall, the selected conjugants did not show a similar behavior as in the rescreening. Most of the chosen conjugants from the rescreening showed lower levels of (+)-valencene than the reference strain #88. But standard deviations of conjugants and #88 often overlapped. For further analysis in the 96-well DWP with n-dodecane, the conjugants V8-C3, V2-F6, V4-D9 V6-D10, V6-D9, V10-G7, V2-G5, V2-D5 and V3-B5 were chosen. Although some conjugants had not been significantly improved in the 24-well DWP cultivation, they showed a high mean valencene concentration.

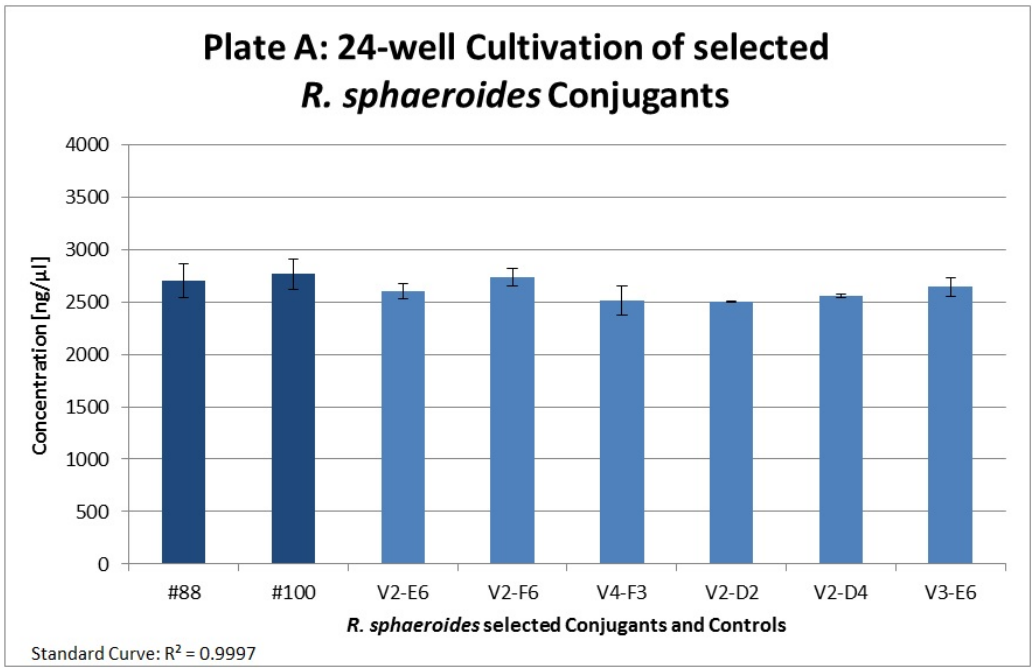

Figure 29: **Cultivation of promising conjugants in 24-well deep well plates.** Strains marked with an asterisk were measured in duplicates. Other strains were measured in triplicates. Depicted (+)-valencene concentration refers to concentration in n-dodecane. Mean values and standard deviation are given.

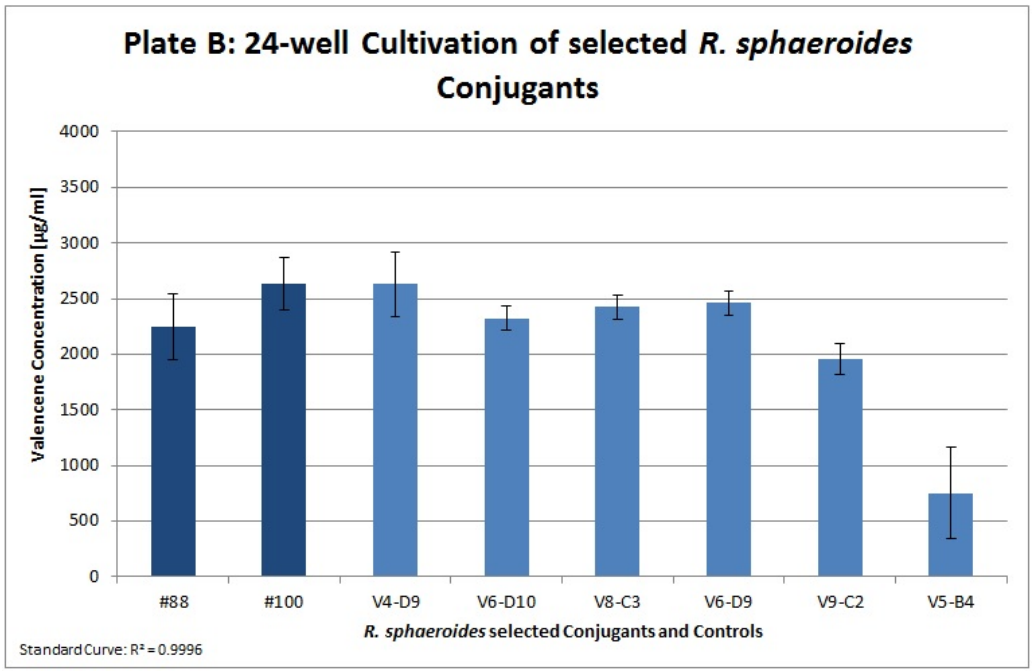

Figure 30: **Cultivation of promising conjugants in 24-well deep well plates.** See legend of Figure 29.

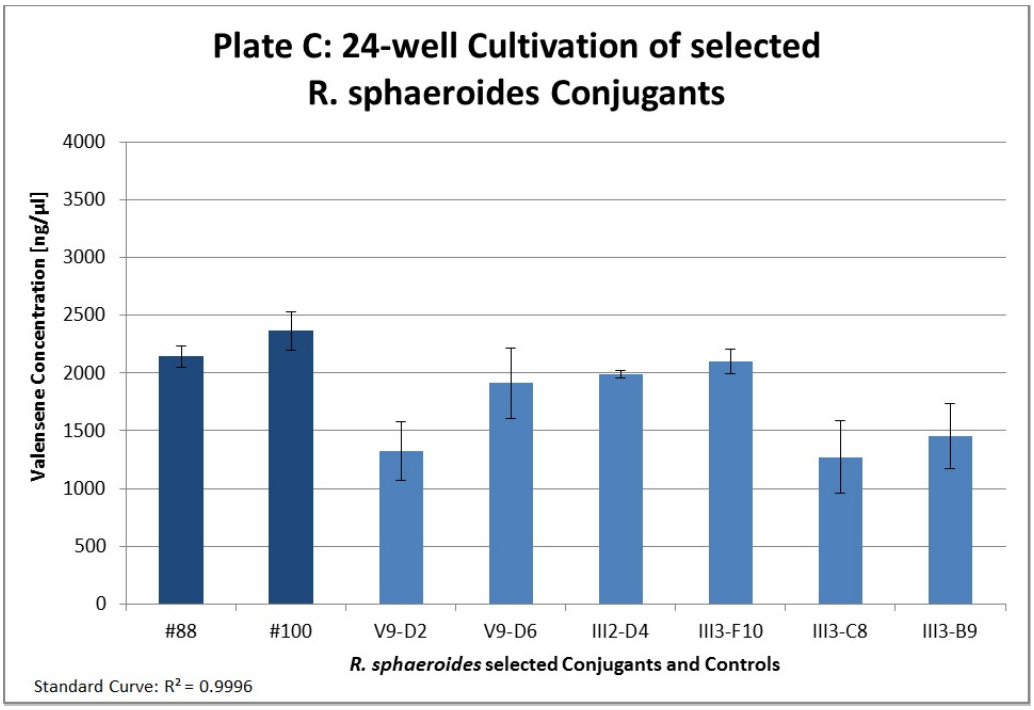

Figure 31: **Cultivation of promising conjugants in 24-well deep well plates.** See legend of Figure 29.

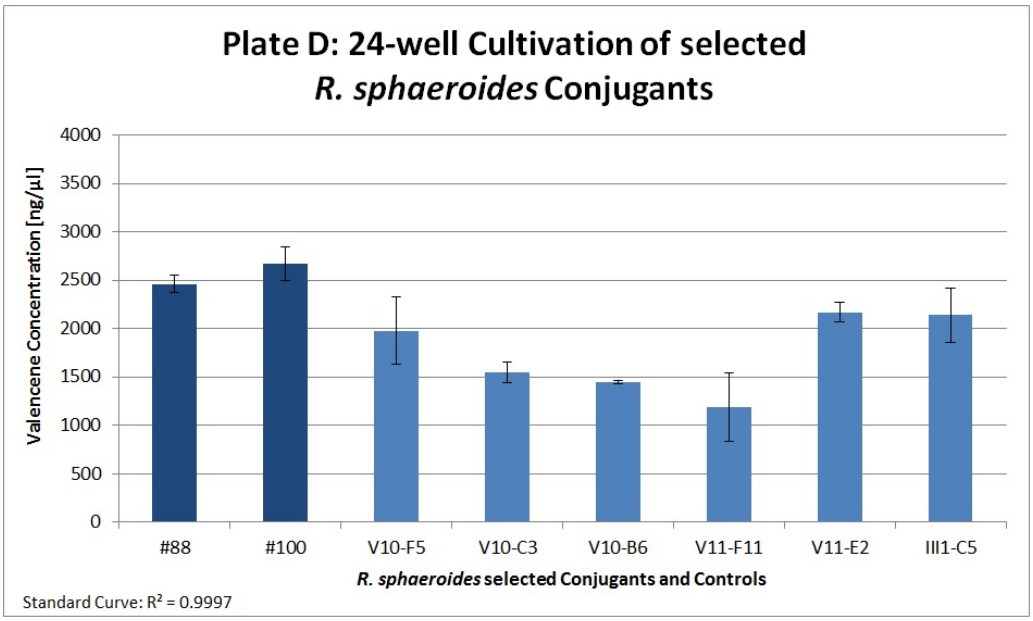

Figure 32: **Cultivation of promising conjugants in 24-well deep well plates.** See legend of Figure 29.

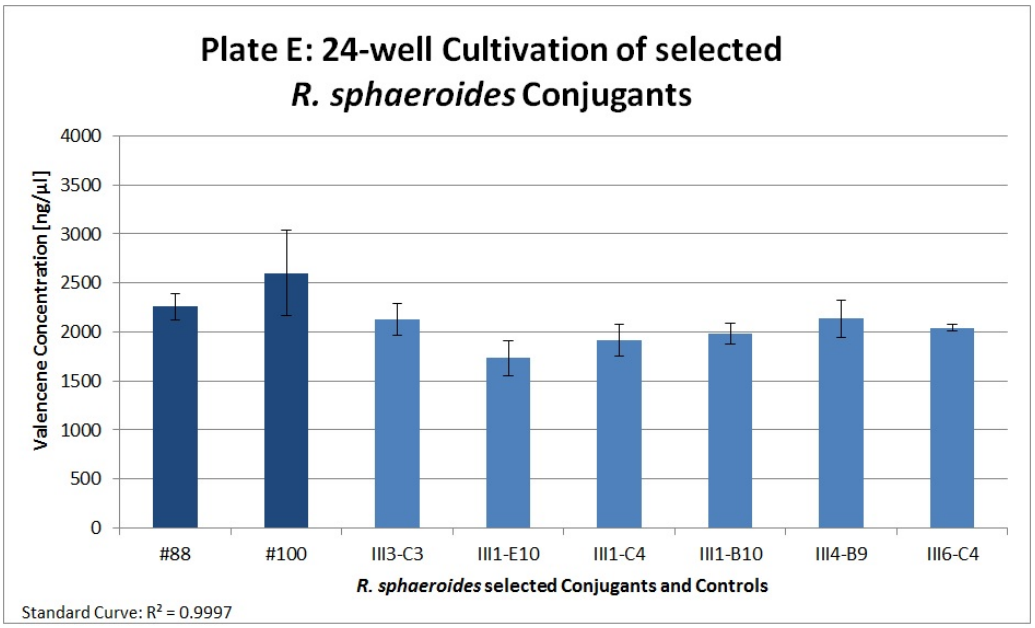

Figure 33: **Cultivation of promising conjugants in 24-well deep well plates.** See legend of Figure 29.

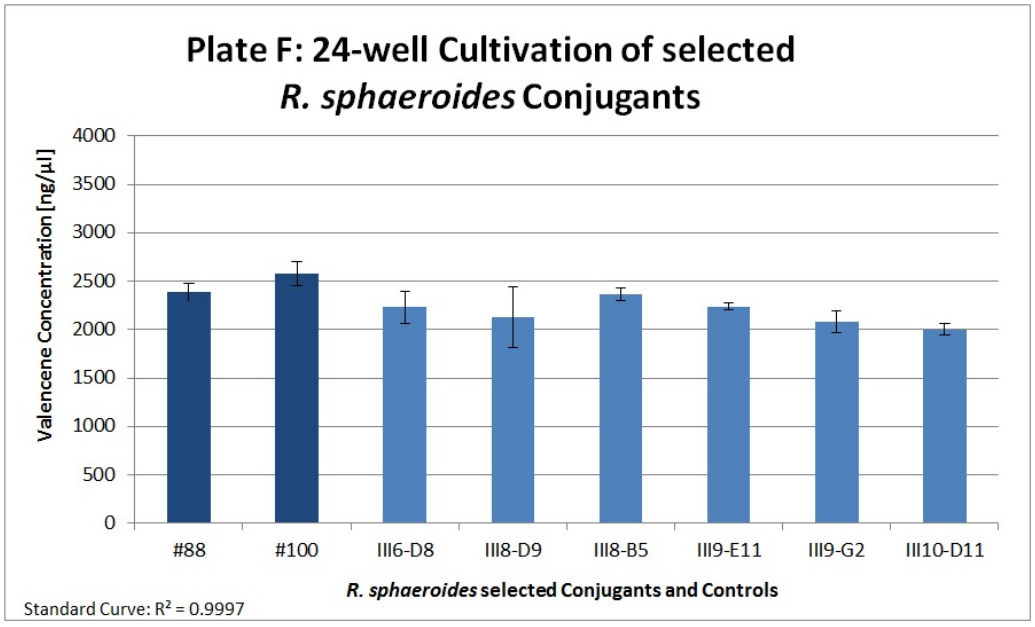

Figure 34: **Cultivation of promising conjugants in 24-well deep well plates.** See legend of Figure 29.

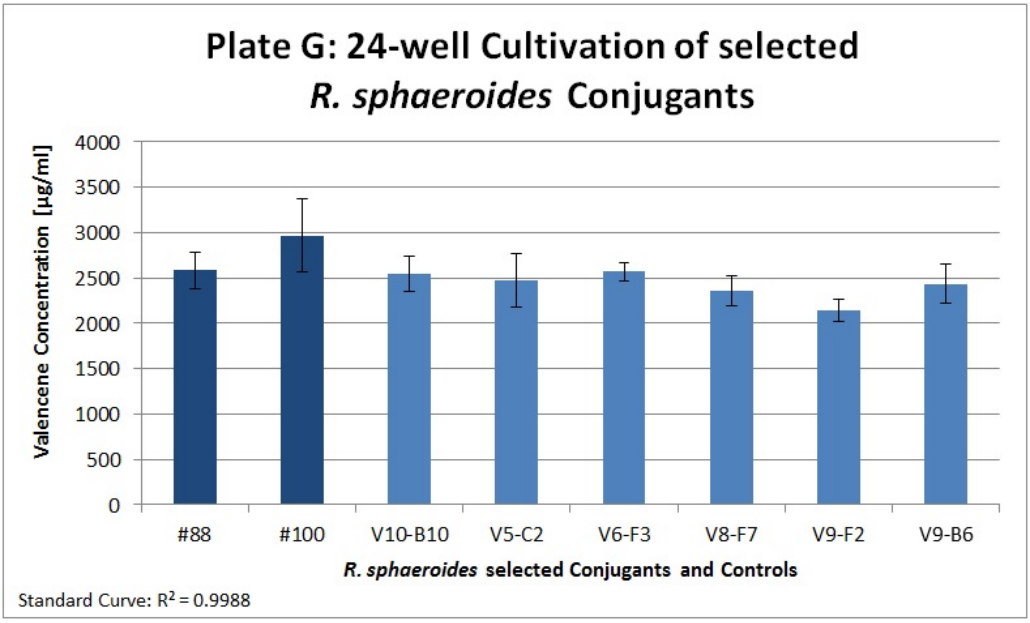

Figure 35: **Cultivation of promising conjugants in 24-well deep well plates.** See legend of Figure 29.

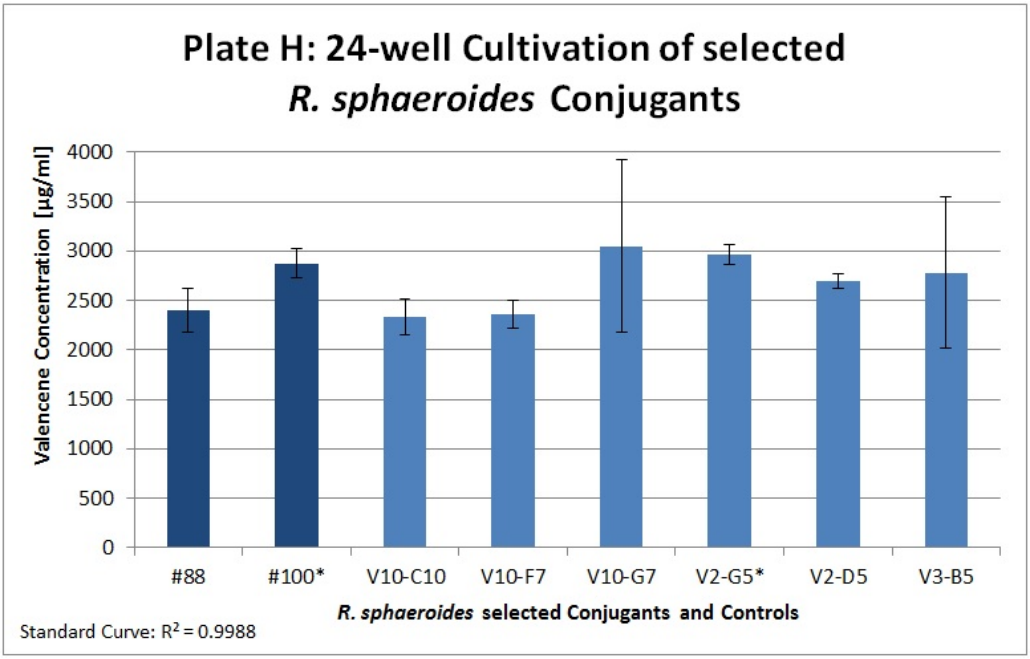

Figure 36: **Cultivation of promising conjugants in 24-well deep well plates.** See legend of Figure 29.

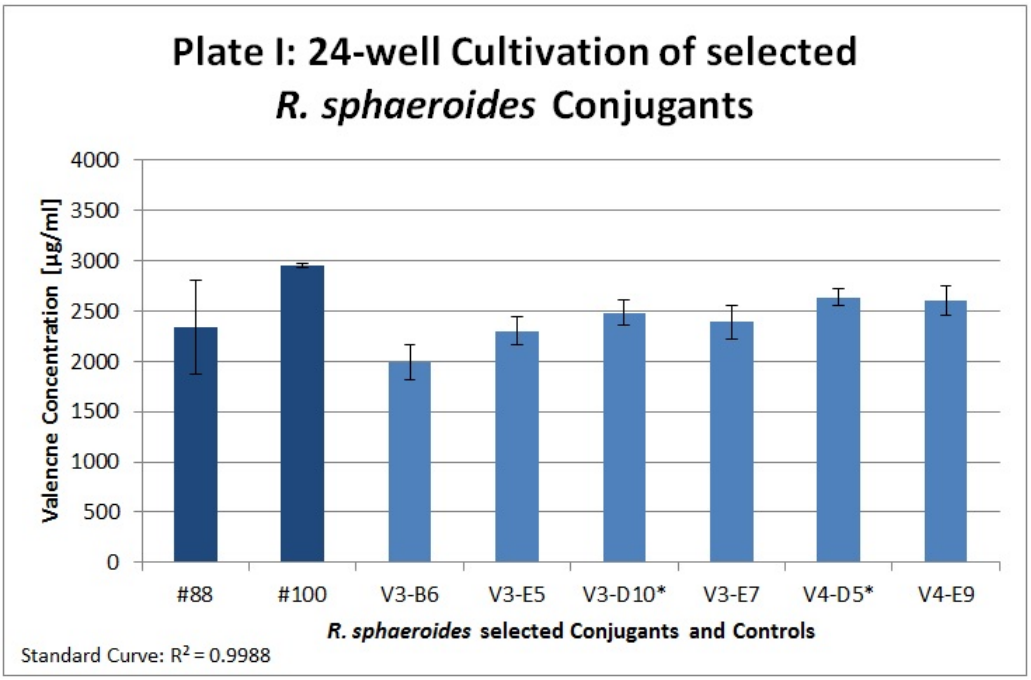

Figure 37: **Cultivation of promising conjugants in 24-well deep well plates.** See legend of Figure 29.

6.3.4 Promising conjugants in 96-well DWP cultivation

The 24-well cultivations did not give a clear indication whether any ot the conjugants yielded in improved (+)-valencene production (Figure 38). Therefore, a 96-well DWP cultivation was performed. Again n-dodecane and GC-FID was used. The control strain #100 was analyzed 6 times. All other strains were analyzed 5 times. The results of the cultivation showed a significant difference between the two reference strains. The mean values of strains were 1809 ng/μl (#88), 2089 ng/μl (#100), 1882 ng/μl (V8-C3), 1831 ng/μl (V2-F6), 1826 ng/μl (V4-D9), 1705 ng/μl (V6-D10), 1869 ng/μl (V6-D9), 1943 ng/μl (V10-G7), 1860 ng/μl (V2-G5), 1870 ng/μl (V2-D5) and 1781 ng/μl (V3-B5). Only one conjugant had a standard deviation that overlapped slightly with the one of control strain #100. The other conjugants were all in the range of #88. There was no evidence for an improved *Pppa* mutant. Still, three conjugants (V2-G5, V4-D9 and V10-G7), which had looked most promising in the rescreening, 24-well DWP cultivation and in the 96-well cultivation were also cultivated in flasks.

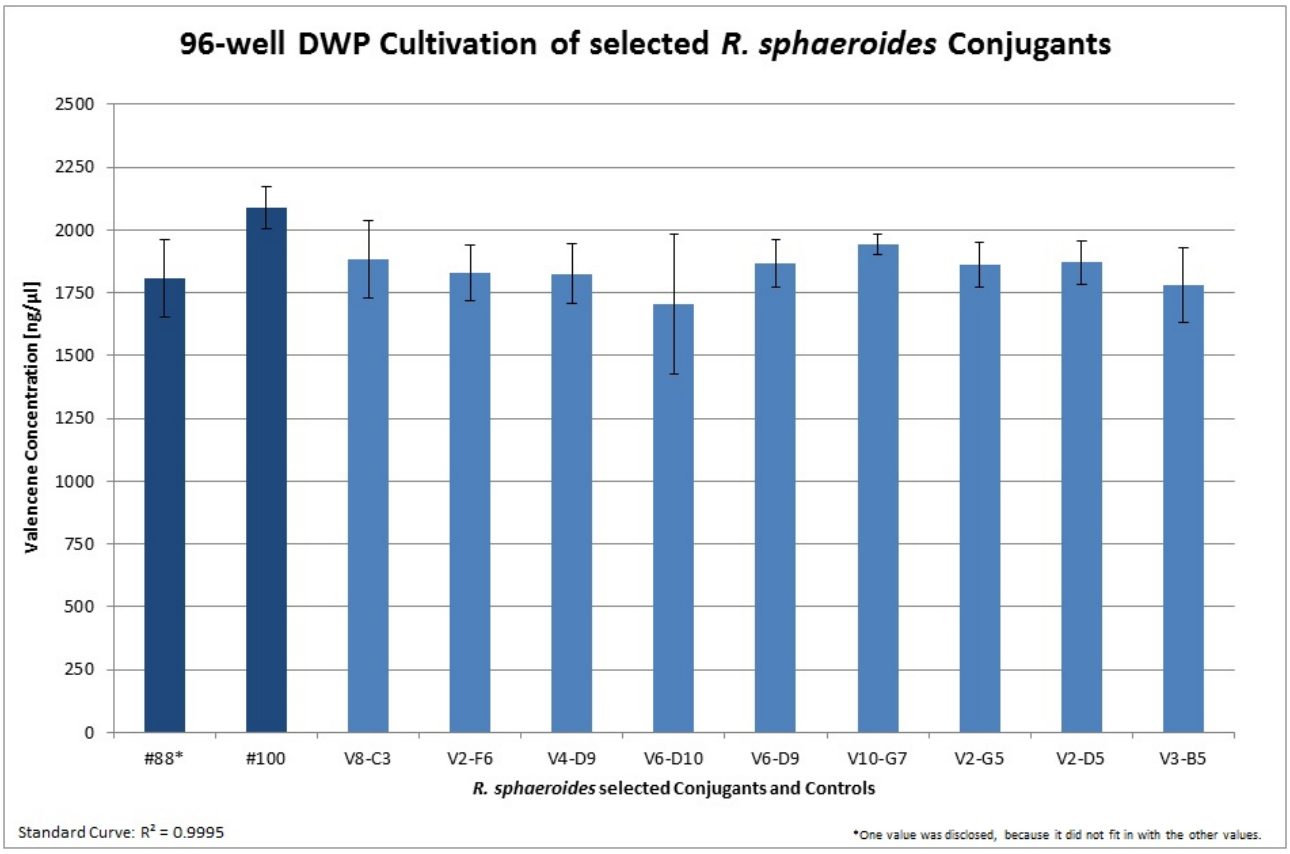

Figure 38: **Cultivation of promising conjugants in 96-well deep well plates.** Control strains were measured 6 times and *Pppa* mutant strains 5 times. Depicted (+)-valencene concentration refers to concentration in n-dodecane. Mean values and standard deviation are given.

6.3.5 Promising conjugants in flask cultivation

The most promising conjugants were cultivated in flasks (39). This also appears to be the standard measurement method of our company partner. The results showed again that a significant improvement of the conjugants was not achieved. The #88 and #100 reference strain differed significantly. All three conjugants overlapped with the standard deviation of #88. The mean values of the strains were 6605 ng/μl (#88), 8447 ng/μl (#100), 5532 ng/μl (V2-G5), 6859 ng/μl (V4-D9) and 7160 ng/μl (V10-G7).

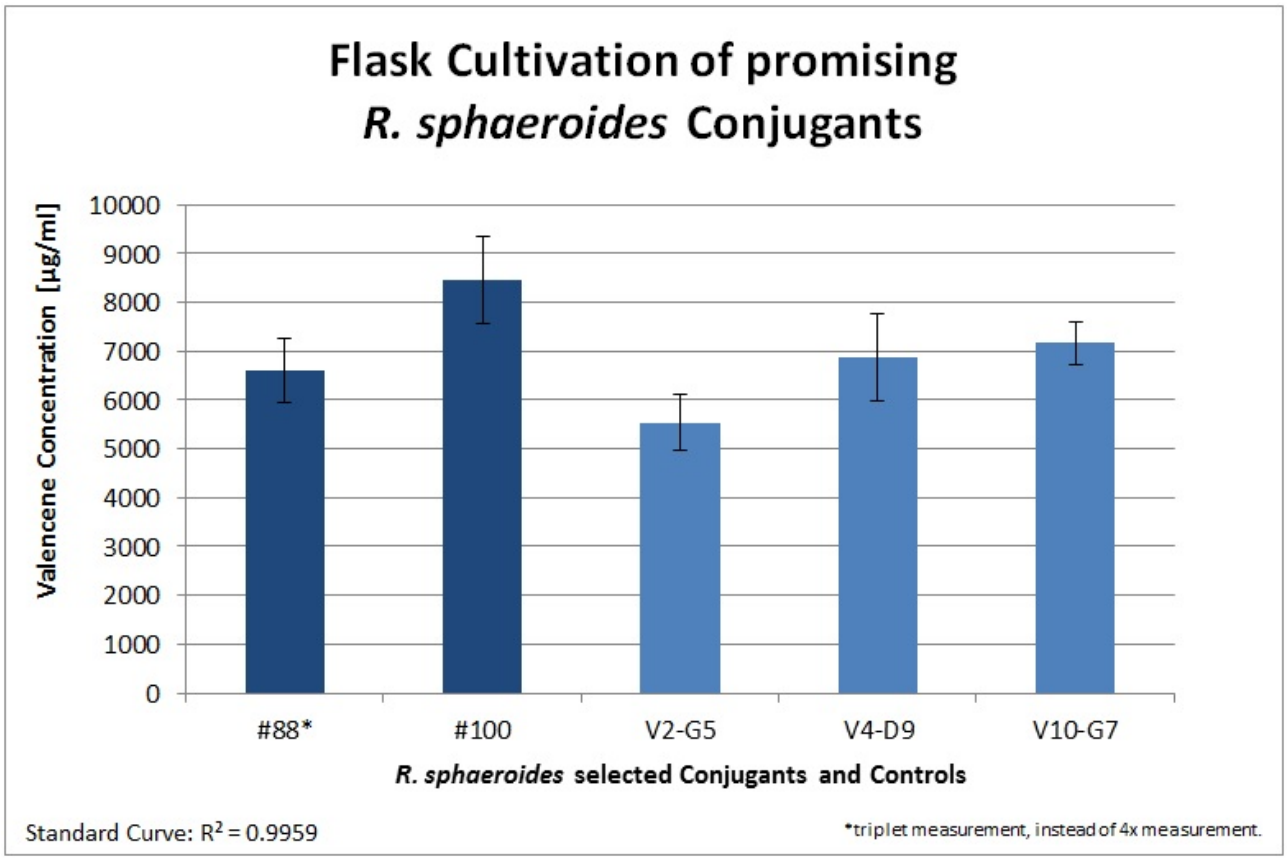

Figure 39: **Cultivation of promising conjugants in flasks** Depicted (+)-valencene concentration refers to concentration in n-dodecane. Mean values and standard deviation are given.

6.3.6 Sequencing and restriction analysis of plasmids from conjugants not producing (+)-valencene

After transformation of the two libraries into *R. sphaeroides* it turned out that 80% of conjugants did not produce (+)-valencene detectable in the screening assay. Since they were growing on media with kanamycin, they apparently still had the resistance cassette, which is encoded on the plasmid. The resistance gene on the plasmid was seemingly intact. But what happened to the rest of the plasmid? To find an answer to this question we decided to sequence the isolated plasmids. For the sequencing, seven conjugants were used that did not create a signal on the screening films. Starting location was the *Pppa* promoter region. From this point sequencing primers spread further. Sequencing failed most of the time. Apparently, sequencing primers were unable to bind to the complementary regions. Finally three plasmids could be sequenced. We found out that each plasmid lacked about 7000 bp at different loci on the plasmid.

For III6-C2 (Rev-LibSeq-6) the region from 11319 bp to 813 bp was deleted. Size of deletion was 7339 bp. This knocked out the genes hcs, mvk, pmk, mvd, valencene synthase and Pz-mvk-alt. The deletion sides were not connected to the cloning strategy. For III11-F6 (Rev-LibSeq-4) the deletion took place from 8652 bp to 16323 bp. Deleted part was 7671 bp. At 16321 bp the SgrDI restriction site is located, that was used in the cloning strategy. This knocked out the genes mvaA, idl, hcs, mvk, pmk, mvd and the valencene synthase. For III13-F9 (Rev-LibSeq-4) the region from 9244 bp to 16321 bp was deleted. Deleted part was 7085 bp. Situation was similar as in the strain above.

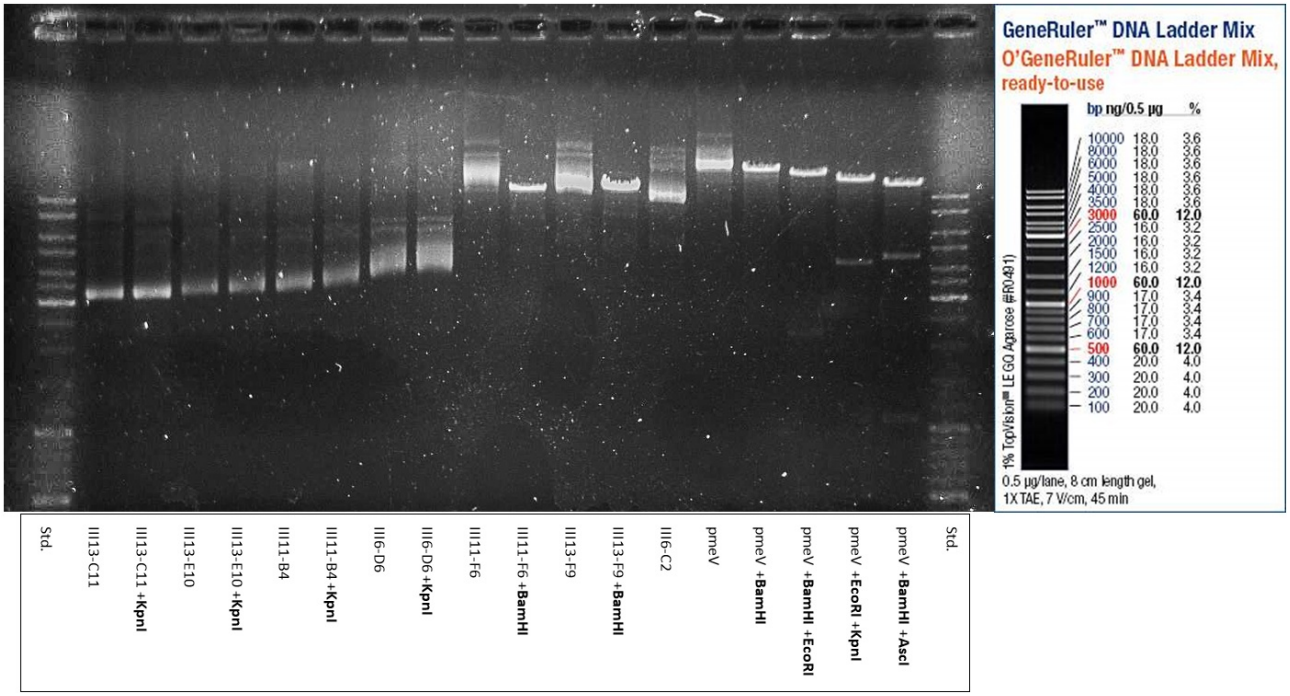

Figure 40: **Restriction analysis.** Gel ran 90 min at 120 V. Each lane contained about 300 ng DNA. The wild type plasmid (pmeV) was strategically cut to serve as an extended standard. pmeV +BamHi +EcoRI: 2250 bp + 15600 bp. pmeV +EcoRi +KpnI: 4250 bp + 13500 bp. pmeV +BamHI +AscI: 1100 bp + 4500 bp + 12200 bp. Image was linearly modified for better depiction.

Since sequencing continuously failed for the other four plasmids, a restriction analysis was per-

formed (Figure 40). The restriction analysis showed that the plasmids of the conjugants III11-F6 and III13-F9 had been linearized by BamHI. The size of the two plasmids on gel fits the calculation with the deletions. III13-F9 even showed a band that ran a little higher, since the deletion is around 600 bp shorter. Based on the information from sequencing, it was apparent that the isolated plasmid could not be cut by any restriction enzyme available in house. The plasmids of conjugants that could not be sequenced, were also not cut by KpnI. The running behavior of the plasmids in gel was not similar. They all showed a band that was between 3,000 bp and 4,000 bp. Size may vary, because plasmids were not linearized.

Overall, seven negative conjugants were analyzed. Two of them had a 7000 bp deletion that took place at a restriction site used in the cloning strategy. One conjugant had a 7,000 bp deletion, that could not be linked to the cloning strategy. Four out of seven conjugants had approximately a 14,000 bp deletions. Only about 4,000 bp remained. The minimal vector backbone is at least 3706 bp large (4913 bp to 8619 bp) and contains the origin of replication, the kanamycin resistance and the mobility gene for plasmid transfer. This seems like a fitting explanation for the remaining 4,000 bp plasmid and explains why the conjugants still grew in the presence of kanamycin.

6.4 Biological example: *Pichia pastoris* and the *GAP* promoter

In order to prove that *P. pastoris* is a promising host that might be used in the developed screening assay we chose two different approaches. The first and easier approach is described in this chapter. In *R. sphaeroides* we had used a constitutive promoter for (+)-valencene production. We adopted this concept to the yeast *P. pastoris* by using the constitutive *GAP* promoter. This approach gave us the opportunity to use our knowledge from screening *R. sphaeroides* to find a representative time interval for screening. Additionally, a GC-FID measurement was performed to compare the results from the screening with the actual (+)-valencene concentrations in n-dodecane after 72 h. Switching to *Pichia pastoris* as a plattform for the screening assay was of special interest, because we knew from previous studies that production of (+)-valencene was about a factor 10 lower compared to *R. sphaeroides*. Achieving results at that low concentrations would set a new benchmark for our screening.

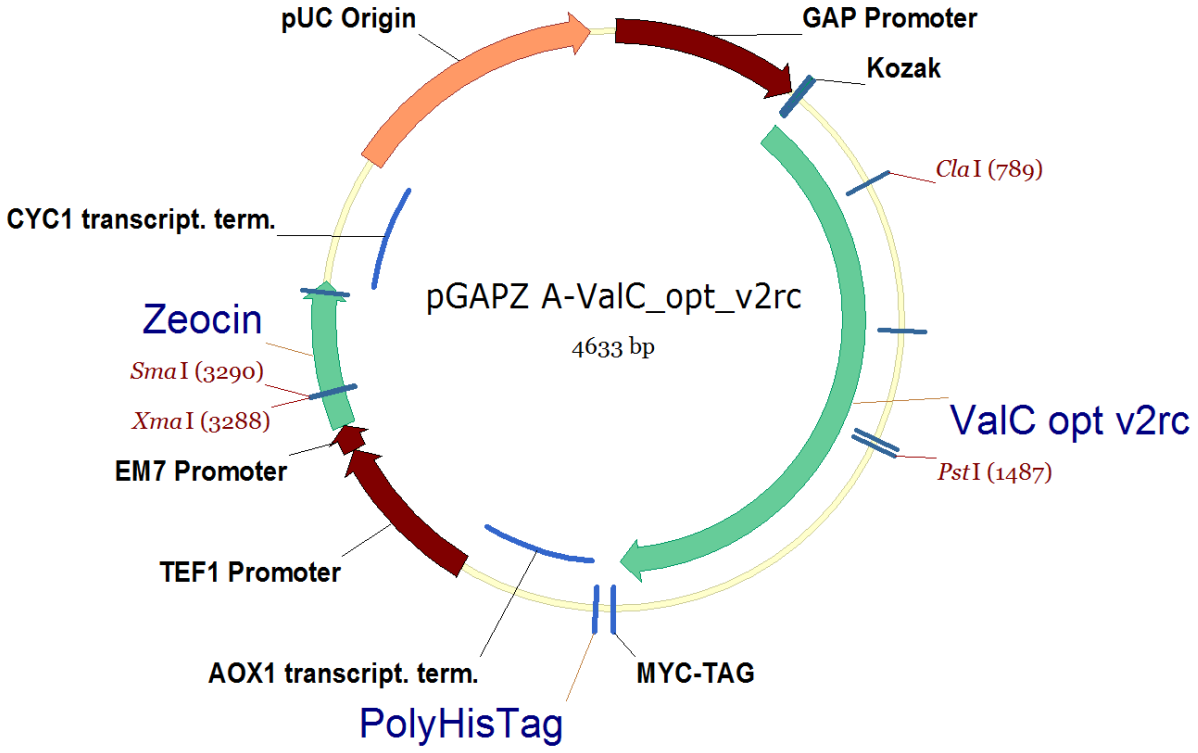

Figure 41: **Plasmid transformed into *Pichia pastoris***

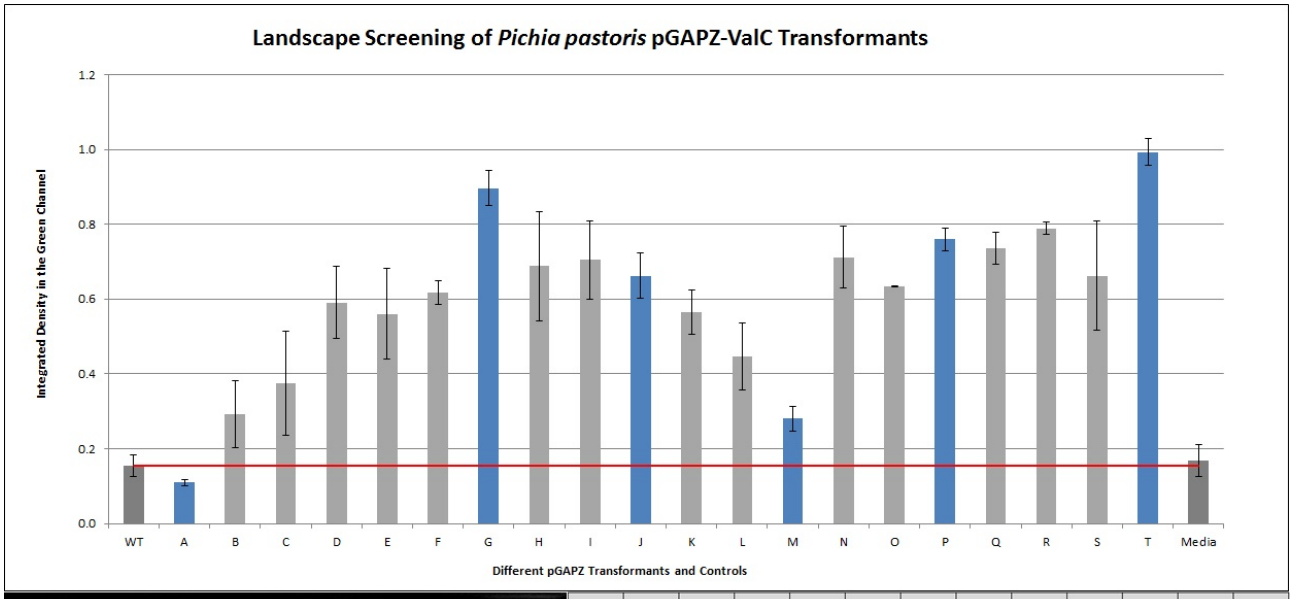

	1	2	3	4	5	6	7	8	9	10	11	12
A	-	-	-	-	-	-	-	-	-	-	-	-
B	-	-	-	-	-	-	-	-	-	-	-	-
C	-	A	B	C	D	E	F	G	H	I	J	-
D	-	A	B	C	D	E	F	G	H	I	J	-
E	-	WT	WT	WT	WT	WT	Media	Media	Media	Media	Media	-
F	-	K	L	M	N	O	P	Q	R	S	T	-
G	-	K	L	M	N	O	P	Q	R	S	T	-
H	-	-	-	-	-	-	-	-	-	-	-	-

Figure 42: **Screening for (+)-valencene production in pGAPZ A-ValC_opt_v2rc transformants.** The wild type (WT) strain *P. pastoris* CBS7435 and the media showed a faint signal. The strains transformed with the plasmid pGAPZ A-ValC_opt_v2rc show signals varying in strength.

We used genomic integration to create *P. pastoris* strains containing the *GAP* promoter in front of a valencene synthase. A linear plasmid was transformed into competent *P. pastoris* cells. The use of linearized plasmid (AvrII) increases the chance of genomic integration by insertion or replacement mechanisms. After transformation 20 transformants were randomly picked from the plate, cultivated in hDWP and screened in duplicates (Figure 42). Since the generation time of *P. pastoris* and *R. sphaeroides* were nearly the same through a few trials and knowledge about the behavior of *R. sphaeroides* a good screening interval was found. It turned out that the screening interval from 18 h to 22 h after inoculation gave the most promising results (Figure 42). The screening of *GAP-ValS* transformants was the only one that has been evaluated with Image Subtraction (see 6.2.3). The values of the Y-axis differed compared to the other screenings, because of the image subtraction. Each pixel was subtracted from the value before the screening. Therefor the remaining pixel values were quite low since they represented only the the alteration during the screening. The transformants were measured in biological duplicates with the same positioning as the GC-FID samples since both of them originated from the same preculture. The wild type (WT) strain and the media (YPD) control were measured 5 times. The screening showed clearly that the WT did not give a signal compared to

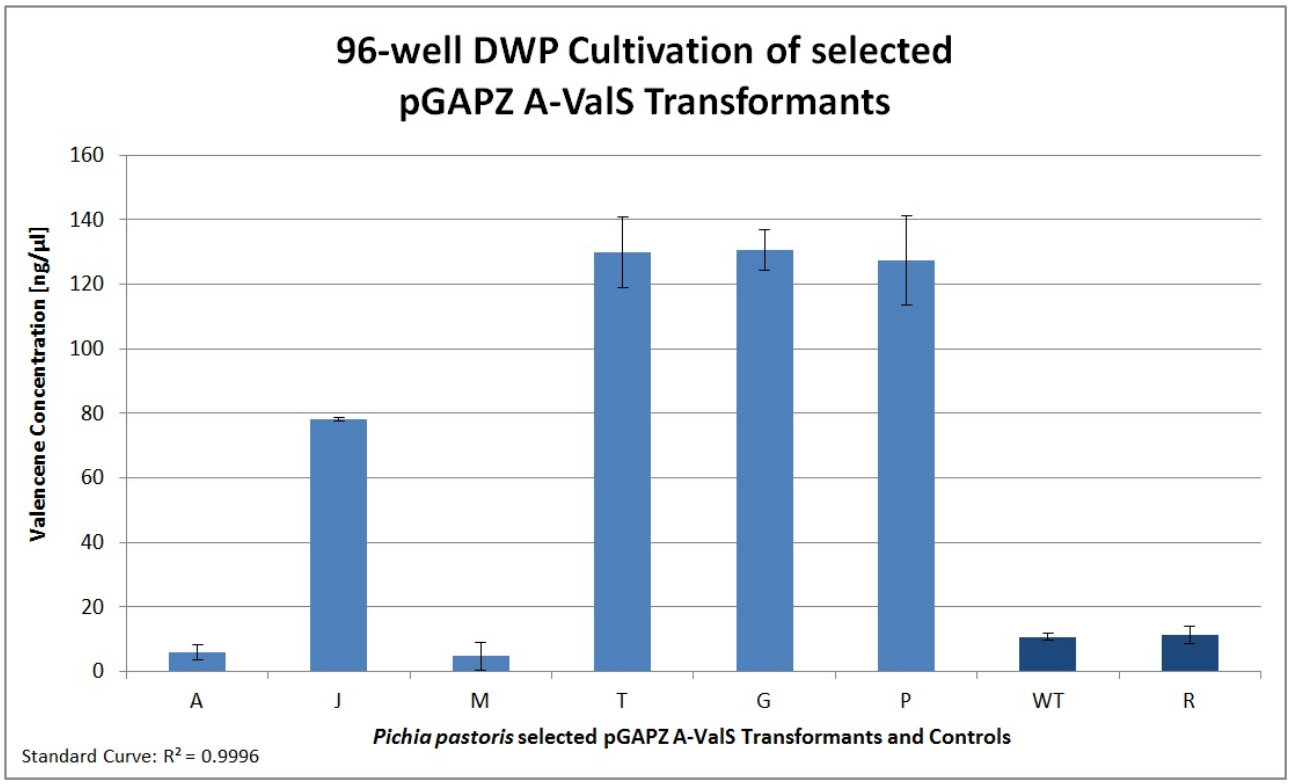

Figure 43: **(+)-Valencene endpoint measurement of *GAP-ValC* transformants with GC-FID.** Alphabetical letters label 6 selected *GAP-ValC* transformants. The depicted concentrations refer to the concentration in the n-dodecane phase after 72 h. Each transformant was measured in triplicates. A contamination peak close to (+)-valencene led to misidentification of small (+)-valencene concentration for media and WT control. Mean values and standard deviation are given.

the media. This result was expected since the CBS7435 strain does not have the intrinsic features to produce terpenes or other volatile hydrophobic compounds in large quantities. Also YPD media did not emit high amounts of volatile hydrophobic compounds as expected. Therefore, the signal of the transformants must originated from the genomically integrated plasmid. This integration event may happen randomly. Depending on where in the genome the integration event takes place, the activity might vary. This is due to the fact that some genomic reagions are more silenced than others. This variation in activity was seen in all the measurements. In the landscape screening the transformants G and T were the strongest. The weakest performers according to the screening were the transformants A and M. In addition to the two weakest and two strongest producers, two transformants with mediocre (+)-valencene production were picked for rescreening and GC-FID measurement. The GC-FID measurement showed the (+)-valencene concentration in the n-dodecane phase in ng/μl after a cultivation time of 72 h for the 6 selected transformants (Figure 43). The antibiotic resistance of the *Pichia pastoris GAP-ValC* transformants was not a direct prove for successful production of (+)-valencene or for the integration of the gene of interest. GC-FID showed differences in production of (+)-valencene between the strains. A supposed contamination complicated the evaluation of the GC data and created a small overlapping peak area of about 10 right next to the (+)-valencene peak. This peak was automatically included in the evaluation and, thus, explains why the wild type and media positions featured a small (+)-valencene content. The *GAP*-ValS transformants G, P and

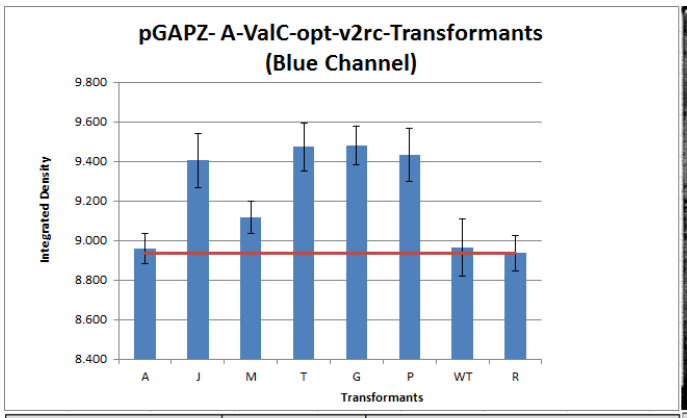

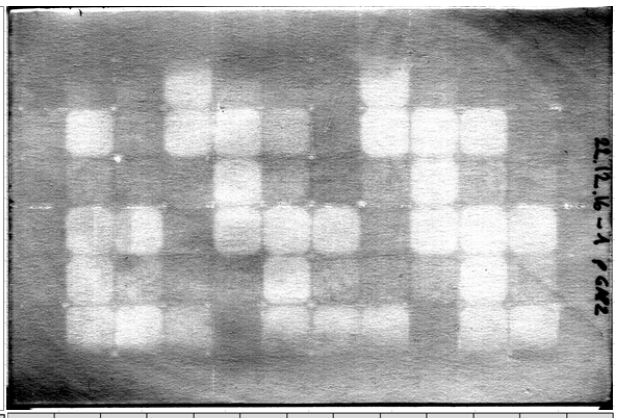

	Mean	Standard Deviation
A	8.962	0.076
J	9.406	0.138
M	9.118	0.082
T	9.475	0.120
G	9.480	0.097
P	9.435	0.134
WT	8.965	0.143
R	8.936	0.088

	1	2	3	4	5	6	7	8	9	10	11	12
A	-	-	-	-	-	-	-	-	-	-	-	-
B	-	A	WT	G	M	A	WT	G	M	A	WT	-
C	-	J	R	P	T	J	R	P	T	J	R	-
D	-	M	A	WT	G	M	A	WT	G	M	A	-
E	-	T	J	R	P	T	J	R	P	T	J	-
F	-	G	M	A	WT	G	M	A	WT	G	M	-
G	-	P	T	J	R	P	T	J	R	P	T	-
H	-	-	-	-	-	-	-	-	-	-	-	-

Figure 44: **Screening for (+)-valencene production in pGAPZ A-ValC_opt_v2rc transformants.** The wild type (WT) strain *P. pastoris* CBS7435 and the media do not show a signal. The strains transformed with the plasmid pGAPZ A-ValC_opt_v2rc show signals varying in strength.

T seemed to be the strongest (+)-valencene producers. On the other hand the transformants A and M did not seem to produce (+)-valencene at all. The transformant J was a mediocre (+)-valencene producer in the GC-FID measurement. A comparison between landscape screening and GC-FID measurement showed the same results with one exception. The transformant P showed mediocre (+)-valencene production in the landscape screening, however higher (+)-valencene productivity in the GC-FID measurement. One has to take into account, that the cultivation parameters differed between the screening and the GC-FID. The GC-FID measurement was an end-point measurement while the screening only showed a representative interval of 3 h. Cultivation conditions were also slightly different, since n-dodecane influenced oxygen transfer and other parameters in culture.

The rescreening (Figure 44) of the 6 transformants showed similar results as the landscape screening. In the rescreening the mediocre transformants P and J showed (+)-valencene production similar to the transformants G and P. In general the results matched perfectly the GC-FID. Only the transformant M showed low production in the screening, but none in the GC-FID measurement. A possible explanation for this small rise in signal intensity of transformant M can be the oxygen sensitivity of *Pichia pastoris*. The cultivation conditions for GC-FID measurement deprived *Pichia pastoris* of oxygen with 18.2% n-dodecane and the microaerobic lid on top.

6.5 Biological example: *Pichia pastoris* and the *AOX1* promoter

The method to use a constitutive promoter in *Pichia pastoris* was shown in the previous chapter (see 6.4) and the *GAP* promoter). In this chapter we focused on the approach of using the tightly regulated *AOX1* promoter. The *AOX1* promoter has been vastly investigated and is used by industry, because of its tight regulation and strong transcriptional activity. By integrating a gene of interest in this locus in front of the *AOX1* promoter one can use its properties for gene of interest expression. The strains for this experiment were created by Wriesnegger et al..[20]

To test our screening assay under the inducing conditions of methanol, we used three different strains. Again, we chose to use n-dodecane cultivation in parallel to compare the results. The ValS strain only produced (+)-valencene. The HCV strain produced not only (+)-valencene, but also high levels of trans-nootkatol and small amounts of (+)-nootkatone. In the HCVA/tHMG strain the production of (+)-nootkatone is further pushed. It was accomplished by integrating not only the *ValC* gene, but also the *CPR* gene for the cytochrome P450 reductase and the *HPO* gene for the premnaspirodiene oxygenase of *Hyoscyamus muticus*.

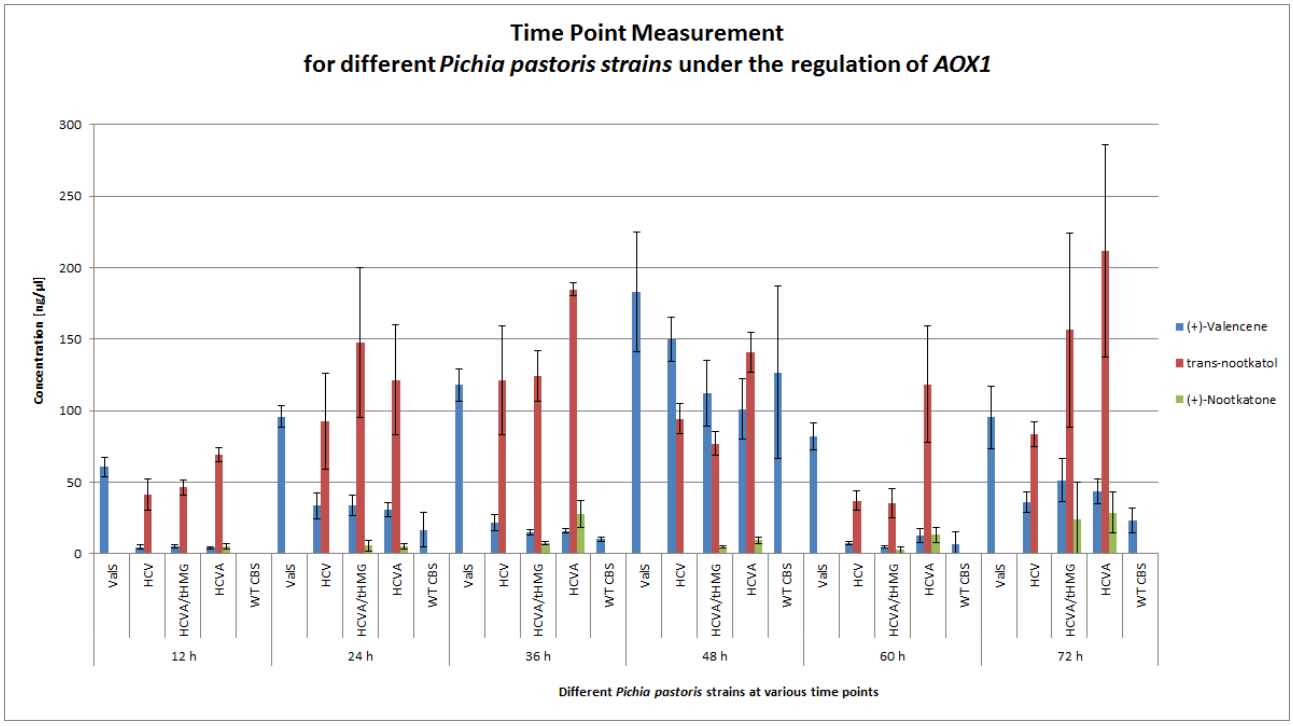

Figure 45: **Time point GC-FID measurement of *Pichia pastoris* strains ValS, HCV, HCVA/tHMG and HCVA under the control of the *AOX1* promoter.** Each time point was one DWP. Depicted concentrations refer to the concentration in the n-dodecane phase. Mean values and standard deviation are given in triplicates.

The GC-FID measurement of the 4 strains and one wild type control was largely not leading to the expected resuls (Figure 45). Although we tried three times, samples always showed cross-contamination and terpenoid concentrations that did not match the expectations. Only the DWP for 24 h did not show (+)-valencene concentrations for the wild type. In the DWP at 60 h some of the concentrations were even lower than for the 12 h DWP. The time points 12 h, 24 h and 36 h could be interpreted. The ValS strain showed a constant increase in (+)-valencene concentration. In addition

the strongest increase was seen between 12 h and 24 h. For the HCV strain the development looked similar, but standard deviations were high at 24 h and 36 h. In the case of the HCVA/tHMG strain results did not reflect expectations. First, the graph did not show an increase of concentrations between 24 h and 36 h, and standard deviations were high. Second, the HCVA/tHMG strain was expected to produce significant amounts of (+)-nootkatone, which had never been seen during the measurements. The HCVA strain showed again a constant rise in concentrations from 12 h to 36 h. These results led to the conclusion that the HCVA/tHMG strain might have some genetic problems and cannot be further interpreted or compared with the screening. Additionally, the biggest difference in concentration levels was observed between 12 h and 24 h for all strains. This time interval was therefore considered for screening.

Since the results for the HCV/tHMG strain showed a discrepancy compared to the expected behavior the strain should be reconstructed. The fact that all of the genes were integrated at the same gene locus might have caused a desintegration event to take place. A possibility for the future might be the use of 2A peptides.[28]

In order to find the right screening interval with the *AOX1* promoter, a few trial studies were conducted. The time interval from 14 h to 19 h seemed to be the most promising one (Figure 46, 47). To investigate the influence of methanol in the screening we had chosen to treat one well without methanol induction. Again the CBS7435 was used as a wild type control since all other strains are based thereon. The three strains ValS, HCV and HCVA/tHMG were chosen for screening. The screening evaluation showed that, by choosing the right screening interval, an influence of methanol in the screening can be prevented. During the trial studies it was tried to screen directly after the induction. In these trials the control always showed a high signal and made the screening not evaluable. Waiting a few hours for the methanol to evaporate solved this problem. In the screening, the ValS strain gave the strongest signal. This might be due to the high sensitivity of nile red to (+)-valencene as seen in the compound-only experiment. The HCV strain gave a signal that was lower than the ValS strain, but still significantly stronger than the media and wild type control. Since we do not yet know a lot about the behavior of trans-nootkatol or (+)-nootkatone in combination with the screening assay, it is hard to give a precise explanation. In the compound-only experiment it was shown that trans-nootkatol did not give a signal, probably because of it's crystallization. In the case of (+)-nootkatone the concentration had to be increased by a factor of 5 to get significant color changes. The low response of nile red or the low volatility of (+)-nootkatone and trans-nootkatol might be an explanation for the low signals of the strains HCV and HCVA/tHMG. In the GC-FID measurement it was shown that the HCVA/tHMG strain did not behave as expected. This was also seen in the screening. Another possible explanation is that the strain produced higher amounts of (+)-nootkatone, which gave a weaker signal than trans-nootkatol. The results suggest that the screening assay allows us to distinguish between different *P. pastoris* strains under methanol inducing conditions.

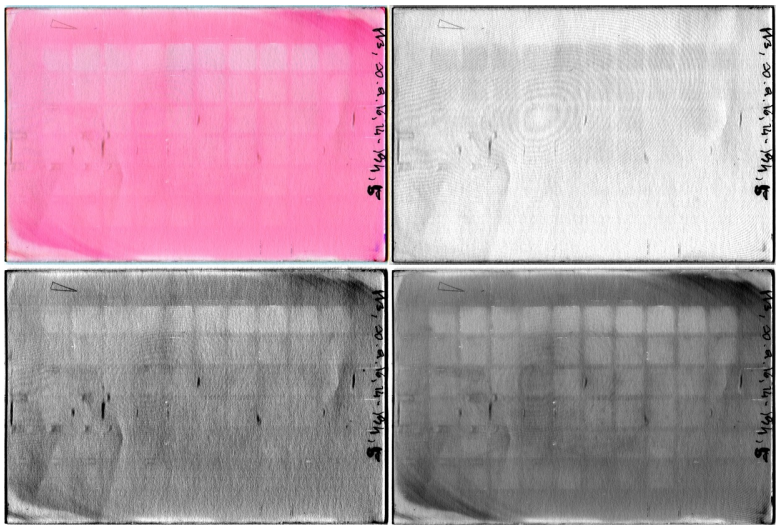

Figure 46: **Different color channels from *AOX1* screening.** Top left: RGB channel; Top right: Red channel; Bottom left: Blue channel; Bottom right: Green channel

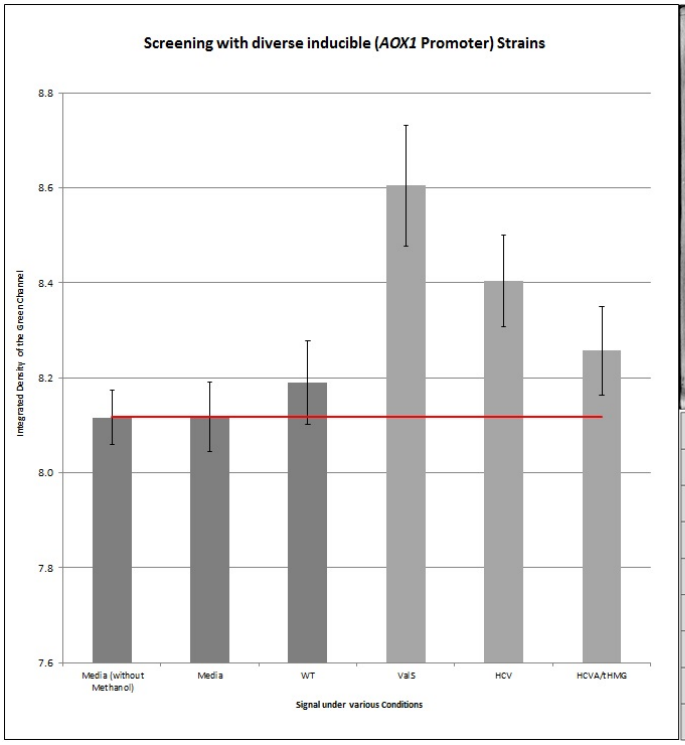

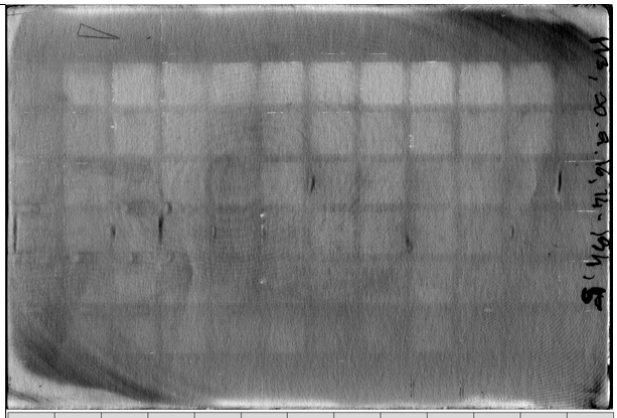

	1	2	3	4	5	6	7	8	9	10	11	12
A	-	-	-	-	-	-	-	-	-	-	-	-
B	-	ValC	ValC	ValC	ValC	ValC	ValC	ValC	ValC	ValC	ValC	-
C	-	HCV	HCV	HCV	HCV	HCV	HCV	HCV	HCV	HCV	HCV	-
D	-	HCVA/ tHMG	HCVA/ tHMG	HCVA/ tHMG	HCVA/ tHMG	HCVA/ tHMG	HCVA/ tHMG	HCVA/ tHMG	HCVA/ tHMG	HCVA/ tHMG	HCVA/ tHMG	-
E	-	WT	WT	WT	WT	WT	WT	WT	WT	WT	WT	-
F	-	Media	Media	Media	Media	Media	Media	Media	Media	Media	Media	-
G	-	Media w/o Methanol	Media w/o Methanol	Media w/o Methanol	Media w/o Methanol	Media w/o Methanol	Media w/o Methanol	Media w/o Methanol	Media w/o Methanol	Media w/o Methanol	Media w/o Methanol	-
H	-	-	-	-	-	-	-	-	-	-	-	-

Figure 47: **Screening under methanol inducing conditions.** Left: Screening interval started 14 h after first induction and lasted 5 h. At the 12 h time point another induction took place. Media (without methanol) refers do non induced media. Media refers to a mixture of BMGY and BMMY media that contained methanol. Top right: Evaluated screening film; Bottom right: Distribution over the plate.

7 Conclusion

The simple glass plate with a redish surface might tempt us to underestimate this piece of technology. The method of production is highly versatile. By using another material instead of trimethylsilylcellulose (TMSC) the polarity of the environment may be altered. Nile red is widely used for staining of cell cultures, but a whole spectrum of other dyes is on the market. According to our observations, chemical properties of each volatile compound interacting with the assay might influence the color on the screening film differently. In future, it could be possible to asses two or more compound concentrations simultaneously. Another approach could be to screen cultures with two different spin-coated screening assay films to evaluate the compound concentrations for two different substances. Furthermore, the screening evaluation is now established to be cheap and easy to set up. This is done by using light of the visible spectrum, but fluorescence has the potential to show signals in higher resolution by eliminating the stray light with filters.

The compound-only experiment already showed that more than a dozen compounds created a color change of the film. Only cis-nootkatol failed to create a signal, due to significant crystallization in the well. Since these compounds included also non-terpenoids, the assay is expected to detect many volatile, hydrophobic compounds under certain conditions. In addition, the ability to use the screening assay beyond microbiologically setups broadens the applicabilty to almost all molecules that are volatile and hydrophobic. The application area might reach from greenhouse gas detection to medical or pharmaceutical research. But main focus will currently remain on screening microbially produced terpenes.

Although the screening of the *Pppa* library failed for several reasons explained in this thesis, some valuable lessons have been learned. The failure was not associated to the screening principle. Due to the general cloning approach containing a large plasmid, conjugation as a transfer method and *E. coli* contamination or tellurite use, over 80% of the library lost their ability to produce (+)-valencene. With only about a population of 200 conjugants the chance to find an improved *Pppa* variant was drastically decreased. For the future it is important to create mutant libraries in *R. sphaeroides* that have a high proportion of active mutants. Taking a retrospective look at the rescreening results of the *Pppa* library shows that the assay did not mislead us. Focusing on the standard deviations of the reference strain #88 and the conjugants shows that hardly any variant of these promoter variants significantly outperforms #88. One of the next steps will be the application of the screening assay on another type of library to find improved strains using the further developed assay including state-of-the-art evaluation procedure. This will finally prove that the screening assay can be applied at least in a medium-throughput manner. Then, efforts can be made to lift the assay up into the category of high-throughput assays.

We managed to adapt the screening assay to the methylotrophic yeast *Pichia pastoris*. Both types of promoters – inducible and constitutive – can be used for the screening assay. The constitutive *GAP* promoter was placed in front of a valencene synthase and the construct was transformed into *Pichia pastoris*. Depending on the locus of genomic integration, the (+)-valencene production

can vary. In this case, landscape screenings are used to find the strongest performers. This has successfully been done with the *GAP* promoter. It seems also possible to use the assay for screening of byproducts. A reaction supposedly creates a hydrophobic and volatile byproduct, in for example an äquimolar ratio, and the signal on the screening assay can be related back to the actual reaction or product.

The *AOX1* promoter is commonly used in biotechnology. After cell growth stalls, when glucose of the growth phase is consumed, cells can be induced with methanol and energy is used for production. The inducer for the *AOX1* promoter is methanol, which is a hydrophobic, volatile compound and, therefore, a possible disturbing factor in our screening. As it turned out, by setting the screening interval to the right time false positive methanol signals can be circumvented.

Since *R. sphaeroides* and *P. pastoris* have been proven to be compatible with the screening assay, the variety of microorganisms should be further enlarged. Another yeast that was shown to produce (+)-valencene and has industrial applications is *Saccharomyces cerevisiae*. [29] Maybe the range of the screening assay can even be broadened to algae, mammalian or plant cells.

8 Appendix

8.1 Strain description

Table 6: **Strain description *Pichia pastoris***[20]

Strain	**Genotype**	**Description**
ValS	CBS7435 Δhis4, Δku70/pPpB1-Zeocin[ValS]	Encodes valencene synthase under the *AOX1* promoter
HCV	CBS7435 Δhis4, Δku70/pPpHIS4[HPO-CPR], pPpB1-Zeocin[ValS]	Encodes premnaspirodiene oxygenase, cytochrome P450 reductase and valencene synthase under the *AOX1* promoter
HCVA	CBS7435 Δhis4, Δku70/pPpHIS4[HPO-CPR], pPpB1-Zeocin[ValS], pPpKan-ADH-C3	Encodes premnaspirodiene oxygenase, cytochrome P450 reductase, valencene synthase and alcohol dehydrogenase under the *AOX1* promoter
HCVA/tHMG	CBS7435 Δhis4, Δku70/pPpHIS4[HPO-CPR], pPpB1-Zeocin[ValS], pPpKan-ADH-C3, pPpHYG[tHMG1]	Encodes premnaspirodiene oxygenase, cytochrome P450 reductase, valencene synthase and truncated hydroxy-methylglutaryl-CoA reductase under the *AOX1* promoter
GAP-ValS	CBS7435 Δhis4, Δku70/pGAPZ A-ValC_opt_v2rc	Encodes valencene synthase under the *GAP* promoter

Table 7: **Strain description *Rhodobacter sphaeroides*.**

Strain	Genotype	Description
#20	Rs265-9c/p-mev-PcrtE-trx-Aaas-mpmii-alt	Encodes amorphadiene synthase; highest terpene titers of all tested strains
#23	Rs265-9c/p-m-4-89-PcrtE-trx-ValC-single mutant	Encodes valencene synthase with a single mutation and the mevalonate pathway
#25	Rs265-9c/p-m-4-89-PcrtE-trx-ValC-H569I	Encodes valencene synthase with a single mutation and the mevalonate pathway
#30	Rs265-9c/p-m-4-89-PcrtE-trx-ValC-single mutant	Encodes valencene synthase with a single mutation and the mevalonate pathway
#37	Rs265-9c/p-m-4-89-PcrtE-trx-ValC-single mutant	Encodes valencene synthase with a single mutation and the mevalonate pathway
#38	Rs265-9c/p-m-4-89-PcrtE-trx-ValC-single mutant	Encodes valencene synthase with a single mutation and the mevalonate pathway
#88	Rs265-9c/p-m-4-89-Pppa-trx-ValC-S439G/Q492K/L566S	Encodes valencene synthase under the *Pppa* promoter with a three mutations and the mevalonate pathway
#100	Rs265-9c/p-m-4-89-Pppa-trx-ValC-S439G/Q492K	Encodes valencene synthase under the *Pppa* promoter with a two mutations and the mevalonate pathway
epi-Cedrol	Rs265-9c/pMevCC-pcrtE-trx-Ae-E-CedSopt	Encodes epi-cedrol synthase and the mevalonate pathway
Germacrene A	Rs265-9c/pMevCC-pcrtE-trx-CiGASshort-opt	Encodes germacrene A synthase and the mevalonate pathway

8.2 Medium

8.2.1 RÄ base medium

Table 8: **RÄ base medium for *R. sphaeroides*.** Selective medium after conjugation.

	1l	500 ml	250 ml
Malic acid	3 g	1.5 g	0.75 g
$MgSO_4$-7H_2O	0.2 g	0.1 g	0.05 g
$(NH_4)_2SO_4$	1.2 g	0.6 g	0.3 g
$CaCl_2$-2H_2O	0.07 g	0.035 g	0.0175 g
Microelements	1.5 ml	0.75 ml	0.375 ml
Adjusted to pH 6.9 with NaOH, bring volume to ___ and autoclaved	972 ml	486 ml	243 ml
Vitamins solution	8 ml	4 ml	2 ml
Phosphate buffer	20 ml	10 ml	5 ml

Table 9: **Mircoelements for the RÄ base medium.** Indicated recipe for a volume of 1 L, filter sterilized afterwards.

Fe(III)-Citrate	500 mg
$MnCl_2$-4H_2O	20 mg
$ZnCl_2$	5 mg
LiCl	5 mg
KBr	2.5 mg
KI	2.5 mg
$CuSO_4$-5H_2O	0.23 mg
Na_2MoO_4 or Na_2MoO4-2H_2O	0.851 mg or 0.999 mg
$CoCl_2$-6H_2O	5 mg
$SnCl_2$-2H_2O	0.5 mg
$BaCl_2$-2H_2O	0.59 mg
$AlCl_3$	1 mg
H_3BO_3	10 mg
EDTA	20 mg

Table 10: **Vitamin solution for the RÄ base medium.** Indicated recipe shows the information for a volume of 0.5 L. Filter sterilize.

Niacin	100 mg
Thiamin-HCl	200 mg
Nicotinamide	100 mg
Biotin	4 mg

Table 11: **Phosphate buffer for RÄ base medium.** Autoclave.

	1l	250 ml
KH_2PO_4	600 mg	150 mg
K_2HPO_4	900 mg	225 mg

8.2.2 PY plates

Table 12: **PY plates.** Conjugation for *R. sphaeroides* takes place on this medium.

	200 ml	400 ml	800 ml
Bacto peptone	2 g	4 g	8 g
Yeast extract	1 g	2 g	4 g
$CaCl_2$ (anhydrous) or $CaCl_2$-$2H_2O$	0.009 g or 0.01224 g	0.018 g or 0.02448 g	0.036 g or 0.04896 g
$MgCl_2$-$6H_2O$	0.0165 g	0.033 g	0.066 g
$FeSO_4$-$7H_2O$	0.011g	0.022 g	0.044 g
Adjusted to pH 7			
Bacto agar	3 g	6 g	12 g

8.2.3 RS102 medium

Table 13: **RS102 medium.** Complex medium for *R. sphaeroides*.

	200 ml	400 ml	900 ml
Yeast extract (Gistex, DSM)	4 g	8 g	18 g
NaCl	0.1 g	0.2 g	0.45 g
Dextrose monohydrate	6.6 g	13.2 g	29.7 g
brought to pH 7.4 with NaOH and autoclaved			
$MgSO_4$-7H_2O (0,5 g/ml; filter sterilized)	0.2 ml	0.4 ml	0.9 ml
Microelements	0.4 ml	0.8 ml	1.8 ml
CaFe	0.4 ml	0.8 ml	1.8 ml

Table 14: **Microelements (left) and CaFe (right) for RS102 medium.** Indicated recipes for 50 ml. Filter sterilize.

$(NH_4)_2Fe(SO_4)_2$-6H_2O	4 g
$ZnSO_4$-7H_2O	0.3 g
$MnSO_4$-H_2O	0.1 g
$NiSO_4$-6H_2O	0.01 g
Vitamin C	0.1 g

$CaCl_2$-2H_2O	3.75 g
$FeCl_3$-6H_2O	0.25 g
HCl (37%)	187.5 µl

8.2.4 Yeast extract peptone dextrose medium - YPD

Table 15: **YPD medium.** Complex medium for *P. pastoris*. The liquid medium was stored at room temperature. YPD slants or plates were stored at 4°C.

	1l
Yeast extract	10 g
Peptone	20 g
H_2O to 900 ml and autoclaved	
10X D	100 ml

8.2.5 Buffered glycerol-complex medium (BMGY)

Table 16: **BMGY medium.** Complex medium for inducible *P. pastoris* strains. Stored media at 4°C.

	1l
Yeast extract	10 g
Peptone	20 g
H_2O to 700 ml and autoclaved	
10X GY	100 ml
500X B	2 ml
10X YNB	100 ml
Potassium phosphate buffer, 1 M, pH 6.0	100 ml

8.2.6 Buffered methanol-complex medium (BMMY)

Table 17: **BMMY medium.** Complex medium for inducible *P. pastoris* strains. Stored media at 4°C.

	1l
Yeast extract	10 g
Peptone	20 g
H_2O to 790 ml and autoclaved	
500X B	2 ml
10X YNB	100 ml
Potassium phosphate buffer, 1 M, pH 6.0	100 ml

8.2.7 LB medium

Table 18: **LB medium.** Complex medium for *E. coli* and *R. sphaeroides*.

	1L
Typtone	10 g
Yeast extract	5 g
NaCl	10 g
autoclaved	

8.2.8 SOC medium

Table 19: **SOC medium.** Regeneration medium for transformation into *E. coli*.

	1l
Bacto™ tryptone	20 g
NaCl	0.58 g
Bacto™ yeast extract	5 g
$MgCl_2$	2 g
KCl	0.16 g
$MgSO_4$	2.46 g
Dextrose	3.46 g
autoclaved	

8.3 Primers

Table 20: **List of primers.** All depicted primers bind to the plasmid p-m-Pppa-trx-ValCO Q492K L566S-mpmii alt-actual Pppa. The term "LibSeq" refers to sequencing primers.

Primer Name	Sequence
Fw_Seqtrx	5‘-GAGTTCCTCGATGCGAACCTC-3‘
Rev_SeqValC_1	5‘-CATGTCCCGGATCTCATCGATC-3‘
Fw_SeqValC	5‘-CAGCTCGACATCCCGAGC-3‘
Rev_SeqValC_2	5‘-GGTTCGAGGAGTTCCTTGTTGAG-3‘
Fw_UPtrxValC_seq	5‘-GAGGTGCTTGAGTTGCCG-3‘
Fw_UpPppaBglII	5‘-AGATCTCCACTGGGTAAGGTTCTGC-3‘
Fw_UPtrxValC	5‘-GAGGTGCTTGAGTTGCCG-3‘
Fw_PppaMut	5‘-CCTGAGCAAACTGGCCTCAGAATTC-3‘
Rev_PppaMut	5‘-CAGGTGGATGATCTTGTCCGACATATG-3‘
LibSeq_1	5‘-GCGCTATGCGGGCTACAAGAC-3‘
LibSeq_2	5‘-CTGCGGATCACGACGCAG-3‘
LibSeq_3	5‘-GAAGGGCCAGCTGAAGGAGTTCC-3‘
rev_LibSeq_4	5‘-GATCGCGGACGAGTTCTTCC-3‘
rev-LibSeq_5	5‘-CGATCAAACCGTTGCTCC-3‘
rev-LibSeq_6	5‘-CCAATTTGGCTCGTAATCCG-3‘
rev_LibSeq_7	5‘-TCGGTCATTCGTCCCTCCTC-3‘
rev_LibSeq_8	5‘-TGCATGGCGAGCGCATTG-3‘
rev_LibSeq_9	5‘-AGCCTCCTGAACGCGGAG-3‘
LibSeq_10	5‘-GCCCAGATCGAGGAGGCGG-3‘
LibSeq_11	5‘-CGCACGACATTCGCCAATCTC-3‘
LibSeq_12	5‘-ACCGAGGATATCATGGATTTCTGGC-3‘

References

[1] N. L. R. Croteau, T.M. Kutchan, "Natural products (secondary metabolites)," *Biochem. Mol. Biol. plants 24*, pp. 1250–1319, 2000.

[2] K. S.-T. Malgorzata Wanke and E. Swiezewska, "Isoprenoid biosynthesis via 1-deoxy-d-xylulose 5-phosphate/2-cmethyl-d-erythritol 4-phosphate (doxp/mep) pathway," *Acta Biochim. Pol.*, vol. 48, p. 663–72, 2011.

[3] A. Doran, W. Morden, K. Dunn, and V. Edwards-Jones, "Vapour–phase activities of essential oils against antibiotic sensitive and resistant bacteria including mrsa," *Letters in Applied Microbiology*, vol. 48, pp. 387–392, 2009.

[4] D. E. Cane, "Enzymic formation of sesquiterpenes," *Chemical Reviews*, vol. 90, pp. 1089–1103, 1990.

[5] J. Inglese, R. L. Johnson, A. Simeonov, M. Xia, W. Zheng, C. P. Austin, and D. S. Auld, "High-throughput screening assays for the identification of chemical probes," *Nat Chem Biol*, vol. 3, pp. 466–479, Aug. 2007.

[6] A. Emmerstorfer-Augustin, S. Moser, and H. Pichler, "Screening for improved isoprenoid biosynthesis in microorganisms," *Journal of Biotechnology*, vol. 235, pp. 112 – 120, 2016. Special Issue on ACIB, Dedicated to the Occasion of Prof. Dr. Helmut Schwab's 65th Birthday.

[7] G.-H. An, J. Bielich, R. Auerbach, and E. A. Johnson, "Isolation and characterization of carotenoid hyperproducing mutants of yeast by flow cytometry and cell sorting," *Nat Biotech*, vol. 9, pp. 70–73, Jan. 1991.

[8] M. Furubayashi, M. Ikezumi, J. Kajiwara, M. Iwasaki, A. Fujii, L. Li, K. Saito, and D. Umeno, "A high-throughput colorimetric screening assay for terpene synthase activity based on substrate consumption," *PLOS ONE*, vol. 9, pp. 1–11, 03 2014.

[9] J. UBERSAX and L. Frenz, "Methods and compositions for detecting microbial production of water-immiscible compounds," Nov. 22 2012. WO Patent App. PCT/US2012/037,351.

[10] H. Tajalli, A. G. Gilani, M. Zakerhamidi, and P. Tajalli, "The photophysical properties of nile red and nile blue in ordered anisotropic media," *Dyes and Pigments*, vol. 78, pp. 15 – 24, 2008.

[11] J. Kirby, M. Nishimoto, R. W. Chow, V. N. Pasumarthi, R. Chan, L. J. G. Chan, C. J. Petzold, and J. D. Keasling, "Use of non-ionic surfactants for improvement of terpene production in saccharomyces cerevisiae," *Applied and Environmental Microbiology*, 2014.

[12] M. Vardakou, M. Salmon, J. A. Faraldos, and P. E. O'Maille, "Comparative analysis and validation of the malachite green assay for the high throughput biochemical characterization of terpene synthases," *MethodsX*, vol. 1, pp. 187 – 196, 2014.

[13] R. Lauchli, K. S. Rabe, K. Z. Kalbarczyk, A. Tata, T. Heel, R. Z. Kitto, and F. H. Arnold, "High-throughput screening for terpene-synthase-cyclization activity and directed evolution of a terpene synthase," *Angewandte Chemie International Edition*, vol. 52, pp. 5571–5574, 2013.

[14] M. Ahmad, M. Hirz, H. Pichler, and H. Schwab, "Protein expression in pichia pastoris: recent achievements and perspectives for heterologous protein production," *Applied Microbiology and Biotechnology*, vol. 98, pp. 5301–5317, 2014.

[15] H. R. Waterham, M. E. Digan, P. J. Koutz, S. V. Lair, and J. M. Cregg, "Isolation of the pichia pastoris glyceraldehyde-3-phosphate dehydrogenase gene and regulation and use of its promoter," *Gene*, vol. 186, pp. 37 – 44, 1997.

[16] C. M. et al., "Postgenomic adventures with rhodobacter sphaeroides," *Annual Review of Microbiology*, vol. 61, pp. 283–307, 2007. PMID: 17506668.

[17] *GeneJET PCR Purification Kit, Thermo Fisher Scientific*. URL: `https://www.thermofisher.com/order/catalog/product/K0701`, 2016-12-11.

[18] *GeneJET Plasmid Miniprep Kit, Thermo Fisher Scientific*. URL: `https://www.thermofisher.com/order/catalog/product/K0502`, 2016-12-11.

[19] B. Dougherty and W. Rasband, *MicroArray Profile*. URL: `http://www.optinav.info/MicroArray_Profile.htm`, 2017-01-18.

[20] T. Wriessnegger, P. Augustin, M. Engleder, E. Leitner, M. Müller, I. Kaluzna, M. Schürmann, D. Mink, G. Zellnig, H. Schwab, and H. Pichler, "Production of the sesquiterpenoid (+)-nootkatone by metabolic engineering of pichia pastoris," *Metabolic Engineering*, vol. 24, pp. 18 – 29, 2014.

[21] Townswebarchiving. URL: `https://www.townswebarchiving.com/2015/01/how-to-digitise-glass-plate-negatives/`, 2017-04-03.

[22] S. Große, P. Wilke, and H. G. Börner, "Easy access to functional patterns on cellulose paper by combining laser printing and material-specific peptide adsorption," *Angewandte Chemie International Edition*, vol. 55, pp. 11266–11270, 2016.

[23] S. Sternberg, "Biomedical image processing," *IEEE Computer*, 1983. URL: `https://imagej.nih.gov/ij/developer/source/ij/plugin/filter/BackgroundSubtracter.java.htm`, 2017-04-03.

[24] R. Borghese, F. Borsetti, P. Foladori, G. Ziglio, and D. Zannoni, "Effects of the metalloid oxyanion tellurite (teo32−) on growth characteristics of the phototrophic bacterium rhodobacter capsulatus," *Applied and Environmental Microbiology*, vol. 70, pp. 6595–6602, 2004.

[25] D. E. Taylor, "Bacterial tellurite resistance," *Trends in Microbiology*, vol. 7, pp. 111–115.

[26] M. D. Moore and S. Kaplan, "Identification of intrinsic high-level resistance to rare-earth oxides and oxyanions in members of the class proteobacteria: characterization of tellurite, selenite, and rhodium sesquioxide reduction in rhodobacter sphaeroides.," *Journal of Bacteriology*, vol. 174, pp. 1505–1514, 1992.

[27] H. Moscoso, C. Saavedra, C. Loyola, S. Pichuantes, and C. Vásquez, "Biochemical characterization of tellurite-reducing activities of bacillus stearothermophilus v," *Research in Microbiology*, vol. 149, pp. 389 – 397, 1998.

[28] M. Geier, P. Fauland, T. Vogl, and A. Glieder, "Compact multi-enzyme pathways in p. pastoris," *Chem. Commun.*, vol. 51, pp. 1643–1646, 2015.

[29] A. Emmerstorfer, M. Wimmer-Teubenbacher, T. Wriessnegger, E. Leitner, M. Müller, I. Kaluzna, M. Schürmann, D. Mink, G. Zellnig, H. Schwab, and H. Pichler, "Over-expression of ice2 stabilizes cytochrome p450 reductase in saccharomyces cerevisiae and pichia pastoris," *Biotechnology Journal*, vol. 10, pp. 623–635, 2015.